

LARGE DEFORMATION FINITE ELEMENT ANALYSIS OF
PARTIALLY EMBEDDED OFFSHORE PIPELINES FOR VERTICAL
AND LATERAL MOTION AT SEABED

SUJAN DUTTA

**LARGE DEFORMATION FINITE ELEMENT ANALYSIS OF PARTIALLY
EMBEDDED OFFSHORE PIPELINES FOR VERTICAL AND LATERAL
MOTION AT SEABED**

by

© **Sujan Dutta**

A Thesis submitted to the

School of Graduate Studies

in partial fulfillment of the requirements for the degree of

Masters in Engineering

Faculty of Engineering and Applied Science

Memorial University of Newfoundland

September, 2012

St. John's

Newfoundland

Canada

ABSTRACT

Subsea pipelines play a significant role in transporting hydrocarbon from offshore. For both shallow and deep water, an effective means of hydrocarbon transportation is the usage of pipeline. However, deep water pipelines are expensive to bury and an economic way is to lay the pipelines on seabed. Due to pipe installation procedures (e.g. wave action, pipelines self weight etc.), pipelines could penetrate into the seabed a fraction of its diameter. Pipelines might experience thermal expansion (due to low ambient and high internal temperature) during operation cycles which can cause pipelines to expand axially. But due to restraining conditions from accumulated soil/pipe interaction and effective longitudinal force along the pipeline, bending moments can develop in the pipelines, which cause pipelines to buckle laterally. This lateral buckling is resisted mainly through soil/pipe interaction. In addition, the berm formed around the pipe (during installation period) plays a vital role in resisting the lateral pipe movements. Thus, accurate prediction of soil/pipe interaction of an as-laid pipeline is very important for the development of pipeline design guidelines. To address this critical phenomenon, the first step is to capture the soil behaviour during pipe vertical penetration along with the berm formulation mechanism. This is a large deformation problem. To solve the problem numerically, a large deformation numerical tool is required. In this study, the Coupled Eulerian Lagrangian (CEL) finite element method is used for analysis of partially embedded pipelines. Analyses are performed using ABAQUS 6.10-EF1 software. In the deep sea, the undrained shear strength of clay typically increases with depth. In addition, the undrained shear strength is strain rate dependent. Moreover, strain softening

behaviour of clay is another critical phenomenon that should be considered. The standard von Mises yield constitutive model available in ABAQUS cannot capture this clay behaviour. Therefore, in this study an advanced soil constitutive model that considered these phenomena is implemented in ABAQUS using user subroutines programmed in FORTRAN. Results from the analysis are compared with centrifuge test results and other available solutions in the literature. It is shown that the Coupled Eulerian Lagrangian (CEL) approach together with the advanced soil constitutive model is a very effective tool for modelling large deformation behaviour of partially embedded pipelines in seabed both for vertical penetration and lateral movement.

ACKNOWLEDGEMENTS

The research work was carried out under the supervision of Dr. Bipul Hawlader, Associate professor, Memorial University, NL, Canada, Dr. Ryan Phillips, Principal Consultant, C-CORE, NL, Canada and Dr. Shawn Kenny, Associate professor, Memorial University, NL, Canada. I would like to express my gratitude to them from the very core of my heart for their keen supervision, invaluable suggestion, and affectionate encouragement throughout the work. I thank MITACS, School of the Graduate Studies, Memorial University and C-CORE for their financial support which helped me to make my thesis possible. Also, my sincerest thanks go to Mr. John Barrett of C-CORE for his invaluable suggestions for finite element analysis. I would like to extend my sincere thanks to my parents. Without their support, it was not possible to finish the thesis.

Table of Contents

ABSTRACT.....	ii
ACKNOWLEDGEMENTS.....	iv
Table of Contents.....	v
List of Tables.....	x
List of Figures.....	xi
List of Symbols.....	xx
Chapter 1.....	1-1
Introduction.....	1-1
1.1 General.....	1-1
1.2 Objective.....	1-3
1.3 Outline of Thesis.....	1-4
1.4 Contribution in Offshore Pipeline Analysis.....	1-5
Chapter 2.....	2-1
Literature Review.....	2-1
2.1 Introduction.....	2-1
2.2 Pipeline Embedment.....	2-2
2.3 Modelling of Partially Embedded Pipelines.....	2-4
2.4 Modelling of Vertical Penetration.....	2-5

2.4.1 Theoretical modeling	2-5
2.4.2. Physical modeling	2-12
2.4.3. Numerical modeling.....	2-18
2.5. Development of Lateral Pipe Resistance Theorem.....	2-34
2.5.1 Theoretical modeling of pipe lateral resistance	2-37
2.5.2 Physical modelling of pipe lateral resistance.....	2-45
2.5.3 Numerical modelling of pipe lateral resistance.....	2-64
2.6 Conclusion	2-71
Chapter 3	3-1
Finite Element Modeling of Vertical Penetration of Offshore Pipelines using Coupled Eulerian Lagrangian Approach	3-1
3.1 Abstract	3-1
3.2 Introduction.....	3-2
3.3 Problem Definition.....	3-4
3.4 Finite Element Model Formulation.....	3-5
3.5 Parameter Selection	3-7
3.6 Model Validation and Results.....	3-9
3.7 Mesh Sensitivity.....	3-9
3.8 Comparison with Centrifuge Test Results	3-10

3.9 Soil Deformation around the Pipe.....	3-13
3.10 Strain in Soil Mass	3-14
3.11 Berm Development Mechanism	3-16
3.12 Conclusions.....	3-17
3.13 Acknowledgements.....	3-18
3.14 References	3-18
Chapter 4.....	4-1
Strain Softening and Rate Effects on Soil Shear Strength in Modelling of Vertical Penetration of Offshore Pipelines	4-1
4.1 Abstract	4-1
4.2 Introduction.....	4-2
4.3 Problem Definition.....	4-4
4.4 Strain Rate and Strain Softening Effects on Undrained Shear Strength of Clay	4-5
4.5 Finite Element Model	4-6
4.6 Parameter Selection	4-9
4.7 Model Validation and Results.....	4-11
4.7.1 Mesh sensitivity	4-11
4.7.2 Comparison with existing models.....	4-12
4.8 Effect of Strain Softening and Strain Rate.....	4-15

4.8.1 Comparison with centrifuge test results.....	4-16
4.8.2 Plastic strain in soil mass	4-16
4.9 Parametric Study	4-19
4.9.1 Effect of μ	4-19
4.9.2 Effect of S_t	4-19
4.9.3 Effect of ξ_{95}	4-20
4.10 Conclusion	4-22
4.11. Acknowledgments.....	4-23
4.12. References.....	4-23
Chapter 5	5-1
Lateral Movement of Partially Embedded Offshore Pipelines	5-1
5.1 Introduction.....	5-1
5.2 Comparison between Numerical and Centrifuge Models	5-2
5.2.1 Vertical penetration.....	5-3
5.2.2 Lateral movement	5-4
5.3 Alternative interpretation of pipe lateral resistance	5-36
5.4 Comparison with Other Analytical Solutions	5-42
5.4 Conclusion	5-45
Chapter 6.....	6-1

Conclusions and Recommendations for Future Research..... 6-1

 6.1 Conclusions..... 6-1

 6.2 Recommendations for Future Research 6-3

References..... 1

List of Tables

Table 2.1 Summary of small to large scale test for vertical penetration (Revised from Verley and Lund, 1995).....	2-13
Table 2.2 Progressive development of numerical analysis in pipe penetration.....	2-33
Table 2.3 Pipe Classification (Based on operative load).....	2-35
Table 2.4 Parameters used for analysis (White and Dingle, 2011).....	2-55
Table 3.1 Geometry and parameters used in the analyses.....	3-8
Table 4.1 Geometry and parameters used in the analyses.....	4-10
Table 5.1 Centrifuge test conditions (White and Dingle, 2011; Dingle et al., 2008)..	5-3

List of Figures

Fig. 1.1 Side-scan sonar image of lateral buckle (Bruton et al., 2006).....	1-2
Fig. 2.1 Problem Statement: (a) initial embedment, (b) lateral movement for heavy pipe, (c) lateral movement of light pipe.....	2-3
Fig. 2.2 Failure modes: (a) strip footing (b) offshore pipelines (Small et al., 1971)...	2-8
Fig. 2.3 Vertical resistance (Small et al., 1971).....	2-8
Fig. 2.4 Velocity field around the pipeline (Murff et al., 1989).....	2-9
Fig. 2.5 Extended upper bound mechanism for pipe penetration depth of above half pipe diameter (Aubeny et al., 2005).....	2-10
Fig. 2.6 Comparison between various models (Cathie et al., 2005).....	2-12
Fig. 2.7 Comparison between various models for pipe vertical penetration (Cheuk et al., 2007).....	2-14
Fig. 2.8 Vertical pipe penetration resistance with embedment (Dingle et al., 2008)...	2-15
Fig. 2.9 Shear zone formation during vertical penetration (Dingle et al., 2008).....	2-16
Fig. 2.10 Pipe penetration resistance with depth (Hu et al., 2009).....	2-17
Fig. 2.11 (a) Small strain analysis (WIP pipe) (b) Large strain analysis (PIP pipe)....	2-18
Fig. 2.12 Comparison between numerical and theoretical solution (Aubeny et al., 2005).	2-20
Fig. 2.13 Comparison of vertical penetration resistance (redrawn from Bransby et al., 2008).....	2-21
Fig. 2.14 Comparison between numerical and theoretical solution (Merifield et al., 2008) (a) Smooth pipe (b) Rough pipe.....	2-22

Fig. 2.15 Typical shear strength profile (Morrow and Bransby, 2010).....	2-23
Fig. 2.16 Comparison of pipe penetration resistance (a) Smooth (b) Rough (Morrow and Bransby, 2010).....	2-24
Fig. 2.17 Variation of bearing capacity factor (Barbosa-Cruz and Randolph, 2005)..	2-25
Fig. 2.18 Variation of nominal bearing capacity factor (Barbosa-Cruz and Randolph, 2005).....	2-26
Fig. 2.19 Comparison between large strain and small strain (Bransby et al., 2008)....	2-27
Fig. 2.20 Comparison between FE analyses and centrifuge test results (Wang et al., 2010).....	2-29
Fig. 2.21 Comparison of vertical bearing capacity factor (Tho et al., 2010).....	2-30
Fig. 2.22 Comparison between finite element model and centrifuge test (Chatterjee et al., 2012a).....	2-32
Fig. 2.23 Pipe vertical penetration with depth (Chatterjee et al., 2012a).....	2-32
Fig. 2.24 Typical behaviour of light and heavy pipe.....	2-36
Fig. 2.25 Bi-linear model (White and Cheuk, 2008).....	2-37
Fig. 2.26 Effective embedment parameters (White and Cheuk, 2008).....	2-38
Fig. 2.27 Theoretical failure loci for surface foundations and pipes (White and Cheuk, 2008).....	2-39
Fig. 2.28 Geometry of upper bound solution for breakout resistance (Cheuk et al., 2007).....	2-40
Fig. 2.29 Prediction of breakout resistance using upper bound solution (Cheuk et al., 2007).....	2-41

Fig. 2.30 Upper bound mechanism (Merifield et al., 2008).....	2-42
Fig. 2.31 Yield envelope at different embedment (a) Smooth pipe (b) Rough pipe (Merifield et al., 2008).....	2-43
Fig. 2.32 Theoretical yield envelope for soil shear strength proportional to depth (a) Smooth pipe (b) Rough pipe. (Randolph and White, 2008).....	2-44
Fig. 2.33 Upper bound geometry solution for lateral resistance (Cheuk et al., 2007).	2-45
Fig. 2.34 Schematic diagram of test (Lyons, 1973).....	2-46
Fig. 2.35 Variation of co-efficient of friction (a) with submerged weight, soil/pipe interface, pipe diameter (b) with hydrostatic test and without hydrostatic test (Lyons, 1973).....	2-47
Fig. 2.36 Comparison with analytical model and experimental results (Wagner et al., 1987).....	2-48
Fig. 2.37 Comparison of Verley and Lund's model with experimental results (Verley and Lund, 1995).....	2-50
Fig. 2.38 Comparison of experimental data and analytical model (Bruton et al., 2006).....	2-51
Fig. 2.39 Pipe lateral resistance during steady cyclic lateral movements (Cheuk et al., 2007).....	2-52
Fig. 2.40 Typical pipe lateral resistance during pipe steady movement (Cheuk et al., 2007).....	2-52
Fig. 2.41 Normalised pipe lateral resistance during pipe lateral movement (Dingle et al., 2008).....	2-53

Fig. 2.42 Soil velocity field during pipe lateral breakout (Dingle et al., 2008).....	2-54
Fig. 2.43 Pipe lateral resistance during lateral movement (White and Dingle, 2011).	2-55
Fig. 2.44 Development of effective embedment using soil berm and softening (White and Dingle, 2011).....	2-56
Fig. 2.45 Variation of pipe lateral resistance with effective embedment (White and Dingle, 2011).....	2-58
Fig. 2.46 Variation of pipe lateral resistance with embedment (White and Dingle, 2011).....	2-58
Fig. 2.47 Comparison of normalised residual horizontal and vertical load (Bruton et al., 2006).....	2-60
Fig. 2.48 Comparison between model data base and empirical equation (Bruton et al., 2006).....	2-62
Fig. 2.49 Comparison between measured and predicted equivalent friction factor (Cardoso et al., 2010).....	2-62
Fig. 2.50 Pipe horizontal resistance during lateral travel (White and Dingle, 2011)...	2-63
Fig. 2.51 Pipe residual friction factor co-relation (White and Dingle, 2011).....	2-64
Fig. 2.52 Details of mesh size (Lyons, 1973).....	2-65
Fig. 2.53 Comparison with numerical and physical experiments (Lyons, 1973).....	2-65
Fig. 2.54 Details of pipe lateral movement (Merifield et al., 2008).....	2-67
Fig. 2.55 Resultant pipe resistance during relative pipe movement (a) Smooth pipe (b) Rough pipe (Merifield et al., 2008).....	2-67
Fig. 2.56 Comparison with yield envelope (Wang et al., 2010).....	2-70

Fig. 2.57 Comparison with yield envelope (Chatterjee et al., 2012b).....	2-70
Fig. 3.1 Problem definition.....	3-4
Fig. 3.2 Finite element model used in this study.....	3-9
Fig. 3.3 Effect of mesh size on vertical reaction.....	3-11
Fig. 3.4 Comparison between finite element and centrifuge test results.....	3-12
Fig. 3.5 Predicted and observed velocity vectors at different depth of penetration.....	3-14
Fig. 3.6 Equivalent plastic strain around the pipe at $w/D=0.45$: (a) smooth (b) rough.....	3-15
Fig. 3.7 Vertical penetration and berm formation (Dingle et al., 2008).....	3-16
Fig. 3.8 Predicted and observed berm size at $w/D=0.45$	3-17
Fig. 4.1 Problem definition.....	4-5
Fig. 4.2 Finite element model used in this study.....	4-8
Fig. 4.3 Effect of mesh size on pipe vertical penetration resistance for smooth pipe-soil interface.....	4-12
Fig. 4.4(a) Comparison with previous solutions for smooth pipe-soil interface.....	4-14
Fig. 4.4(b) Comparison with previous solutions for rough pipe-soil interface.....	4-15
Fig. 4.5 Comparison between finite element and centrifuge test results.....	4-17
Fig. 4.6(a) Equivalent plastic shear strain around the pipe at $w/D = 0.45$ for smooth pipe-soil interface.....	4-18
Fig. 4.6(b) Equivalent plastic shear strain around the pipe at $w/D = 0.45$ for rough pipe-soil interface.....	4-18
Fig. 4.7 Effect of strain rate parameter, μ for smooth pipe-soil interface.....	4-20

Fig. 4.8 Effect of remoulded sensitivity, S_t for smooth pipe-soil interface.....	4-21
Fig. 4.9 Effect of strain softening parameter, β_{95} for smooth pipe-soil interface.....	4-22
Fig. 5.1 Variation of pipe vertical penetration resistance with embedment depth.....	5-5
Fig. 5.2(a) Pipe resistance during lateral movement (Case-D1: Dingle et al., 2008)..	5-6
Fig. 5.2(b) Pipe invert trajectory (Case-D1: Dingle et al., 2008).....	5-6
Fig. 5.2 (c) Equivalent plastic strain around pipeline and (d) Velocity field during pipe lateral movement at (i) breakout point (ii) lateral displacement of one pipe diameter (iii) lateral displacement of three pipe diameter.....	5-7
Fig. 5.2 (e) Equivalent plastic strain around pipeline and (f) Velocity field during pipe lateral movement at (i) breakout point (ii) lateral displacement of one pipe diameter (iii) lateral displacement of three pipe diameter.....	5-8
Fig. 5.3(a) Pipe resistance during lateral movement (Case-L1).....	5-9
Fig. 5.3(b) Pipe invert trajectory (Case-L1).....	5-9
Fig. 5.3 (c) Equivalent plastic strain around pipeline and (d) Velocity field during pipe lateral movement at (i) breakout point (ii) lateral displacement of one pipe diameter (iii) lateral displacement of three pipe diameter.....	5-10
Fig. 5.3(e) Equivalent plastic strain around pipeline and (f) Velocity field during pipe lateral movement at (i) breakout point (ii) lateral displacement of one pipe diameter (iii) lateral displacement of three pipe diameter.....	5-11
Fig. 5.4(a) Pipe resistance during lateral movement (Case-L2).....	5-12
Fig. 5.4(b) Pipe invert trajectory (Case-L2).....	5-12
Fig. 5.4 (c) Equivalent plastic strain around pipeline and (d) Velocity field during	

pipe lateral movement at (i) breakout point (ii) lateral displacement of one pipe diameter (iii) lateral displacement of three pipe diameter.....	5-13
Fig. 5.4(e) Equivalent plastic strain around pipeline and (f) Velocity field during pipe lateral movement at (i) breakout point (ii) lateral displacement of one pipe diameter (iii) lateral displacement of three pipe diameter.....	5-14
Fig. 5.5(a) Pipe resistance during lateral movement (Case-L3).....	5-15
Fig. 5.5(b) Pipe invert trajectory (Case-L3).....	5-15
Fig. 5.5 (c) Equivalent plastic strain around pipeline and (d) Velocity field during pipe lateral movement at (i) breakout point (ii) lateral displacement of one pipe diameter (iii) lateral displacement of three pipe diameter.....	5-16
Fig. 5.5 (e) Equivalent plastic strain around pipeline and (f) Velocity field during pipe lateral movement at (i) breakout point (ii) lateral displacement of one pipe diameter (iii) lateral displacement of three pipe diameter.....	5-17
Fig. 5.6(a) Pipe resistance during lateral movement (Case-L4).....	5-18
Fig. 5.6(b) Pipe invert trajectory (Case-L4).....	5-18
Fig. 5.6 (c) Equivalent plastic strain around pipeline and (d) Velocity field during pipe lateral movement at (i) breakout point (ii) lateral displacement of one pipe diameter (iii) lateral displacement of three pipe diameter.....	5-19
Fig. 5.6 (e) Equivalent plastic strain around pipeline and (f) Velocity field during pipe lateral movement at (i) breakout point (ii) lateral displacement of one pipe diameter (iii) lateral displacement of three pipe diameter.....	5-20
Fig. 5.7(a) Pipe resistance during lateral movement (Case-L5).....	5-21

Fig. 5.7(b) Pipe invert trajectory (Case-L5).....	5-21
Fig. 5.7 (c) Equivalent plastic strain around pipeline and (d) Velocity field during pipe lateral movement at (i) breakout point (ii) lateral displacement of one pipe diameter (iii) lateral displacement of three pipe diameter.....	5-22
Fig. 5.7 (e) Equivalent plastic strain around pipeline and (f) Velocity field during pipe lateral movement at (i) breakout point (ii) lateral displacement of one pipe diameter (iii) lateral displacement of three pipe diameter.....	5-23
Fig. 5.8(a) Pipe resistance during lateral movement (Case-L6).....	5-24
Fig. 5.8(b) Pipe invert trajectory (Case-L6).....	5-24
Fig. 5.8 (c) Equivalent plastic strain around pipeline and (d) Velocity field during pipe lateral movement at (i) breakout point (ii) lateral displacement of one pipe diameter (iii) lateral displacement of three pipe diameter.....	5-25
Fig. 5.8 (e) Equivalent plastic strain around pipeline and (f) Velocity field during pipe lateral movement at (i) breakout point (ii) lateral displacement of one pipe diameter (iii) lateral displacement of three pipe diameter.....	5-26
Fig. 5.9 Variation of pipe rear end surface area with pipe travel direction.....	5-27
Fig. 5.10 Six pipe locations (A, B, C, D, E & F) on load-displacement plot (Dingle et al. 2008).....	5-32
Fig. 5.11 (a) Predicted and observed velocity vectors at pipe displacement of $0.04D$ (location A) and $0.1D$ (location B).....	5-33
Fig. 5.11 (b) Predicted and observed velocity vectors at pipe lateral displacement of $0.15D$ (location C) and $0.53D$ (location D)	5-34

Fig. 5.11 (c) Predicted and observed velocity vectors at pipe lateral displacement of 2.11 <i>D</i> (location E) and 2.95 <i>D</i> (location F)	5-35
Fig. 5.12 Variation of smooth pipe lateral resistance with embedment from CEL analysis	5-37
Fig. 5.13 Variation of rough pipe lateral resistance with embedment from CEL analysis	5-38
Fig. 5.14 Variation of smooth pipe lateral resistance for CEL analysis with effective embedment (w' = effective embedment).....	5-40
Fig. 5.15 Variation of rough pipe lateral resistance for CEL analysis with effective embedment.....	5-41
Fig. 5.16 Comparison of lateral breakout resistance.....	5-43
Fig. 5.17 Variation of lateral residual resistance with initial pipe embedment.....	5-44
Fig. 5.18 Comparison of lateral residual resistance.....	5-45

List of Symbols

Symbol	Descriptions
A_{berm}	Area of berm
B	Effective pipe width
c_u	Undrained shear strength of soil
D	Pipe diameter
D_f	Depth of footing from mudline
D'	Effective pipe width
E_u	Undrained elastic modulus
f_{brk}	Normalized breakout resistance
F_{brk}	Breakout resistance
F_h	Horizontal force per unit length
G	Dimensionless soil strength
h_{berm}	Berm height
h'_{berm}	Berm height after sensitivity effect
h_{res}	Normalized residual resistance
H_{res}	Residual resistance
k	Gradient of undrained shear strength of soil
L	Length of slip surface
N_c or N_{cv}	Bearing capacity factor
N_{sw}	Soil self weight factor
P'	Net force on pipe allowing buoyancy

q_u	Ultimate bearing capacity
R	Over penetration ratio
r	Pipe radius
r_o	Radius of slip circle
S	Dimensionless vertical force
S_t	Soil sensitivity
s_u	Undrained shear strength of soil
s_{u0}	Intact undrained soil shear strength
s_{um}	Undrained shear strength of soil at mudline
s_{uzp}	Undrained shear strength of soil at pipe invert
$s_{u_D'_{max}}$	Undrained shear strength of soil at maximum pipe contact width
$\bar{s}_{u,1D}$	Mean undrained shear strength of soil between soil surface and at one pipe diameter
$s_{u0(i)}$	undrained shear strength of clay at the invert of the pipe
U_l	Pipe lateral displacement
V	Vertical penetration resistance
v'	Pipe velocity
v	Normalized vertical resistance
w	Distance of pipe invert from mudline
w'	Effective pipe embedment
w'_p	Effective pipe weight per unit length
w_s	Submerged pipe weight

w'_{s1}, w'_{s2}	Effective weight of soil masses per unit length
x_{s1}, x_{s2}	Moment arm
z	Depth from mudline
α	Roughness factor for pipe/soil interface
θ	Angle with horizontal axis
γ	Soil unit weight
γ'	Submerged soil unit weight
$\dot{\gamma}$	Strain rate
$\dot{\gamma}_{ref}$	Reference strain rate
η	Normalised gradient of undrained shear strength of soil
η_e	Aspect ratio for berm area calculation
μ	Rate of strength increase per decade
μ_f	Friction factor
δ_{rem}	Inverse of soil sensitivity
ξ	Accumulated plastic shear strain
ξ_{95}	The value of accumulated strain where 95% of soil strength is reduced
λ	Sensitivity reduction factor
ν_u	Poisson's ratio
ϵ^{pl}	Plastic strain

Chapter 1

Introduction

1.1 General

Demand for offshore technological development is increasing daily for increased hydrocarbon production. One of the major challenges is the safe and efficient transportation of hydrocarbon offshore. Among the possible options, an effective way to transport the hydrocarbon from offshore to onshore is the use of pipelines especially for high yield reservoirs. Depending upon shallow or deep water, pipelines can be either buried or kept in as-laid state on the seabed. In deep water, installations of buried pipe are expensive. Thus, pipelines are normally laid on the seabed in deep water. As-laid pipeline can penetrate a fraction of its diameter owing to self weight along with its laying effects. Sediment transportation, liquefaction, consolidation in soil along with installation process may also cause self burial of pipeline (Cathie et al., 2005); however, it is not of interest in the present study.

After installation, pipelines may be operated under high temperature and pressure to transport the hydrocarbon whereas the ambient temperature around the pipeline is very low (Merifield et al., 2008). High temperature and pressure is required to ease the fluid flow through the pipe and to reduce the wax solidifications (Cheuk et al., 2007). But high

temperature and pressure can create effective longitudinal forces along the pipelines, which is resisted by soil reaction (due to embedment). The developed longitudinal force might cause the pipeline to buckle laterally to release the energy. Thus, the pipeline might suffer from lateral buckling along with thermal expansion. This phenomenon can be best described in Fig.1.1 where as-laid pipeline moves away from its original position. Besides thermal expansion, geo-hazards like submarine slide can also cause pipeline to move laterally up to 2 to 10 m (Bruton et al., 2008).

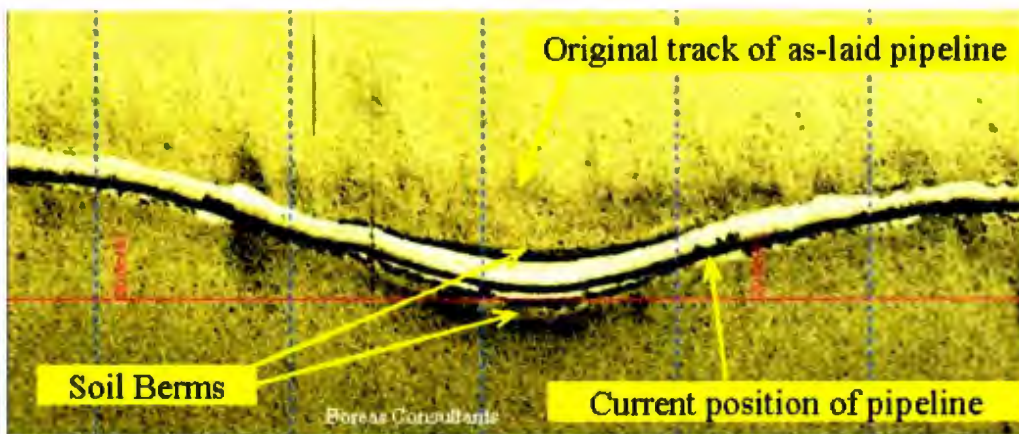


Fig. 1.1 Side-scan sonar image of lateral buckle (Bruton et al., 2008)

Also, temperature variation within the pipeline might occur during operation at shut down and restart effects. It causes pipe thermal expansion and contraction, which is responsible for the variation of pipe effective axial force. This may cause cyclic lateral pipeline movement. The developed stress along the pipeline can be relieved by the usage of inline expansion spools or lateral buckle (snake lying) along the unburred pipeline. But inline spools are not cost effective (Dingle et al., 2008) and for snake lying, it is difficult to estimate the boundary condition, mode of lateral buckling and the pipe feed that must be

allowed for expansion. Therefore, pipelines are kept as-laid and the challenge is to estimate the pipe lateral resistance from soil/pipe interaction. Pipe embedment during pipe installation is a governing factor affecting the lateral pipe resistance. Based on different theoretical (lower bound theory, upper bound theory), experimental (full scale, centrifuge) and numerical solutions, vertical penetration has been studied by different authors.

1.2 Objective

The purpose of this study is to understand the soil failure and flow mechanism for vertical and lateral pipe movements through numerical investigation using large deformation finite element tools. Among the available limited large deformation finite element (LDFE) tools, Coupled Eulerian-Lagrangian technique (CEL) is adopted in commercially available software package ABAQUS 6.10-EF1. However, the built-in constitutive models available in ABAQUS do not model properly the soil typically found in deep sea under large strain. Therefore, in this study an advanced soil constitutive model is implemented using user subroutines to show the strain-softening and strain rate effects on undrained shear strength of soil. Numerical analyses are performed both for vertical and lateral movement of partially embedded pipeline. The effect of pipe weight during applied vertical condition on lateral movement of the pipe is also shown.

1.3 Outline of Thesis

This thesis presents the outcome of this research work in a systematic way in six chapters. The First chapter demonstrates introduction and objectives along with the contribution to the problem. Chapter 2 describes the research works that have been performed in the analysis of vertical penetration of offshore pipeline during installation phase and lateral displacement during pipeline operational period. Moreover, development of bearing capacity theorem and its application in vertical pipeline penetration problems is also outlined. Finite element model development, simulation and problem idealizations are discussed in Chapter 3. Finite element model was evaluated using existing centrifuge test data and comparison with centrifuge test results is also discussed. This chapter has been published as: Dutta, S., Hawlader, B. and Phillips, R. (2012) "Finite Element Modelling of Vertical Penetration of Offshore Pipelines using Coupled Eulerian Lagrangian Approach," 22nd International Offshore (Ocean) and Polar Engineering Conference & Exhibition, Rodos Palace Hotel, Rhodes (Rodos), Greece, June 17–22, 2012. In Chapter 4, a more realistic numerical model is developed for most sophisticated analysis. A strain rate dependent softening soil model is incorporated to capture more realistic scenario and a detailed parametric study is also demonstrated with their effects. This chapter has been accepted for publication as: Dutta, S., Hawlader, B. and Phillips, R. (2012) "Strain Softening and Rate Effects on Soil Shear Strength in Modelling of Vertical Penetration of Offshore Pipelines," 9th International Pipeline Conference, IPC2012, September 24–28, 2012, Calgary, Alberta, Canada. In Chapter 5, a detailed analysis is performed for lateral pipeline movement. As discussed in the introduction, a pipeline can move several pipe

diameters during its operation and a number of numerical models are developed. Also, developed numerical models are compared with the centrifuge test results discussed. Finally, in Chapter 6 conclusions and recommendations of this research for future study are described.

1.4 Contribution in Offshore Pipeline Analysis

- Applicability and challenges of Coupled Eulerian Lagrangian (CEL) technique in partially embedded offshore pipeline analysis.
- Analysis of large deformation soil behavior at undrained condition using user subroutines written in FORTRAN.
- Effects of strain rate and strain softening on soil behavior are analyzed.

Chapter 2

Literature Review

2.1 Introduction

With increasing demand for energy, offshore oil and gas developments in deep water have significantly increased over the last several decades. Deep sea pipelines are often laid untrenched on the seabed and may not be buried. The pipelines may be operated under high temperature and pressures. Field data from various offshore pipeline projects confirm that the vertical penetration/embedment of pipelines has a strong impact on pipeline lateral displacement (Lyons, 1973; Karal, 1977). Thus, the accurate prediction of pipeline penetration is very important in pipeline design. During installation and operation the deep-sea pipelines might be subjected to two different types of displacements, which are critical in design. The first one is the axial displacement, which is commonly known as “Pipeline Walking.” The second one is due to the effects of pressure and temperature during operating condition, which can cause the pipeline to move laterally and might result in lateral buckling of the pipeline. Lateral buckling can also occur for vertical and horizontal out-of-straightness of pipeline.

In general deep water soils are very soft cohesive soil with high water contents. The problems considered in this study are the soil/structure interaction of a pipeline during vertical embedment and lateral displacement during operating conditions. As the

permeability of these fine-grained soils is very low and the application of the load is relatively fast, then undrained conditions prevail.

The literature review presented in the following sections covers mainly two problems: (i) vertical embedment of pipelines in the seabed, and (ii) the response of the partially embedded pipeline under lateral movement. The soil response for undrained loading conditions is mainly presented.

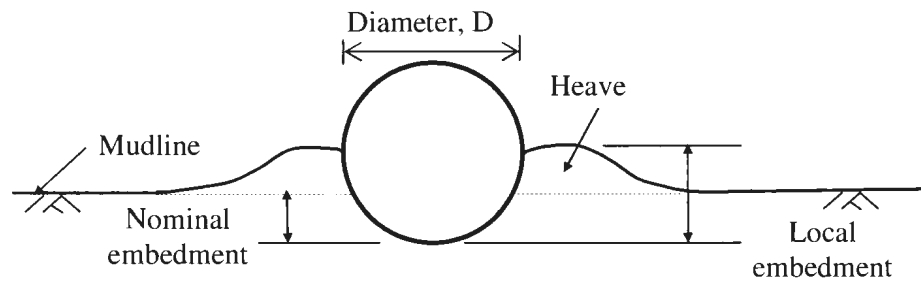
2.2 Pipeline Embedment

The untrenched pipelines generally embed into the seabed by a fraction of their diameter owing to their self-weight and the additional motions imposed during the laying process. The embedment of a partially embedded pipeline is defined as the depth of the pipe invert from soil surface. During penetration, heaving of soil around the pipe occurs as shown in Fig. 2.1 (a). Bruton et al. (2008) defined two depths of embedment for modelling of partially embedded pipelines. As shown in Fig. 2.1(a) the nominal embedment is the depth measured from the undisturbed mudline while the local embedment is the depth measured from the top of the heaved soil. Typically the local embedment is approximately 50% greater than the nominal embedment (Bruton et al., 2008).

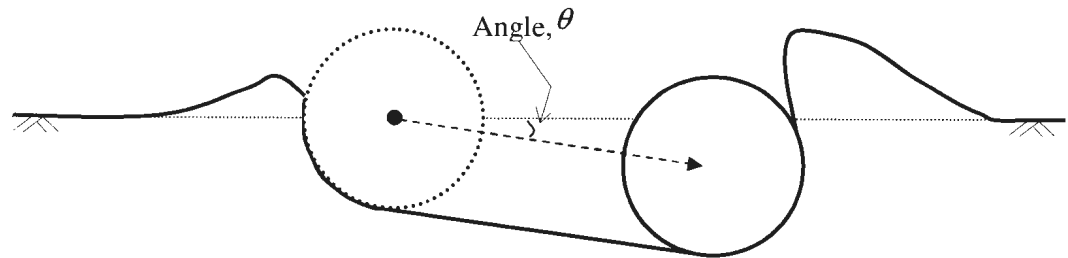
During operation lateral and axial movement of the pipelines might occur. The soil resistance to lateral and axial movement needs to be assessed properly for pipeline design. From physical experiments and field data it has been identified that the direction (angle θ

in Fig. 2.1(b) and (c)) is one of the key factors for estimating lateral resistance (e.g. White and Dingle, 2011). As shown in Fig. 2.1 (b), “heavy” pipes usually penetrate further into the soil during lateral movement. On the other hand “light” pipes might move upward during lateral movement, and if it is very light it might even come to the initial mudline level. The soil berms formed in these two cases are quite different and has a significant effect on lateral resistance, which will be discussed further in the following sections.

(a)



(b)



(c)

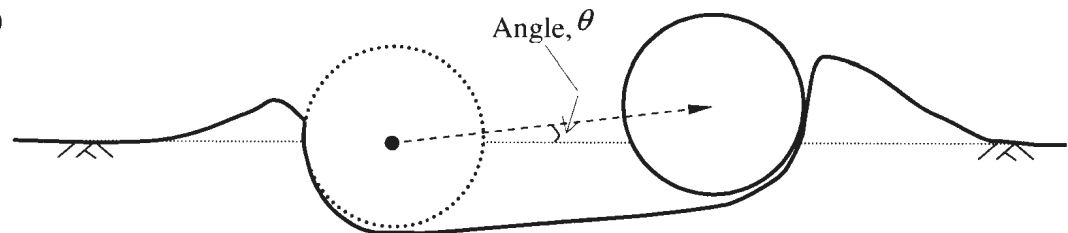


Fig. 2.1 Problem Statement: (a) initial embedment, (b) lateral movement for heavy pipe, (c) lateral movement of light pipe.

2.3 Modelling of Partially Embedded Pipelines

The penetration of a pipeline in the seabed and subsequent lateral movement is fundamentally a large deformation problem. Various approaches have been used in the past for modelling this behaviour. At the early stage the pipeline penetration was modelled using the concept of soil bearing capacity. Guidelines have also been proposed based on physical modelling using geotechnical centrifuge, numerical modelling and field data.

Embedment of a pipeline might occur due to several reasons such as self-weight of the pipe, stress concentration at touchdown zone (where catenary shaped pipeline touches the soil), vertical and lateral oscillation due to sea state including waves and current. Thus, the total pipe penetration, which is also termed as “as-laid” or “initial” pipe embedment, can be divided into two broad categories namely “static” and “dynamic”. The static component includes the penetration due to self-weight of the pipeline and stress concentration at the touchdown zone, while the dynamic component includes the penetrations due to vertical and lateral oscillation of pipelines during installation (Westgate et al., 2010a).

Initial pipe embedment during installation is the combined effects of both static and dynamic effects. Depending upon seabed soil property and laying process (sea state, vessel response, lay ramp configuration, pipeline rigidity, water depth and seabed stiffness), pipe embedment can vary significantly. It has been observed that depending

upon lay process, vertical penetration can increase up to 2 to 10 times static embedment of pipelines (Westgate et al., 2010a).

2.4 Modelling of Vertical Penetration

Previous research on modelling of vertical penetration of pipelines can be broadly categorized into three groups: (i) theoretical modelling, (ii) physical modelling and (iii) numerical modelling. Theoretical modelling includes the models based on bearing capacity equations, upper and lower bound plasticity models and also the empirical models based on laboratory test and field data. The physical modelling includes small or large scale modelling and centrifuge modelling. Finally, the numerical modelling includes the early stage small strain finite element/finite difference modelling in Lagrangian framework and recent large strain finite element modelling.

2.4.1 Theoretical modelling

The vertical penetration of pipelines into the sea-bed can be better understood using the concept of soil bearing capacity and therefore many researchers considered the pipeline as an infinitely long strip footing for predicting depth of penetration and corresponding vertical resistance. The bearing capacity of a shallow foundation for undrained loading can be expressed as:

$$q_u = N_c s_u + \gamma D_f \quad (2.1)$$

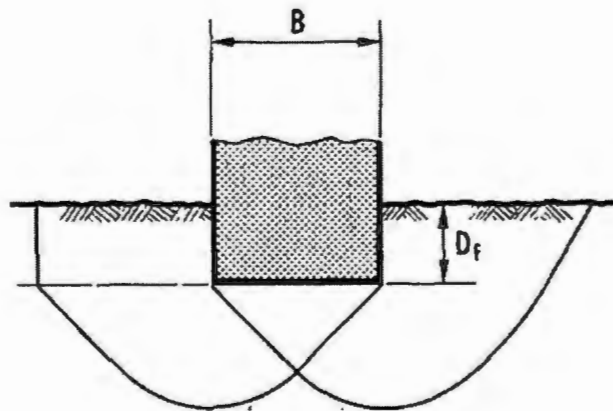
where, q_u is the bearing capacity of the foundation, N_c is the bearing capacity factor, s_u is the undrained shear strength of the soil, γ' is the submerged unit weight of the soil, and D_f is the depth of embedment. For undrained loading the value of N_c is equal to 5.14 when the foundation is at mudline.

The concepts of bearing capacity for a strip footing can be extended further to calculate the vertical penetration resistance of as-laid pipeline as the pipe surface is not rectangular. If the pipeline is placed on the seabed, the unburied pipeline will tend to penetrate through soil up to its bearing capacity level. Small et al. (1971) proposed a method to calculate pipeline embedment into the seabed using the concepts of bearing capacity of a shallow foundation. Fig. 2.2 (b) shows the formation of a soil wedge under the pipe and the soil failure mechanism used in their study. This is very similar to the failure of a shallow foundation as shown in Fig. 2.2 (a). The solutions have been developed for two penetration conditions as shown in Fig. 2.2 (b). The case-I is for shallow embedment that means the center of the pipeline is above the mudline. The case-II is for deeper embedment, which means that the center of the pipeline is below the mudline. No effect of the berm is considered. Vertical load only from the submerged weight (W_s) of the pipe was considered. The failure has been modelled for general (upper line in Fig. 2.3) and local (lower line in Fig. 2.3) shear failure conditions. As shown in this figure that the maximum vertical resistance is mobilized when $D_f = 4.0D$.

While the presented method is very simple it has a number of limitations such as it does not consider the soil/pipe interaction properly and the solutions have been developed only for uniform undrained shear strength.

In addition to pipe/soil interaction and lay process, vertical penetration of a pipeline also depends on undrained shear strength variation of soil. Soil failure mechanism is different for soil with uniform and non-uniform (vary with depth) undrained shear strength. Generally deep sea offshore soils are normally consolidated (NC) to slightly over consolidated (OC) clay and the undrained shear strength of soil varies with depth. Davis et al. (1973) shows that the conventional slip surface failure, such as the one shown above, overestimates the bearing capacity when soil shear strength variation with depth is dominant. In addition to shear strength variation, the roughness of the pipe also has significant influence on vertical resistance.

(a)



Murff et al. (1989) developed upper and lower bound plasticity solutions for partially embedded pipelines based on the failure mechanism of Randolph and Houlsby (1984). The velocity field under the pipeline is shown in Fig. 2.4. Both smooth and rough pipe/soil interface conditions are considered. The analyses were conducted first for wished in place (WIP) pipes (i.e. no berm around the pipe). Note that, WIP condition is different from pushed in place (PIP) condition as shown in Fig. 2.1(a) where berms are formed around the pipe.

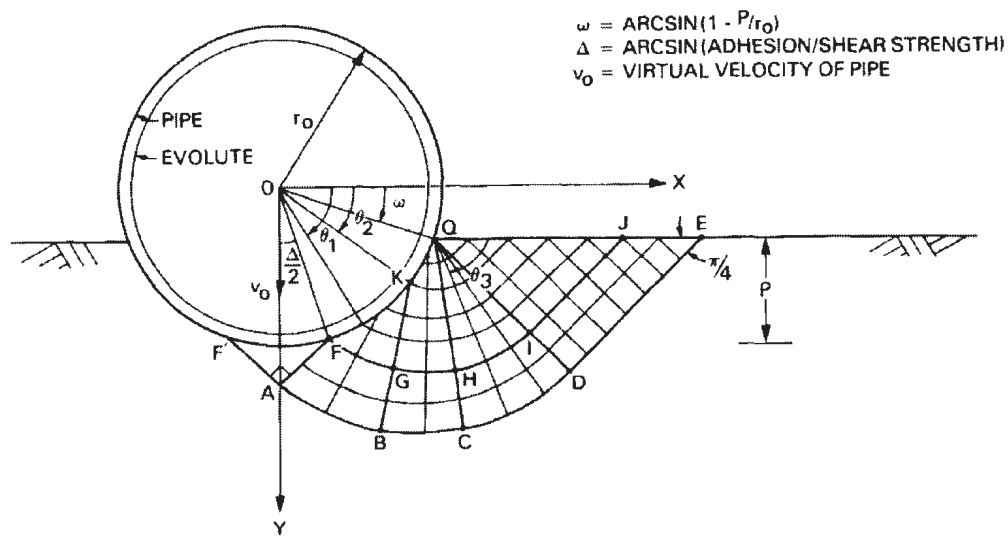


Fig. 2.4 Velocity field around the pipeline (Murff et al., 1989).

Murff et al. (1989) finally extended their model for the effects of a berm using the concept of volume conservation. For example, it is shown that berm formation for a pipe penetration of $0.2D$ can increase resistance by 10-15%. Their analyses are limited to a

vertical penetration of $0.5D$. Also, they did not consider the effects of soil remoulding during penetration and large strain behaviour of soil.

Aubeny et al. (2005) further extended the upper bound solution of Randolph and Houslby (1984) (Fig. 2.5) for pipe embedment greater than $0.5D$. They also considered the variation of undrained shear strength with depth. While compared with finite element analysis, it was found that this solution substantially overestimates the penetration resistance.

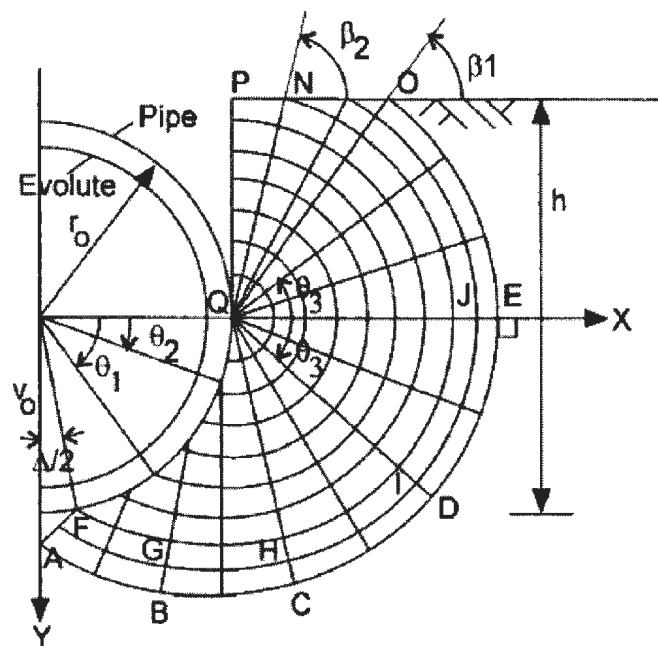


Fig. 2.5 Extended upper bound mechanism for pipe penetration depth of above half pipe diameter (Aubeny et al., 2005).

Besides theoretical modelling, a number of experimental studies were also carried out to simulate vertical embedment of offshore pipelines for a number of projects (e.g. SINTEF 1986a, 1986b, 1987 and TAMU (1992)). Verley and Lund (1995) compiled all the experimental works available in the literature on vertical penetration. Based on this experimental database, Verley and Lund (1995) developed an empirical relationship through dimensionless analysis for vertical penetration in clay which were written in terms of dimensionless soil strength, $G = s_u / D\gamma$ and dimensionless vertical force, $S = w'_p / Ds_u$, where w'_p is the resultant downward force, which is the difference between submerged pipe weight and lift force. The parameters S and G are related as:

$$\frac{z}{D} = 0.0071(SG^{0.3})^{3.2} + 0.062(SG^{0.3})^{0.7} \quad (2.2)$$

Cathie et al. (2005) showed a comparison between the proposed models available in the literature with the data compiled by Murff et al (1989). The comparison is shown in Fig. 2.6 where V = pipe vertical resistance, z = pipe invert embedment from seabed and r = pipe radius.

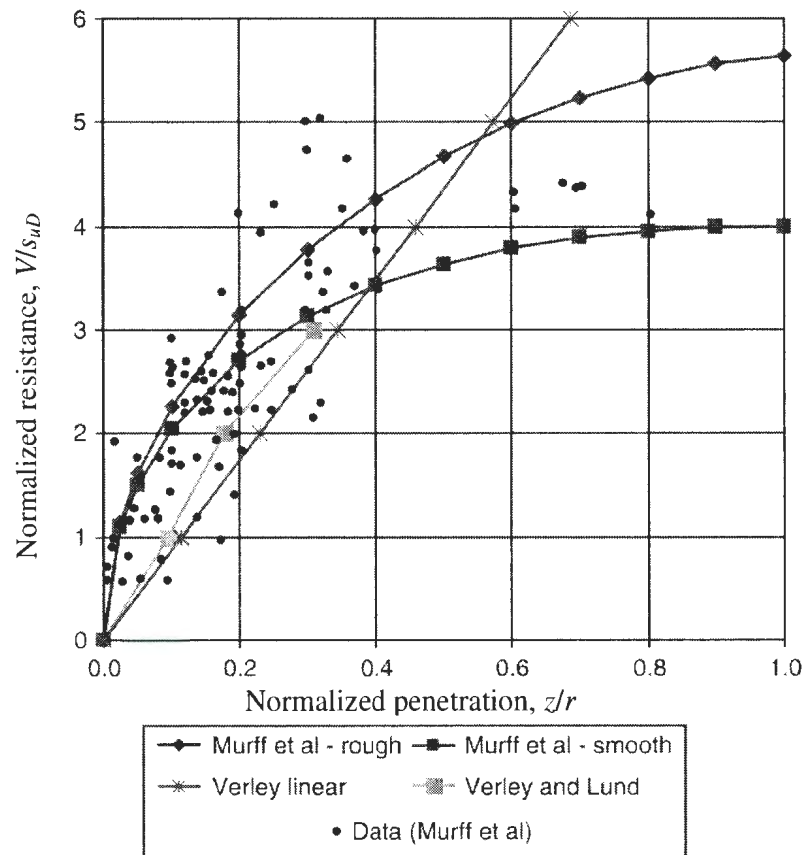


Fig. 2.6 Comparison between various models (Cathie et al., 2005).

2.4.2. Physical modelling

A number of small to large scale laboratory tests have been conducted in the past for modelling vertical penetration of offshore pipelines. Some of them are for large scale offshore projects such as PIPESTAB (Pipeline Stability Design). American Gas Association/Pipeline Research Committee (AGA/PRC) also conducted significant research for modelling on-bottom stability of offshore pipelines. Verley and Lund (1995) compiled all available data. Table 2.1 shows the summary of these experimental studies.

As shown in Table 2.1, tests were conducted mainly for soft clay as typically encounter in the deep sea, except SINTEF (1986b) where undrained shear strength (s_u) of 70 kPa was used. The diameter of the pipes (D) varied between 0.15 m to 1.0 m. The compiled data are shown in Fig. 2.6, based on the available database from experimental study.

Table 2.1 Summary of small to large scale test for vertical penetration (Revised from Verley and Lund 1995).

References	Summary
Lyons, C.G.(1973)	$D = 0.41\text{m}$; $s_u = 2\text{ kPa}$
SINTEF (1986a) (for PIPESTAB)	$D = 1.0(0.5)\text{ m}$; $s_u = 1\text{ kPa}$
SINTEF (1986b) (for PIPESTAB)	$D = 1.0 (0.5)\text{ m}$; $s_u = 70\text{ kPa}$
SINTEF (1987) (for AGA)	$D = 1.0(0.5)\text{ m}$; $s_u = 1.4\text{ kPa}$
Morris et al. (1988)	$D = 0.15\text{ m}$; $s_u = 1\text{ kPa}$
Dunlap et al. (1990)	$D = 0.15\text{ m}$; $s_u = 1.4\text{ kPa}$
Brennodden (1991)	$D = 0.5\text{m}$; $s_u = 1-2\text{ kPa}$
TAMU (1992) (for AGA)	$D = 0.324\text{m}$; $S_u = 1-8\text{ kPa}$

* D =Pipe diameter, s_u = Soil undrained shear strength

Verley and Lund (1995) proposed an empirical equation (Eq. 2.2) to calculate pipe vertical resistance. Although their model reasonably fits with the data they used (standard deviation of 20%), significant variation was observed as shown in Fig. 2.6 for the complete dataset.

Cheuk et al. (2007) conducted a series of large scale tests to simulate pipe penetration and cyclic lateral movement in kaolin (JIP) and West African (WA) clay. Tests were conducted for two pipe sizes ($D=0.283$ m & 0.174 m). The undrained shear strength of clays varied with depth. They compared the test results with two models, namely Verley and Lund (1995) and Murff et al. (1989), as shown in Fig. 2.7.

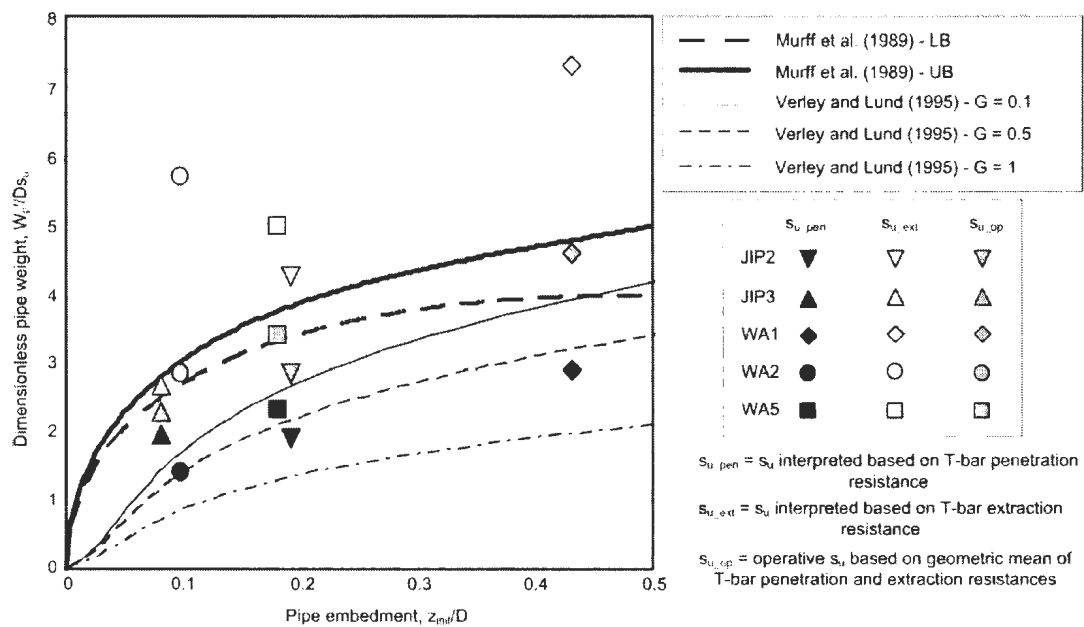


Fig. 2.7 Comparison between various models for pipe vertical penetration (Cheuk et al., 2007).

Dingle et al. (2008) conducted centrifuge tests to understand the mechanism and also to develop solutions for resistance of vertical and lateral pipe movements. A 0.8 m diameter pipe section in prototype scale was pushed into the clay seabed to $0.45D$ at a speed of $0.015D$ per second. The undrained shear strength of the soil varies linearly with depth

with mudline shear strength of 2.3 kPa. Figure 2.8 shows the comparison between centrifuge test results with the empirical model proposed by Murff et al. (2007) and also with the finite element model developed by Merifield et al. (2008). As shown in this figure, the vertical penetration resistance obtained from the centrifuge test is higher than the model predictions. It is noted that vertical penetration resistance is normalized by initial undrained shear strength of clay at the invert of the pipe.

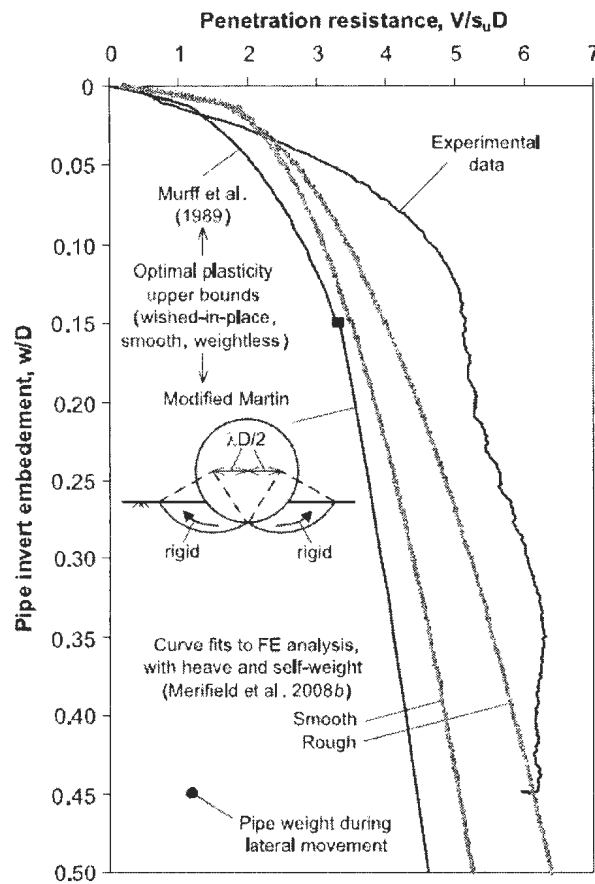


Fig. 2.8 Vertical pipe penetration resistance with embedment (Dingle et al., 2008).

To have better insight, particle image velocity (PIV) techniques were used to capture the soil flow mechanism. Soil deformation was compared with the theoretical upper bound solution and good agreement was achieved. Also, formation of shear zones during pipe vertical penetration was identified (Fig. 2.9) to provide more insight into the soil flow mechanism.

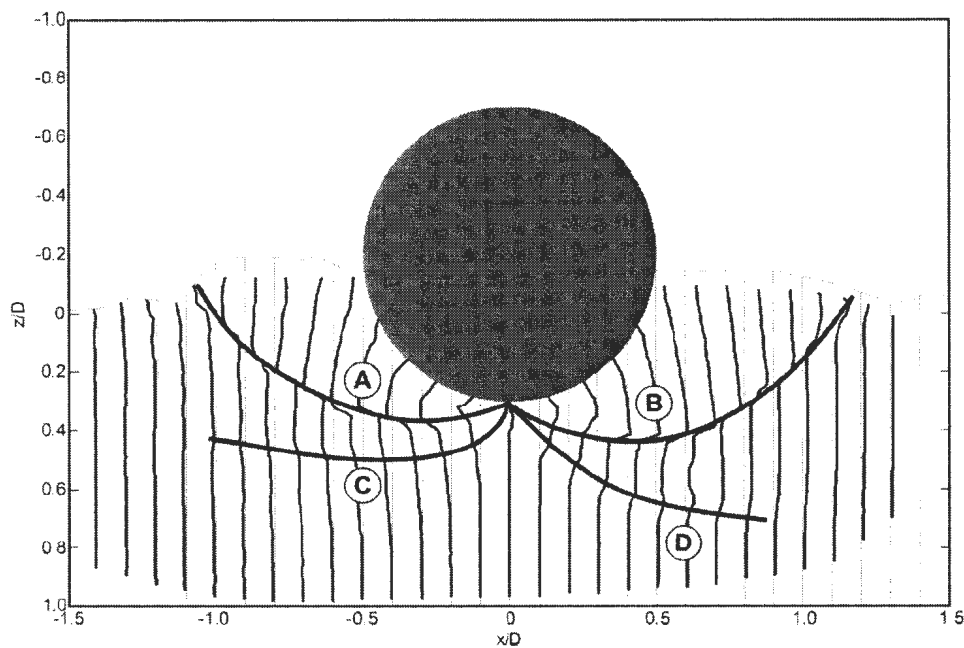


Fig. 2.9 Shear zone formation during vertical penetration (Dingle et al., 2008).

Hu et al. (2009) conducted a number of centrifuge tests for deeper pipe penetration (up to three pipe diameters). The intent of this study was to model cyclic vertical penetration of a steel catenary riser at the touchdown zone. Figure 2.10 shows the penetration resistance during cyclic loading. The numbers 1 to 3 in this figure are the number of cycles. As

2.4.3. Numerical modelling

Pipeline penetration into the seabed is a large deformation process. Most of the available software packages cannot handle such large deformation due to mesh distortion and convergence issue. If the pipe is pushed into the soil, mesh tangling/convergence issues can occur after certain displacement of the pipe. Therefore, in the early stage (e.g. Aubeny et al., 2005, Bransby et al., 2008, Merifield et al., 2008 and Morrow and Bransby, 2010) the analyses were conducted for pre-embedded pipes. That means, the pipe is initially placed at desired depth and displaced further to calculate pipe penetration resistance. This procedure was termed as small strain analysis (Fig. 2.11). With recent technological advancement, issues regarding mesh tangling/convergence are overcome to simulate large deformation problems, which is termed as large strain analysis. For large strain analysis (e.g. Barbosa- Cruz and Randolph, 2005, Bransby et al., 2008, Merifield et al., 2009, Wang et al. 2010, Tho et al., 2011), there are no requirements to put the pipe at different pre-embedment depths and the pipe can penetrate several pipe diameters into the soil. Details of these numerical techniques to calculate the pipe penetration resistance are discussed below in two broad categories: (i) small strain analysis and (ii) large strain analysis.

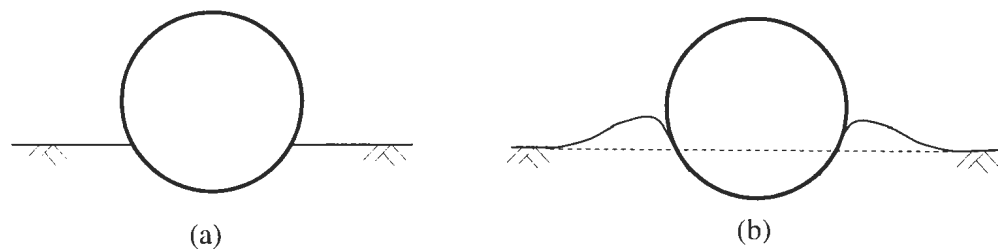


Fig. 2.11 (a) Small strain analysis (WIP pipe) (b) Large strain analysis (PIP pipe).

2.4.3.1 Small strain analysis

Aubeny et al. (2005) performed finite element analyses and compared the results with the extended Randolph and Houlsby (1984) model discussed in Section 2.4.1. Based on their analyses, they proposed analytical models to calculate the pipe penetration resistance. Both uniform and varying undrained shear strength of soil was considered and von Mises yield criterion was adopted. Both smooth and rough pipe/soil interface conditions were considered. Figure 2.12 shows the variation of vertical pipe penetration resistance with pipe penetration depth. In the vertical axis, the normalization was done using the undrained shear strength of clay at the pipe invert. Effects of uniform ($\eta=0$) and triangular ($\eta = \infty$) undrained shear strength profile of clay are discussed where $\eta = kD/s_{um}$ ($k =$ gradient of undrained shear strength of soil, $s_{um} =$ mudline intercept of soil undrained shear strength). Figures 2.12 (a) and (b) show a wide variation in results obtained from FE and closed form solutions for the depth of embedment between one to three pipe diameters for both smooth and rough pipes with uniform soil ($\eta=0$). The difference is less for triangular shear strength profile of clay (Fig. 2.12(c)).

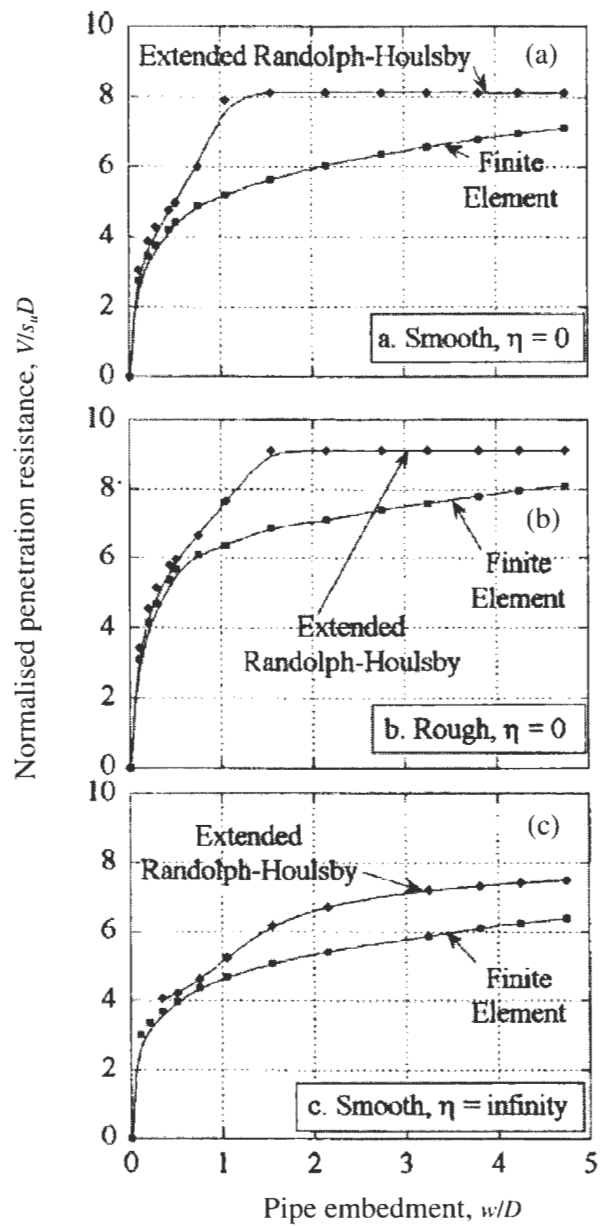


Fig. 2.12 Comparison between numerical and theoretical solution (Aubeny et al., 2005).

Bransby et al. (2008) show the importance the soil berm and soil unit weight on rough pipe penetration resistance from large and small strain finite element analysis. Uniform

undrained shear strength of clay is modelled using Tresca yield criterion. Close agreement (Fig. 2.13) is observed with Murff et al. (1989) but the deviation is higher when compared with Aubeny et al. (2005). Possible reasons might be Aubeny et al. (2005) used the von Mises whereas Bransby et al. (2008) used Tresca yield criterion and mesh distortion for Bransby et al. (2008).

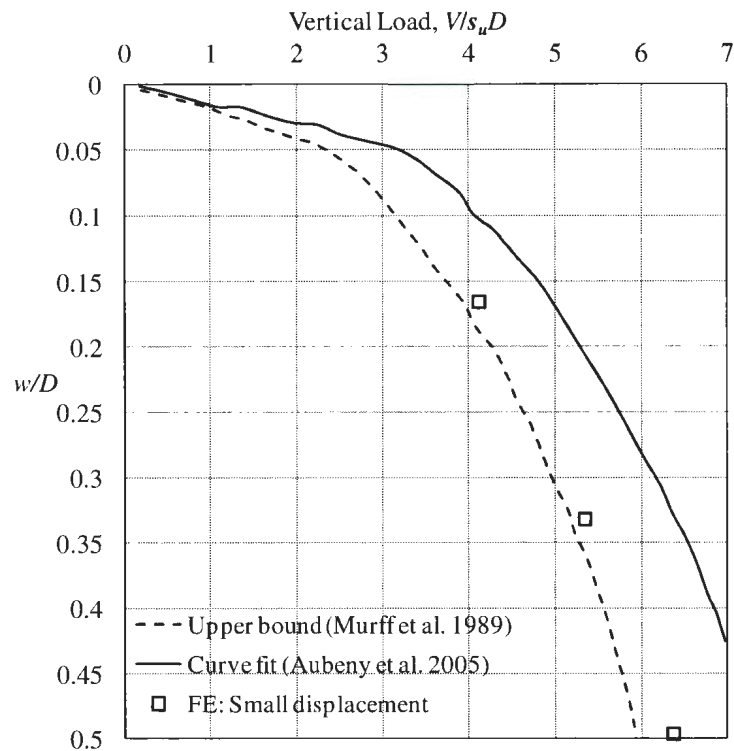


Fig. 2.13 Comparison of vertical penetration resistance (redrawn from Bransby et al., 2008).

Merifield et al. (2008) conducted a series of finite element analyses and compared it with the upper bound theorem (using Martin's mechanism) discussed in Section 2.4.1. Analytical solutions to calculate the pipe vertical resistance were also proposed. Uniform undrained shear strength of soil and the Tresca yield criteria was adopted. Both smooth

and rough pipes were considered for the analysis. The developed finite element model had been compared with theoretical as well as with other numerical models, Fig. 2.14. For smooth pipe, variations were observed with theoretical plasticity solutions whereas for rough pipe closer agreements are observed. In spite of different yield criteria used in FE analyses (Aubeny et al., 2005 used von Mises whereas Merifield et al., 2008 used Tresca) close agreement was observed for both smooth and rough pipe as shown in Fig.2.14.

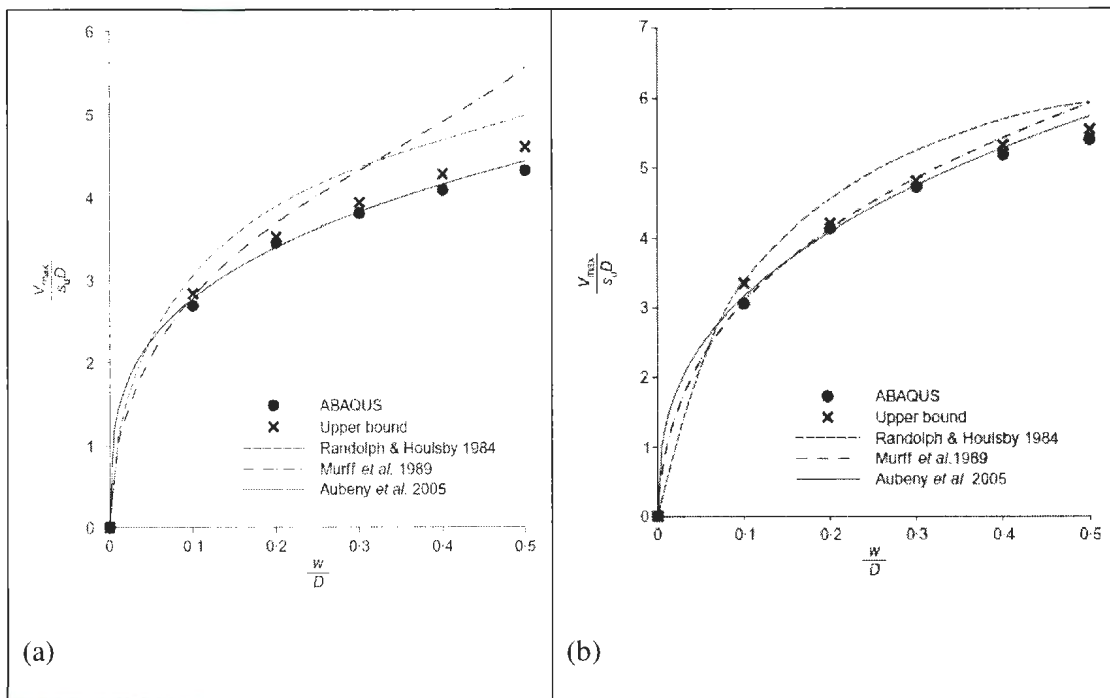


Fig. 2.14 Comparison between numerical and theoretical solution (Merifield et al., 2008) (a) Smooth pipe (b) Rough pipe.

Morrow and Bransby (2010) showed that vertical pipe penetration resistance depends on the soil undrained shear strength gradient (e.g. Fig. 2.15, b, c, d) and shear strength crust

(Fig. 2.15, e). Finite difference technique (FLAC 6.0) was used for the investigation and the Tresca yield criterion was adopted. Four different soil undrained shear strength profiles (Fig. 2.15) were adopted in the analysis. Undrained shear strength of soil at mudline and pipe invert was defined as s_{um} and s_{uzp} respectively. Pipe penetration resistance from developed numerical models were compared with Aubeny et al. (2005) and Merifield et al. (2008) (Fig.2.16). Pipe penetration resistances matches well with the literature for uniform soil undrained shear strength ($s_{um}/s_{uzp} = 1.0$). But significant variation was observed for soil with varying undrained shear strength as shown in Fig. 2.16.

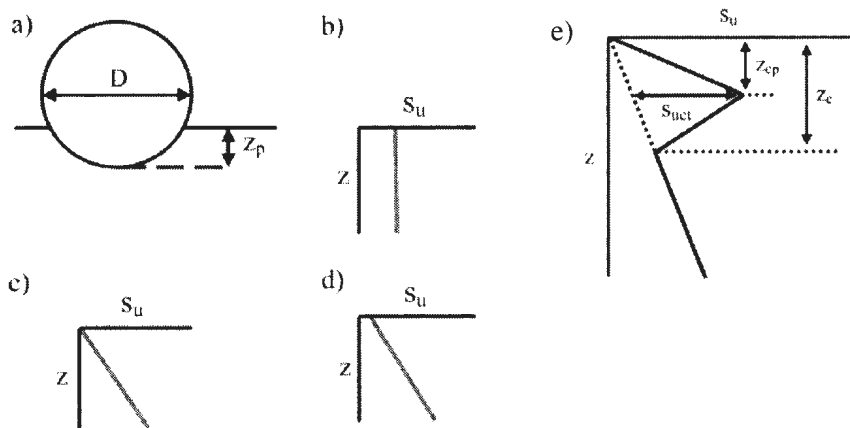


Fig. 2.15 Typical shear strength profile (Morrow and Bransby, 2010).

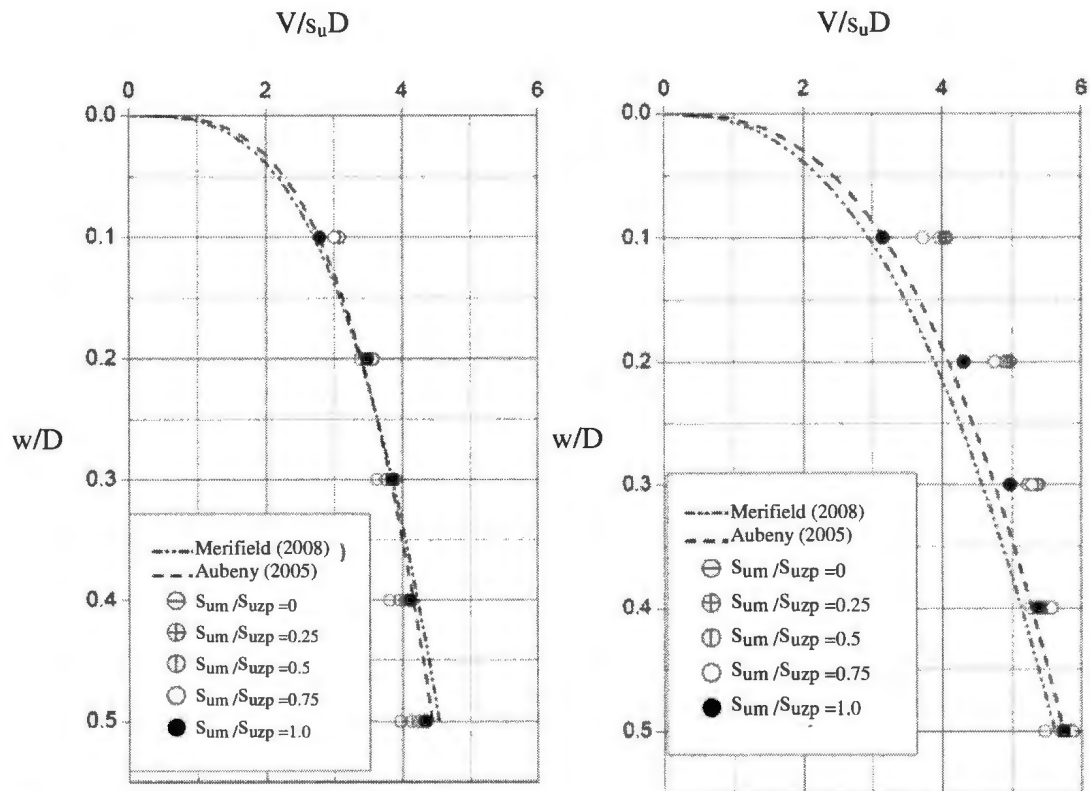


Fig. 2.16 Comparison of pipe penetration resistance (a) Smooth (b) Rough (Morrow and Bransby, 2010).

2.4.3.1 Large strain analysis

As pipe penetration is a large deformation phenomenon the large strain FE analysis might be a better option to simulate this behaviour. Barbosa-Cruz and Randolph (2005) developed a series of numerical models to calculate the pipe vertical bearing capacity factor (explained later) at different penetration depths using “remeshing and interpolation techniques with small strain (RITSS) ” technique with Arbitrary Lagrangian Eulerian (ALE) method to capture large strain behaviour. The details of ALE with RITSS

technique is discussed later in this section. They present the results in terms of pipe vertical bearing capacity factor $N_c (=V/D's_{u,D'max})$ where V was the pipe reaction force, D' was the pipe contact width and $s_{u,D'max}$ was soil undrained shear strength at maximum pipe contact width. Both uniform (homogeneous) undrained soil shear strength and varied (non homogeneous) soil undrained shear strength were considered in the analysis. Figure 2.17 show the bearing capacity factor obtained from the analyses with normalised pipe embedment. Nominal bearing capacity factor (Nominal $N_c = P'/s_{u,D'max}D$ where P' was the net pipe force allowing buoyancy effects, $s_{u,D'max}$ undrained soil shear strength at maximum contact width) was also increased as the pipe penetrates further (Fig. 2.18). Barbosa-Cruz and Randolph (2005) used large strain analysis and the limitations of small strain analysis were overcome. However, strain rate and softening effects on clay shear strength were not incorporated into the analysis.

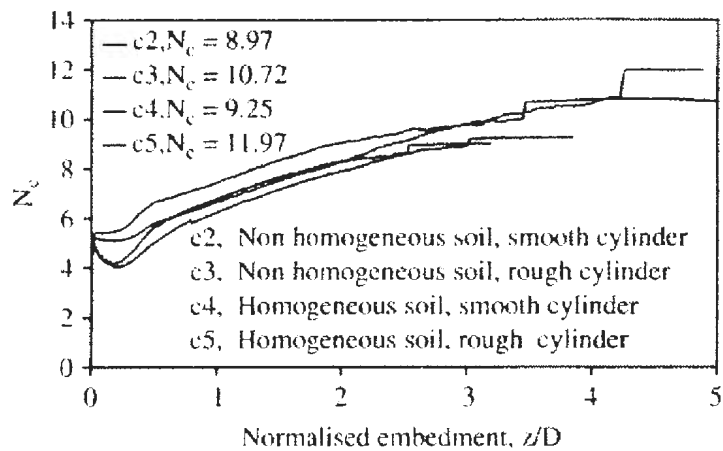


Fig. 2.17 Variation of bearing capacity factor (Barbosa-Cruz and Randolph, 2005).

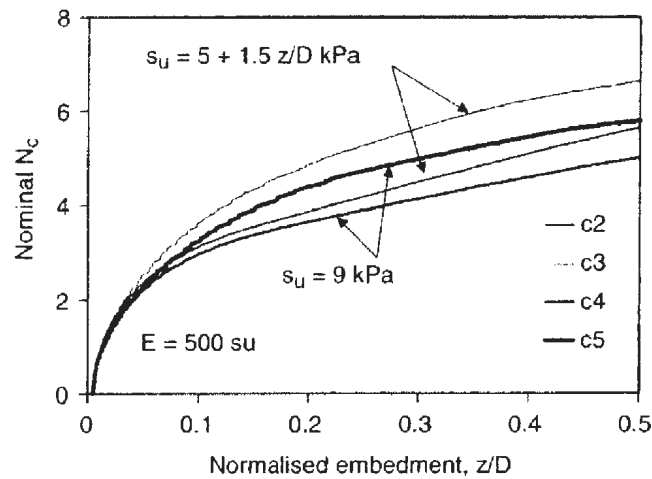


Fig. 2.18 Variation of nominal bearing capacity factor (Barbosa-Cruz and Randolph, 2005).

Bransby et al. (2008) conducted both small and large strain analysis to simulate pipe vertical penetration into seabed with uniform undrained soil shear strength. A rough pipe diameter of 0.3 m was used and the Tresca yield criterion was adopted for the analysis. The pipe was pre-embedded at the same depth for both small and large strain analysis and penetrated further to compare the results from two types of analyses as shown in Fig. 2.19. One of the key findings is that in small-strain analyses the vertical resistance is almost constant after $w \approx 0.15$ m ($w/D \approx 0.5$), however the large strain clearly shows the effects of the berm and the resistance increases with vertical penetration.

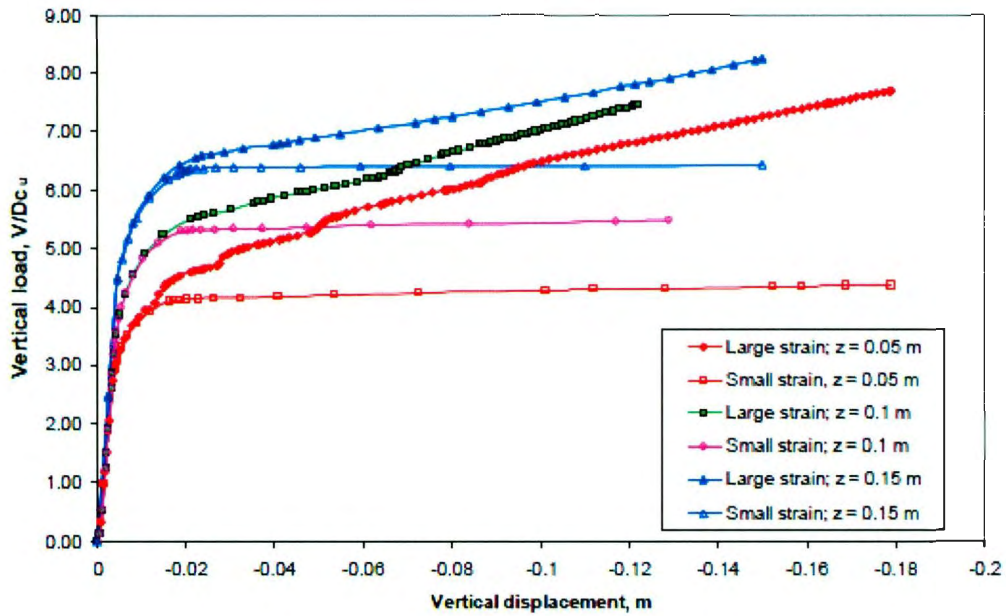


Fig. 2.19 Comparison between large strain and small strain (Bransby et al., 2008).

Merifield et al. (2009) conducted a series of numerical analysis to calculate the effects of the soil berm during pipe penetration both from theoretical and numerical investigations. Analytical solutions were also provided to calculate the pipe penetration resistance. Using conventional bearing capacity solutions for strip footings, a bearing capacity solution was developed first for WIP pipes and extended it to PIP pipes. Using the soil bearing capacity theorem, the developed equation for pipe vertical resistance (V) was:

$$\frac{V}{s_u D} = N_{cv} + N_{swv} \frac{\gamma' w}{s_u} \quad (2.3)$$

where N_{cv} and N_{swv} are two factors and the proposed equations for two factors were

$$N_{cv} = a \left(\frac{w}{D} \right)^b$$

$$N_{swv} = \frac{0.67}{\hat{w}} \left[\frac{\sin^{-1}(\sqrt{4\hat{w}(1-\hat{w})})}{2} - (1-2\hat{w})\sqrt{\hat{w}(1-\hat{w})} \right]$$

Where N_{cv} is the vertical bearing capacity factor, N_{swv} is the self-weight factor, D is the pipe diameter, w is the pipe penetration depth from mudline, a and b are the fitting coefficient for limiting conditions of roughness and $\hat{w} = \frac{w}{D}$. Values of a (5.3-7.1) and b (0.25-0.33) were calculated using large strain modelling through finite element analysis. The arbitrary Eulerian Lagrangian (ALE) technique was adopted for the analysis. Uniform undrained shear strength of soil with Tresca yield criterion was also used in the analysis.

In ALE, elements near the pipeline become distorted after certain displacement and computational issues can occur. Therefore, this technique can only partially simulate large strain behaviour. However, mesh tangling/convergence issues can be overcome using RITSS technique with ALE. Wang et al. (2010) conducted a series of numerical analysis to simulate pipe penetration using “remeshing and interpolation techniques with small strain” (RITSS) technique with ALE to capture large strain behaviour. Undrained shear strength of soil was varied along with depth and a Tresca yield criterion was adopted. A rate dependent softening soil model was incorporated in the analysis performed for both smooth and rough soil/pipe interface conditions. Close agreement was observed with centrifuge test results (Dingle et al., 2008) as shown in Fig. 2.20. In horizontal axis, normalization was done by using undrained shear strength of soil at pipe invert. Wang et al. (2010) modelled the kaolin clay as a rate dependent and strain

softening material. A remoulding sensitivity of 3.2 was used for kaolin clay to match the centrifuge test results although some authors recommended slightly different values of sensitivity (e.g. Sensitivity=2.0 - 2.8 Hossain et al., 2009).

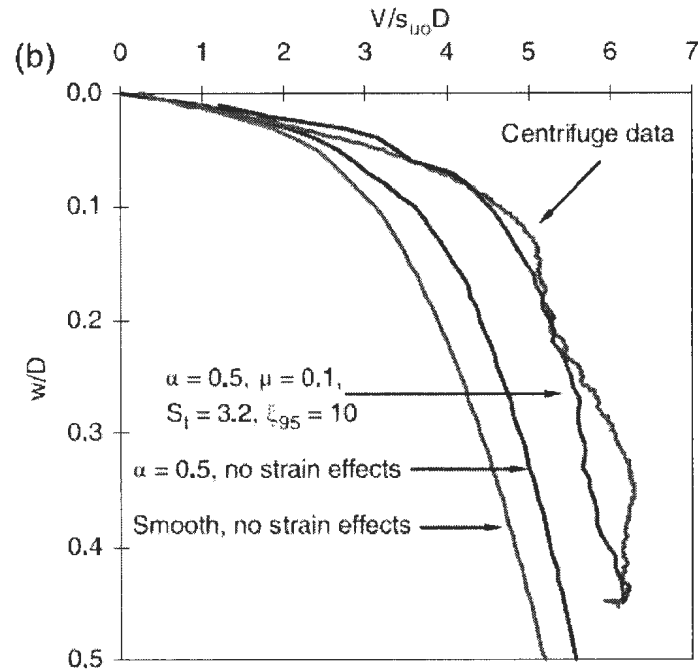


Fig. 2.20 Comparison between FE analyses and centrifuge test results (Wang et al., 2010).

Other than ALE with RITSS, Coupled Eulerian Lagrangian (CEL) technique has the capabilities to model large deformation behaviour. Using CEL, Tho et al. (2011) modelled pipe penetration to have insight into the deep cavity flow mechanism during pipe penetration. With CEL, it is possible to model pipe penetration more than several pipe diameters without mesh tangling or convergence issues. The mesh is fixed in this

case and material can flow within the mesh. Therefore, the numerical issues of mesh tangling or convergence can be avoided. Tho et al. (2011) developed the finite element model for uniform undrained shear strength of soil and the Tresca yield criterion was used. Analyses were conducted only for smooth soil/pipe interfaces. The calculated vertical bearing capacity factor (N_c or N_{cv} , discussed in Section 2.4.3.) were compared with other available solutions in the literature and shown in Fig. 2.21. Note that, strain rate and strain softening effects on shear strength were not considered in their analyses.

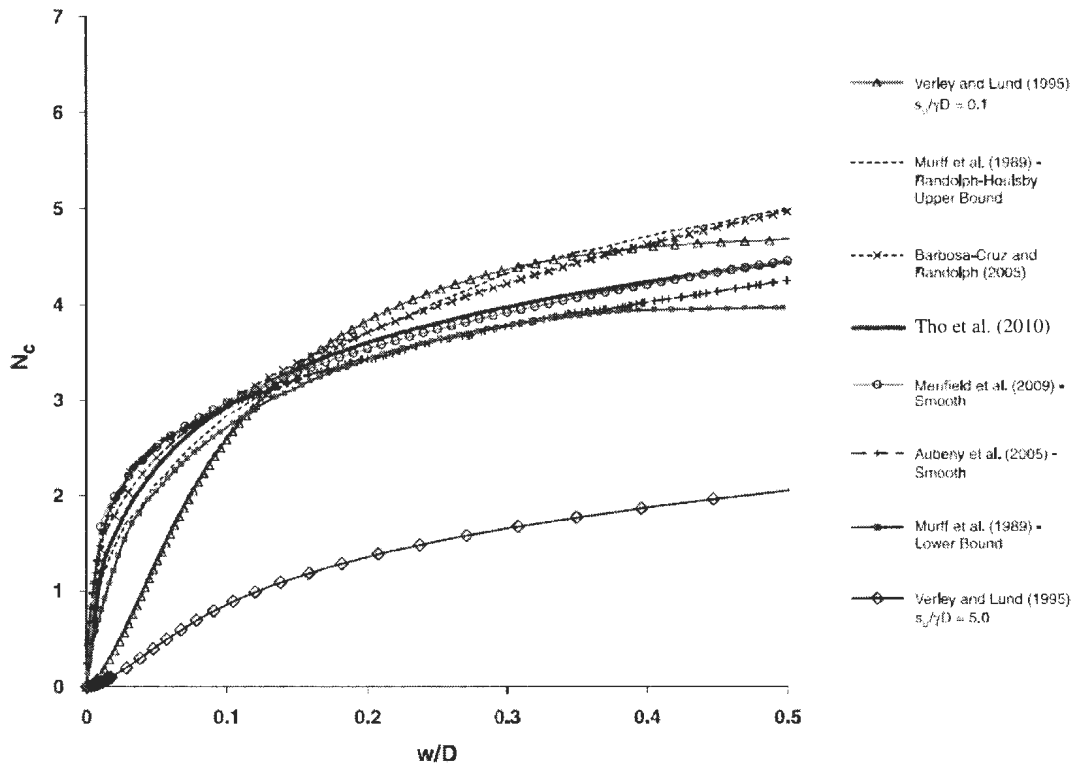


Fig. 2.21 Comparison of vertical bearing capacity factor (Tho et al., 2010).

Chatterjee et al. (2012a) conducted a number of finite element investigations again using ALE with RITSS approach and presented a new concept of estimating pipe vertical penetration resistance for clay. Undrained shear strength of soil was varied with depth and a rate dependent softening soil model was adopted. To define the rate dependent softening soil model, the developed equation of Einav and Randolph (2005) was used (Eq. 2.4). Finite element results were compare with the centrifuge test results of Dingle et al. (2008) as shown in Fig.2.22. Analytical solutions were proposed to calculate the pipe penetration resistance using an equivalent undrained shear strength of soil. The equivalent soil undrained shear strength was calculated using a strain rate ($\dot{\gamma}$) of $0.7 v' / D$ (v' = pipe velocity and D = pipe diameter) and an accumulated strain (ξ) of $0.8 w/D$ (w = pipe penetration depth) in Einav and Randolph's equation (Eq. 2.4). It was observed from finite element investigations that for different values of parameters (Eq. 2.4), pipe resistance varied widely and normalised pipe penetration resistance with equivalent undrained shear strength brought them into a narrow range as shown in Fig. 2.23.

$$s_u = \left[1 + \mu \log \left\{ \frac{\max(\dot{\gamma}, \dot{\gamma}_{ref})}{\dot{\gamma}_{ref}} \right\} \right] \left[\delta_{rem} + (1 - \delta_{rem}) e^{-3\xi/\xi_0} \right] s_{u0} \quad (2.4)$$

In summary, several numerical techniques have been developed in the past to calculate vertical pipe penetration resistance in clay varying from small to large strain finite element analyses with von Mises or Tresca yield criteria. Analysis was performed for uniform or non-uniform undrained shear strength profiles of the seabed. Some of the analyses considered the effects of strain rate and strain softening effects. The progressive

developments of numerical procedures for vertical pipe penetration are summarized in Table 2.2 for ease of comparison.

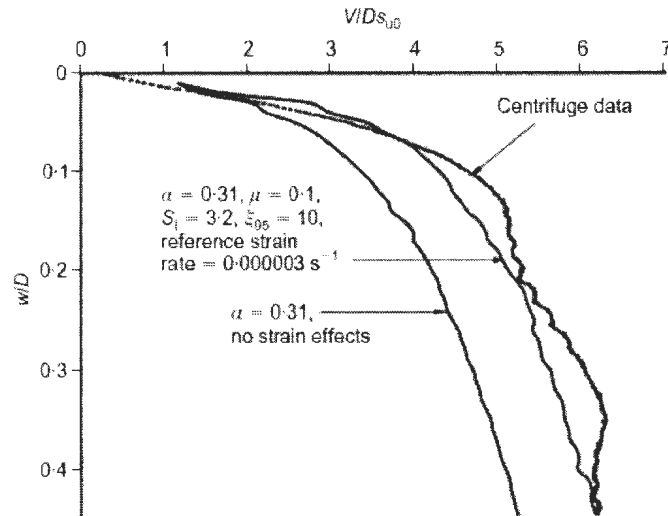


Fig. 2.22 Comparison between finite element model and centrifuge test (Chatterjee et al., 2012a).

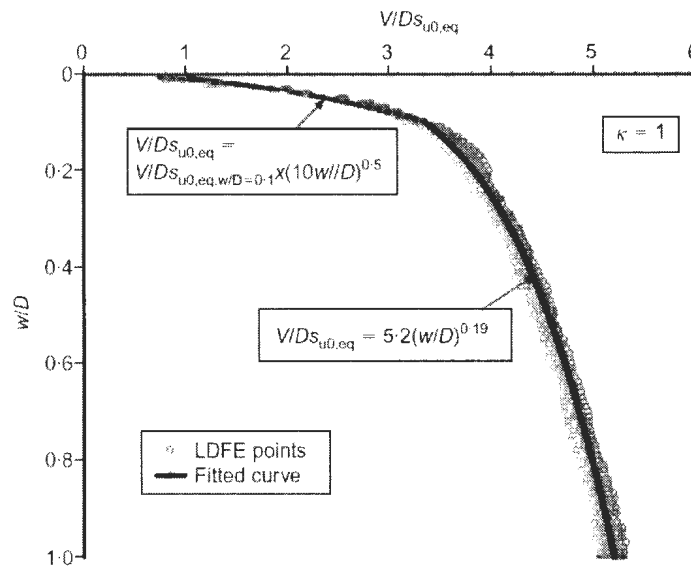


Fig. 2.23 Pipe vertical penetration with depth (Chatterjee et al., 2012a).

Table 2.2 Progressive development of numerical analysis in pipe penetration

Authors	Numerical Technique	Notes
Aubeny et al.(2005)	Small strain analysis using ABAQUS (2000)	von Mises soil for both uniform and increasing strength.
Barbosa-Cruz and Randolph (2005)	Arbitrary Eulerian Lagrangian (ALE) with RITSS technique	Tresca soil with uniform strength and increasing strength
Bransby et al.(2008)	Small strain analysis using ABAQUS	Tresca soil with uniform strength
Merifield et al.(2008)	Small strain analysis using ABAQUS	Tresca soil with uniform strength
Merifield et al.(2009)	Arbitrary Eulerian Lagrangian (ALE) using ABAQUS (2004)	Tresca soil with uniform strength
Morrow, D.R. and Bransby, M.F. (2010)	Finite difference technique using FLAC 6.0 (2008)	Tresca soil with increasing strength
Wang et al. (2010)	Arbitrary Eulerian Lagrangian (ALE) with RITSS technique using ABAQUS 6.5 (2006)	Tresca soil with increasing strength and strain softening and rate effects.
Tho et al.(2011)	Eulerian Technique using ABAQUS 6.8 (2008)	Tresca soil with uniform strength
Chatterjee et al. (2012a)	Arbitrary Eulerian Lagrangian (ALE) with RITSS technique using ABAQUS (2007)	Tresca soil with increasing strength and strain softening and rate effects.

2.5. Development of Lateral Pipe Resistance Theorem

Partially embedded pipelines in deep sea can move laterally up to 10 to 20 pipe diameters due to high temperature and pressure during its operational period (Bruton et al., 2006). However, still today, the guidelines for pipeline design considering such large amplitude lateral displacements are not well-developed. Literature indicates that the controlled lateral buckling is the best available mitigation option for as-laid pipeline (Bruton et al., 2006). For controlled lateral buckling, major uncertainties relate to the in pipe feed calculation. If the amount of pipe feed is less than that required, the pipeline can fail due to developed bending stresses. Accurate estimates of pipeline lateral movement is required in pipeline feed calculations and the expected mode shape. In other word, pipe lateral resistance plays a vital role in pipe feed calculation.

During lateral travel, the resultant direction of as-laid pipe can be either downward or towards the mudline (vertical direction of movement). Pipeline lateral travel direction mainly depends on the soil undrained shear strength, soil unit weight and pipe applied vertical load (vertical load on pipe due to hydrocarbon and pipe self-weight). Based on pipe lateral travel direction, the pipe can be defined as light or heavy. Wang et al. (2010) defined light and heavy pipe in terms of over-penetration ratio (R). Over-penetration ratio (R) is the ratio between maximum vertical load that is required for further vertical penetration and applied vertical load. When the value of R is less than 2, pipe can be defined as heavy pipe (Wang et al., 2010.) and vice versa. However, Cardoso et al. (2010)

defined the pipes more elaborately by a ratio S where $S = \frac{w'}{Ds_u}$ and w' means submerged

pipe unit weight. The details are provided below:

Table 2.3 Pipe Classification (Based on operative load)

	Range
Extra Light Pipe	$S < 0.5$
Light Pipe	$0.5 < S < 1.0$
Heavy Pipe	$1.0 < S < 2.5$
Extra Heavy Pipe	$S > 2.5$

For heavy pipe, pipe lateral resistance is gradually increased with pipe lateral movement. On the other hand, for light pipe, lateral pipe resistance increased at first (known as lateral breakout resistance), then decreases gradually and reaches a constant value known as residual resistance (Fig. 2.24). From observed pipe behaviour, it can be said that accurate assessment of lateral pipe resistance for light pipe is more crucial (as pipe lateral resistance is decreasing) than heavy pipe and therefore the present thesis is limited to investigating the light pipe only.

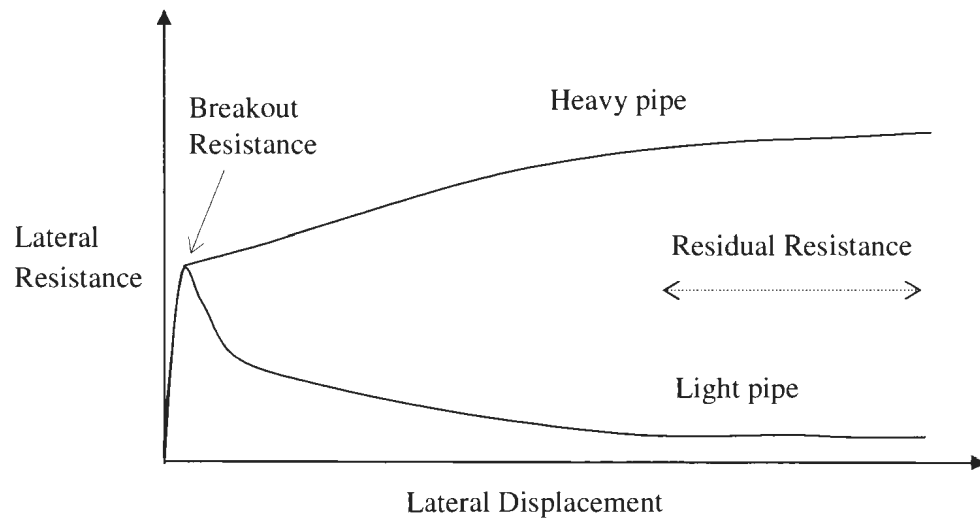


Fig. 2.24 Typical behaviour of light and heavy pipe.

Lateral breakout resistance of pipelines is an important issue because it governs the initiation of pipe lateral buckling (Wagner et al., 1989; Verley and Lund, 1995). Pipe breakout resistance is observed to occur within pipe lateral displacements of $0.5D$ whereas pipe residual lateral resistance occurs within 3 to $4D$ (Bruton et al., 2006). For lateral pipe movement, several empirical expressions had been developed using theoretical works (Merifield et al., 2008, 2009; Randolph and White, 2008), model tests database (Wagner et al., 1989; Verley and Lund, 1995; Bruton et al., 2006; Cheuk et al., 2007; Dingle et al., 2008; White and Dingle, 2011) and numerical works (Merifield et al., 2008; Wang et al., 2010.). For convenience, light pipe lateral travel is described in three separate sections: (i) theoretical, (ii) physical and (iii) numerical modelling. Each section is again divided into two sub-sections: (a) breakout resistance and (b) residual resistance.

2.5.1 Theoretical modelling of pipe lateral resistance

Theoretical modelling of pipe lateral resistance includes Coulombs frictional law, classical metal plasticity theorem or Greens theorem (1954) and solutions of upper bound theorem using Martins mechanism (2006).

2.5.1.1 Lateral breakout resistance

Conventional pipeline design practice includes spring slider elements at an interval along the pipelines to simulate the lateral resistance. A spring slider element simulates linear elastic perfectly plastic response as shown in Fig. 2.25. The ratio of horizontal to vertical force (H/V) increases linearly with lateral displacement and become maximum (H_{\max}/V) at breakout point, which is termed as “friction factor (μ_f)”.

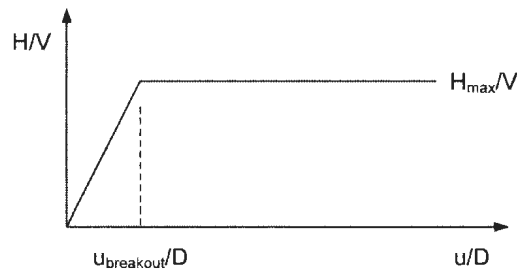


Fig. 2.25 Bi-linear model (White and Cheuk, 2008).

The value of μ_f of 0.2 to 0.8 is recommended for pipeline design (White and Cheuk, 2008). However, Coulomb’s frictional model assumes that the support is rigid and the

pipe slides parallel to the surface of the support. But, in practice, soil (support) cannot be rigid. Therefore, Coulomb's model needs to be modified.

Other than Coulomb's friction model or spring slider elements, Greens theory (Green, 1954) was used to develop theoretical solutions for pipe lateral resistance with some modifications (ISO, 2003). Combination of shear and normal loads are used to define the failure envelope. To develop the failure envelop using Green`s theory, a pipe contact area is required. Although pipes have curved surface, it can be modelled by approximating as a surface strip foundations of width D' (Fig. 2.26). During pipe lateral movement, penetration of pipe will occur until the load path reaches to the corner of the failure surface (Fig. 2.27). This point is known as parallel point. For uniform soil strength, the ratio of $\frac{H_{max}}{V}$ is 0.39 at parallel point but for varying undrained shear strength of soil this value is decreasing up to 0.15 (Gourvenec and Randolph, 2003).

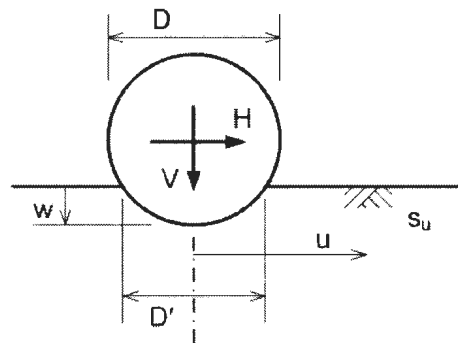


Fig. 2.26 Effective embedment parameters (White and Cheuk, 2008).

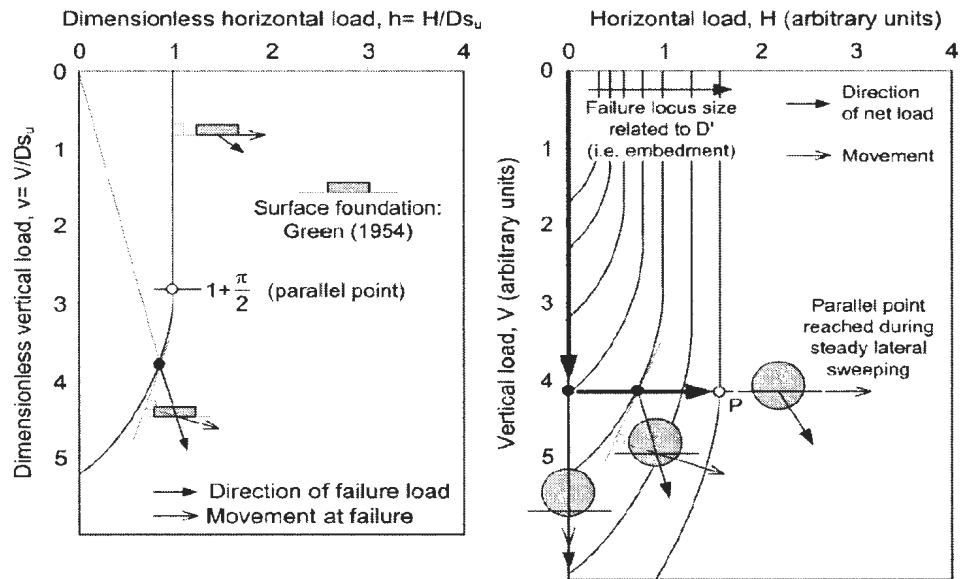


Fig. 2.27 Theoretical failure loci for surface foundations and pipes (White and Cheuk, 2008).

From experimental and numerical investigation, Lyons (1973) showed that the Coulomb friction model is not valid for pipe lateral resistance measurement. Using the concept of wedge indenter and energy equilibrium principle, Karal (1977) calculated pipe horizontal resistance. But wedge indenter is reasonable only for small pipe movements. Later, Cheuk et al. (2007) proposed upper bound theorem where failure surface was assumed to occur along a circular slip surface (Fig. 2.28). Uniform undrained shear strength of soil was adopted for analysis. It was assumed the soil undrained shear strength was mobilised along the pipe slip surface. Maintaining conservation of volume, two semicircular soil berms were also assumed to form around the pipe after pipe vertical penetration. The slip surface passes through the berm at pipe rear end. Therefore, this mechanism is able to

simulate full soil/pipe adhesion i.e. suction at pipe rear end can be simulated. By using a moment equilibrium equation, the required horizontal force for lateral pipe movement can be expressed as:

$$F_h = \frac{S_u l r_0 + w'_{s1} x_{s1} + w'_{s2} x_{s2} - w'_p x_0}{y_0} \quad (2.5)$$

where, F_h = Horizontal force per unit length; l = Length of slip surface; r_0 = Radius of the slip circle; w'_{s1} and w'_{s2} = Effective weights of the soil masses per unit length; x_{s1} and x_{s2} = Moment arm of w'_{s1} and w'_{s2} respectively and w'_p = Effective pipe weight per unit length.

Figure 2.29 compares observed full-scale model test data for first lateral sweep and developed equation.

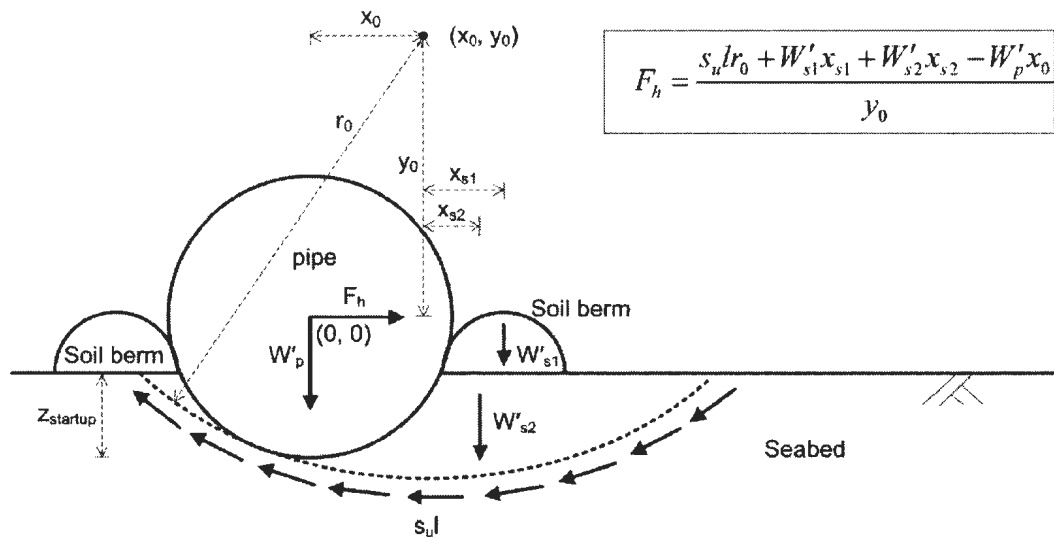


Fig. 2.28 Geometry of upper bound solution for breakout resistance (Cheuk et al., 2007).

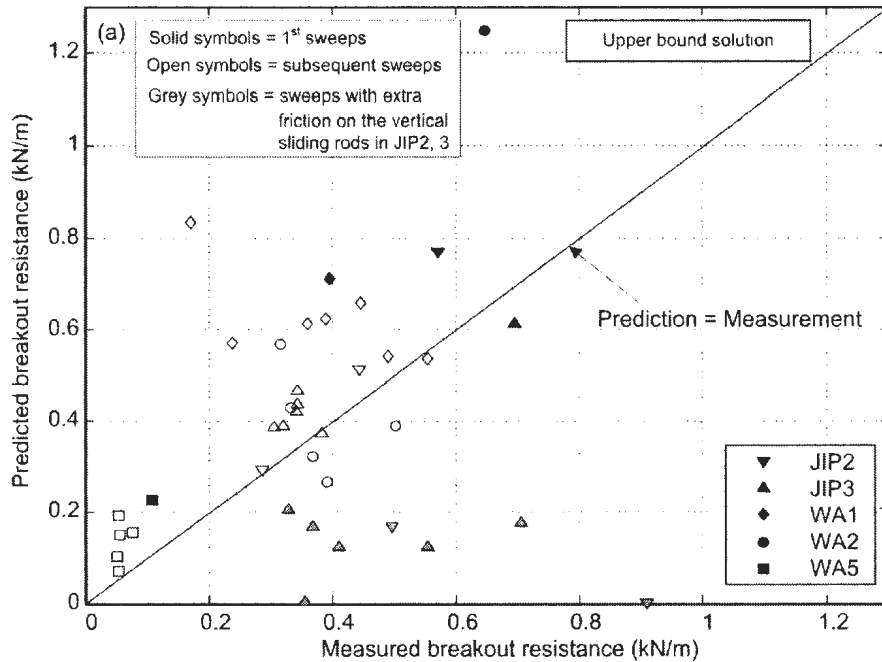


Fig. 2.29 Prediction of breakout resistance using upper bound solution (Cheuk et al., 2007).

Upper bound solution largely depends on the adopted soil flow mechanism. Using Martin's mechanism (Fig. 2.30), a theoretical yield envelope had been proposed by Merifield et al. (2008) (Fig. 2.31). Martin's mechanism consists of two parts. During pipe lateral breakout, a generalised Martin's mechanism was adopted in front of pipe (Fig. 2.30). Generalisation occurs as center of rotation (S) cannot maintain its position on pipe diameter where pipe diameter should be perpendicular to the direction of motion. Second part consists of a rigid portion where the center of rotation was Q . It can maintain its position on the pipe diameter by keeping pipe motion direction perpendicular (Fig. 2.30). It was assumed that the pipe itself does not rotate. For a range of pipe embedment depths

($0.1D$ to $0.5D$), the pipe was moved at different angles (δ , Fig. 2.30) to develop the yield envelope. The developed theoretical model was compared with numerical analysis and a close agreement was observed (Fig. 2.31). Details of the numerical analysis are discussed in Section 2.5.3.1.1. Both smooth and rough pipes were considered for the theoretical analysis with uniform soil undrained shear strength.

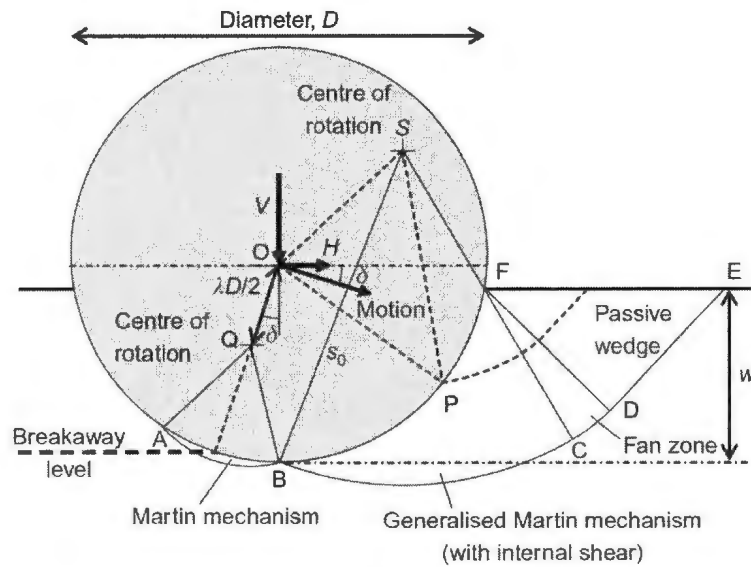


Fig. 2.30 Upper bound mechanism (Merifield et al., 2008).

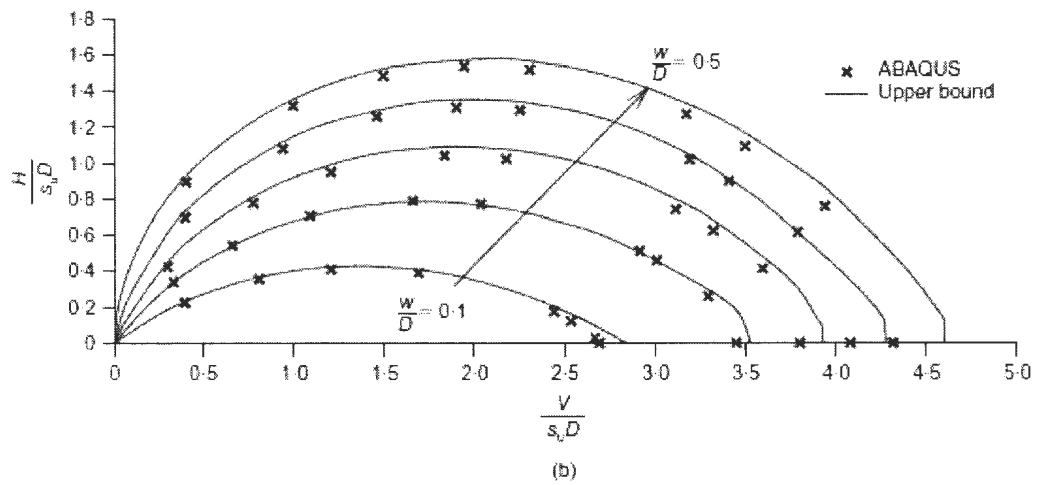
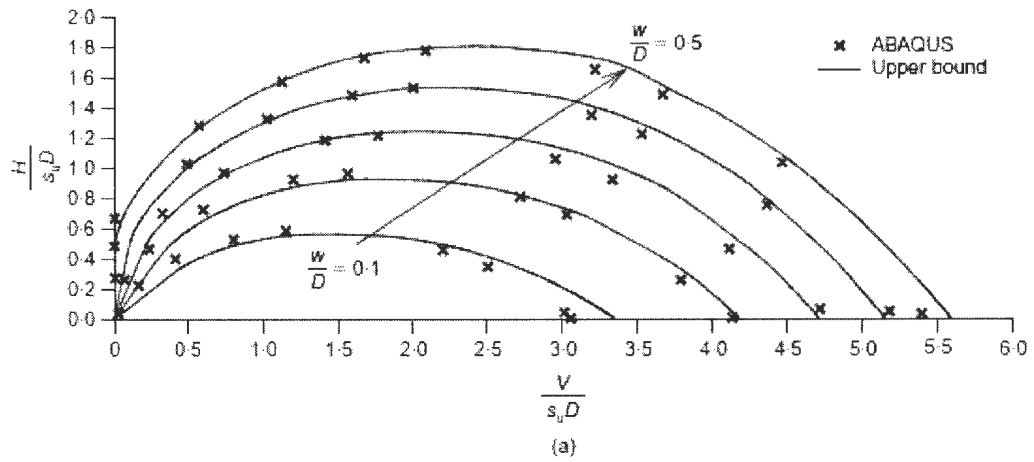


Fig. 2.31 Yield envelope at different embedment (a) Smooth pipe (b) Rough pipe (Merifield et al., 2008).

Merifield et al. (2008) considered uniform undrained shear strength of soil to develop the theoretical yield envelope. Using the upper bound mechanism (Martin's mechanism), Randolph and White (2008) developed a theoretical yield envelope for varying undrained shear strength of soil. For different pipe embedments ($0.1D$ to $0.5D$) and interface

conditions (smooth and rough), theoretical yield envelopes were developed as shown in Fig. 2.32.

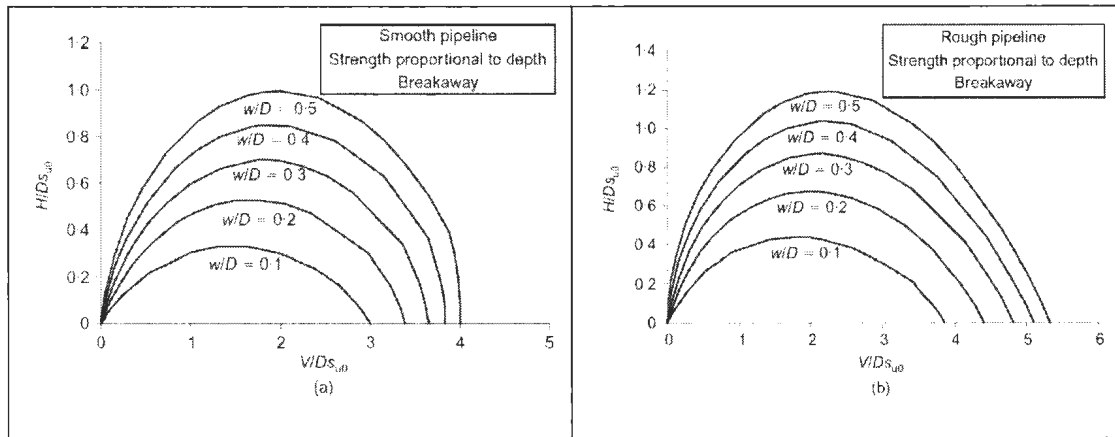


Fig. 2.32 Theoretical yield envelopes for soil shear strength proportional to depth (a) Smooth pipe (b) Rough pipe. (Randolph and White, 2008).

2.5.1.2 Residual lateral resistance

Limited theoretical research is available for estimation of pipe lateral residual resistance. Cheuk et al. (2007) developed theoretical analysis for steady lateral pipe motion (i.e. pipe will not displace in upward or downward direction during horizontal movement) and it can shed light into the theoretical development of pipe lateral residual resistance. Cheuk et al. (2007) proposed an upper bound solution of measuring pipe lateral residual resistance and a new mechanism as shown in Fig. 2.33. Soil deformation in front of pipe was ignored and uniform soil undrained shear strength was adopted for the analysis.

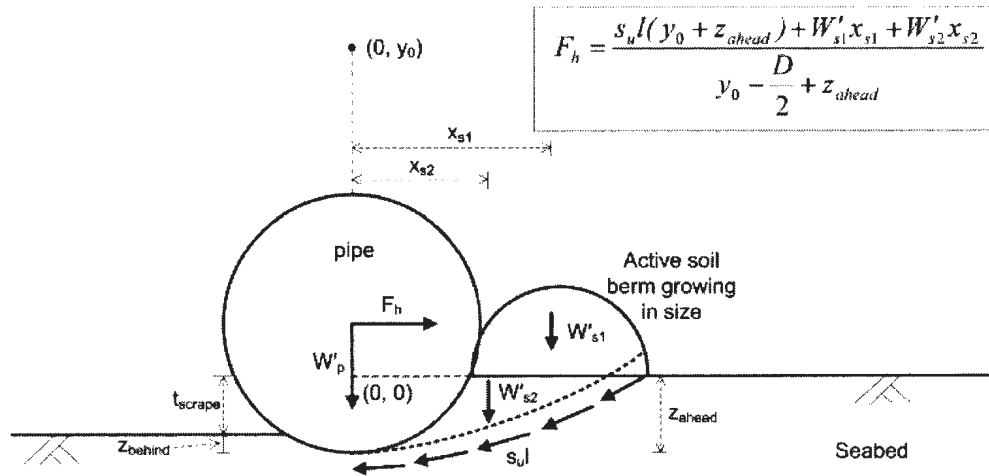


Fig. 2.33 Upper bound geometry solution for lateral resistance (Cheuk et al., 2007).

2.5.2 Physical modelling of pipe lateral resistance

Small to large scale tests (Lyons, 1973, SINTEF 1986a, 1986b, Cheuk et al., 2007) and centrifuge modelling (Dingle et al., 2008, White and Dingle, 2011) were used to model pipe lateral resistance. A number of empirical equations were proposed based on the available experimental database. In order to present these works systematically the physical modelling is also discussed in two broad parts: pipe lateral breakout resistance and residual resistance.

2.5.2.1 Pipe lateral breakout resistance

Lyons (1973) had conducted small and large scale modelling to calculate pipe lateral resistance for both clay and sand. Figure 2.34 shows the typical arrangement for the tests.

For clay, the experiment was performed using an undrained shear strength of 45 psf (2.1 kN/m²), bare and concrete coated pipelines with submerged pipe weights of 10 to 85 lb/ft. Experimental results showed that Coulombs friction law cannot be used to simulate the pipe lateral breakout resistance on clay since a co-efficient of friction was not constant. The co-efficient of friction increased with submerged unit weight and decreased with increasing pipe diameter and higher for bare pipe than concrete coated pipe (Fig. 2.35 (a)). Figure. 2.35 (b) shows that the co-efficient of friction increases as the pipe weight increased (i.e. pipe penetration increased) during hydrostatic testing (performed normally for leak detection).

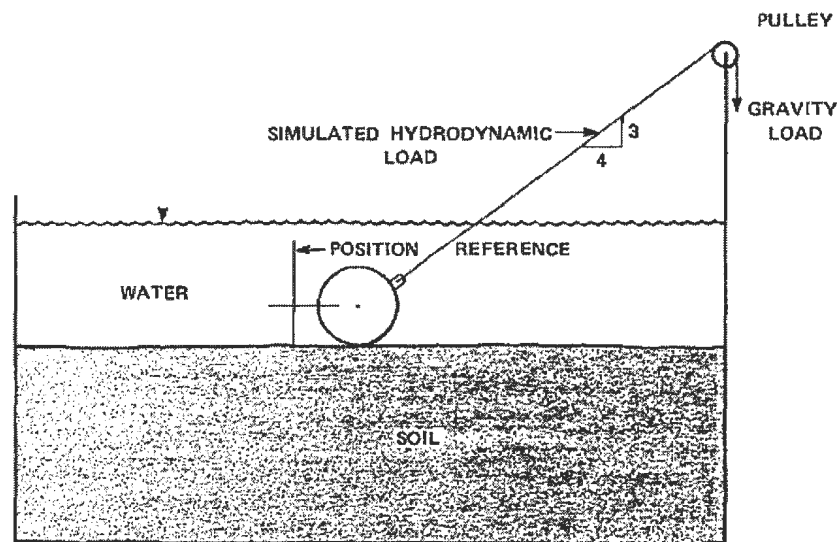


Fig. 2.34 Schematic diagram of test (Lyons, 1973).

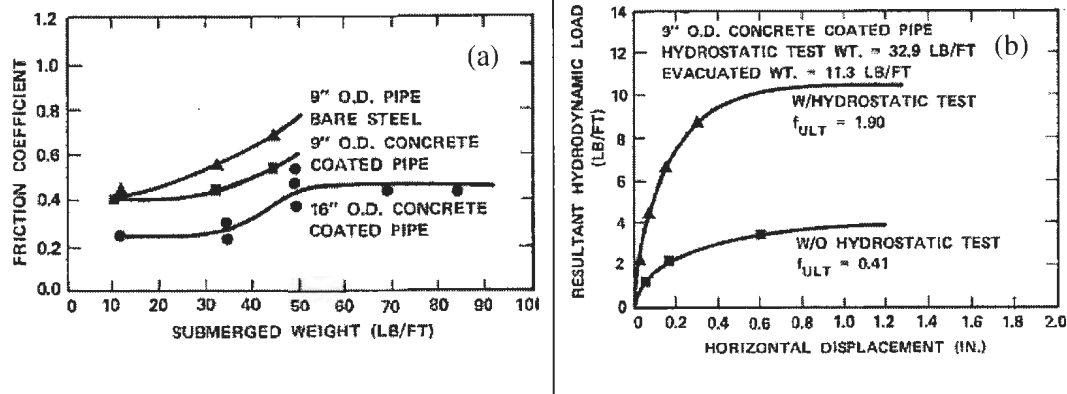


Fig. 2.35 Variation of co-efficient of friction (a) with submerged weight, soil/pipe interface, pipe diameter (b) with hydrostatic test and without hydrostatic test (Lyons, 1973).

Wagner et al. (1987) modified Coulomb's frictional model based on data from 200 tests with five different soil conditions (silty fine sand, loose sand, dense sand, soft clay with undrained shear strength of 1kPa and stiff clay with undrained shear strength of 70kPa) in PIPESTAB project. Using large scale model test program, breakout resistance was calculated for no cyclic loading (simple breakout), after small cyclic loading and after large cyclic loading with different pipe diameters and unit weights. Based on the test data, different analytical models for clay and sand were proposed. Figure 2.36 compares the test results with an analytical solution (for clay only) and reasonable agreement was shown.

American Gas Association/ Pipeline Research Committee (1992) also proposed models for clay to calculate pipe lateral resistance. However, Verley and Lund (1995) show that

PIPESTAB and AGA/PRC models give very different lateral resistance for a given initial embedment. Using the data from physical modelling (SINTEF 1986a, 1986b, 1987; Morris et al. 1988; TAMU 1992), Verley and Lund (1995) combined all the test data in a generalised framework. By modifying Coulomb's equation and

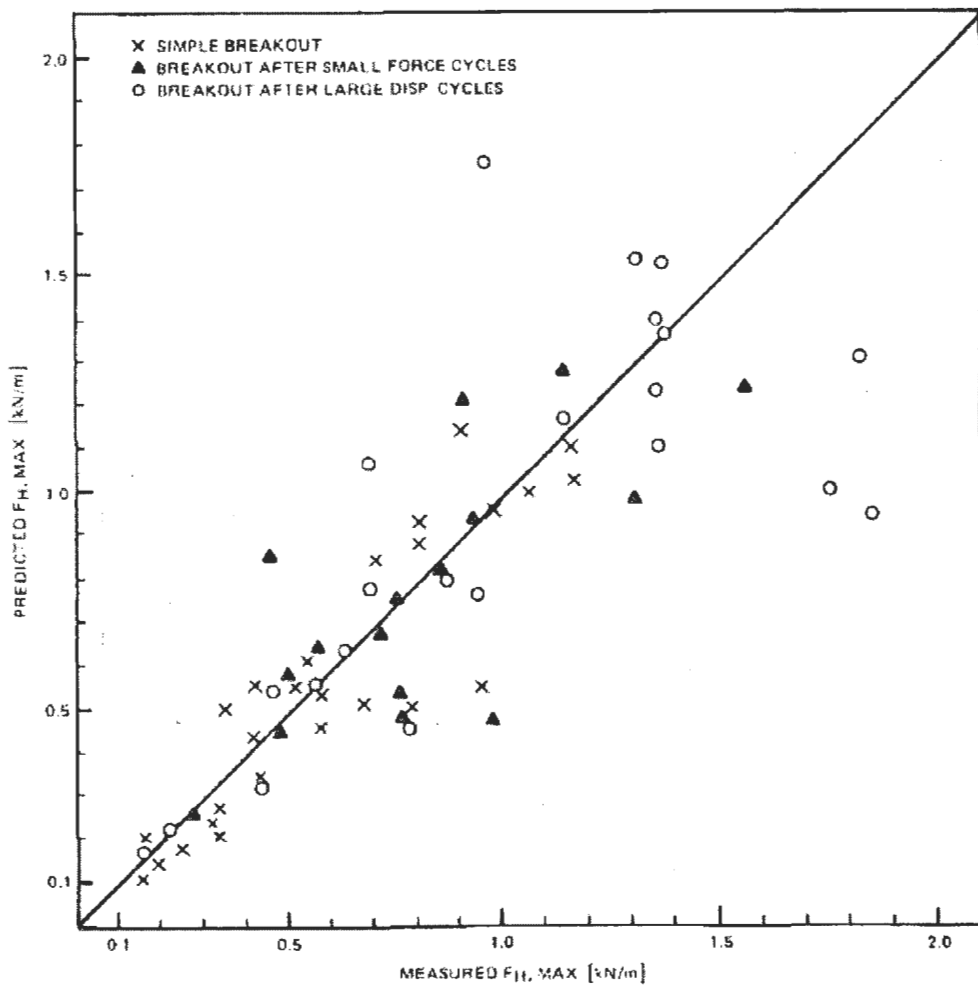


Fig. 2.36 Comparison with analytical model and experimental results (Wagner et al., 1987).

comparing it with the extensive experimental database through dimensionless analysis, Verley and Lund (1995) proposed an empirical equation to model pipe lateral resistance. The proposed equation of Verley and Lund (1995) to calculate the lateral breakout resistance is a function of dimensionless soil weight, $S = w'_p / Ds_u$ and dimensionless soil strength, $G = s_u / D\gamma$. The developed empirical equation can be expressed as:

$$\frac{F_h}{Ds_u} = \mu_f S + 4.13G^{-0.392} \left(\frac{Z}{D} \right)^{1.31} \quad (2.6)$$

Verley and Lund (1995) showed that lateral pipe breakout resistance depended mainly on the vertical load on the pipe, undrained shear strength of soil, soil unit weight, pipe diameter and pipe embedment depth. Although Verley and Lund (1995) observed a standard deviation of 25% with physical modelling (Fig. 2.37), they recommended that more physical experiments are required for analytical model validation.

Bruton et al. (2006) updated Verley and Lund's (1995) equation to calculate pipe lateral resistance based on the experimental database of SAFEBUCK JIP phase I. Pipe lateral breakout resistance was divided into two separate parts: (i) frictional component and (ii) passive component (to lift plus deform the soil in front of pipe). Test data showed that pipe lateral breakout resistance depended on vertical load, pipe embedment and the ratio of soil shear strength to weight ($s_u / \gamma D$). The modified Verley and Lund (1995) equation to measure the pipe lateral breakout resistance can be expressed as:

$$f_{brk} = 0.2\nu + \frac{3}{\sqrt{\frac{s_{u_invert}}{\gamma'}}} \frac{Z}{D} \quad (2.7)$$

where $f_{brk} = \frac{H_{breakout}}{s_u D}$ and $\nu = V/Ds_u$.

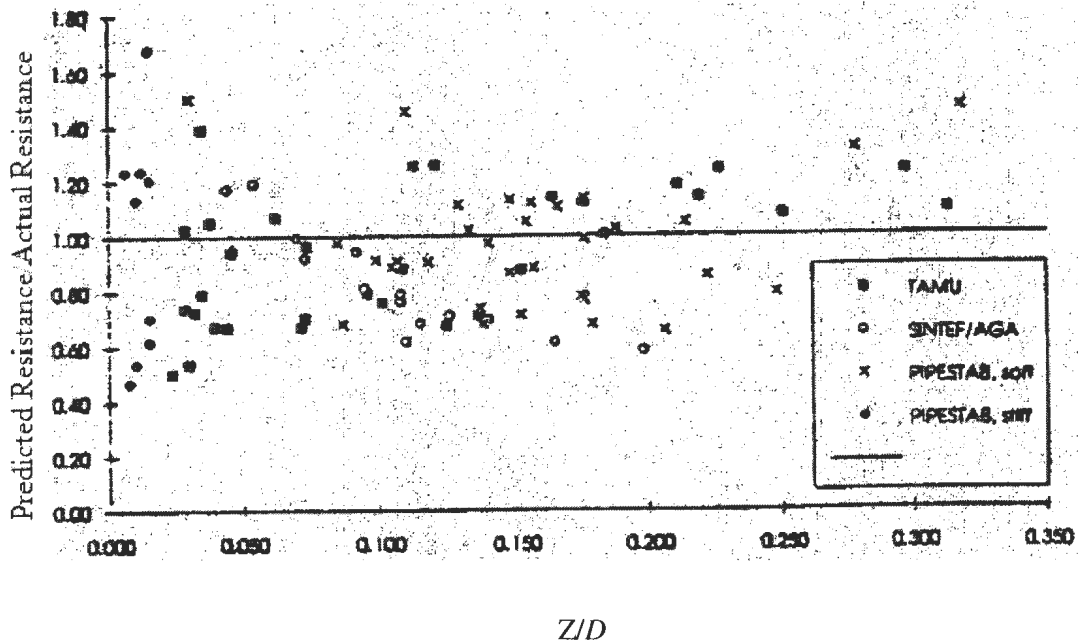


Fig. 2.37 Comparison of Verley and Lund's model with experimental results (Verley and Lund, 1995).

A standard deviation of 37% was observed between the proposed equation and the available experimental database (Fig. 2.38) which was higher than Verley and Lund (1995). Later, Cheuk et al. (2007) conducted a number of full-scale model tests for steady cyclic lateral sweeping of a pipeline followed by initial pipe embedment. Typical light pipe behaviour is shown in Fig. 2.39. As shown, during lateral travel, pipe lateral

resistance shows a peak first and then decrease gradually. Suction (at pipe rear end) had significant contribution in the post peak behaviour of pipe lateral breakout resistance (Fig. 2.40). Results from the experimental analysis were compared with an upper bound solution (Fig. 2.29) and reasonable agreement was observed for first lateral sweep.

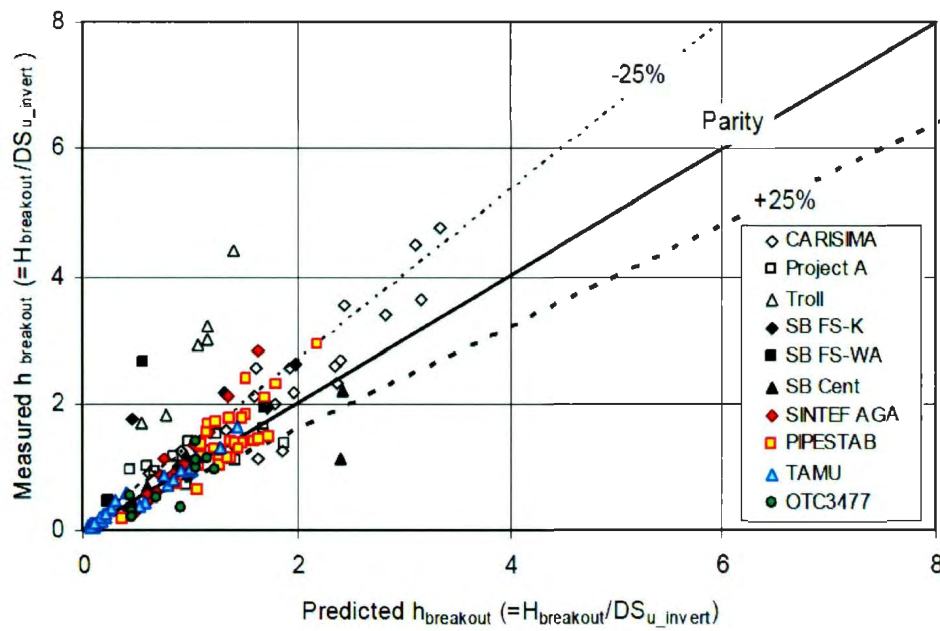


Fig. 2.38 Comparison of experimental data and analytical model (Bruton et al., 2006).

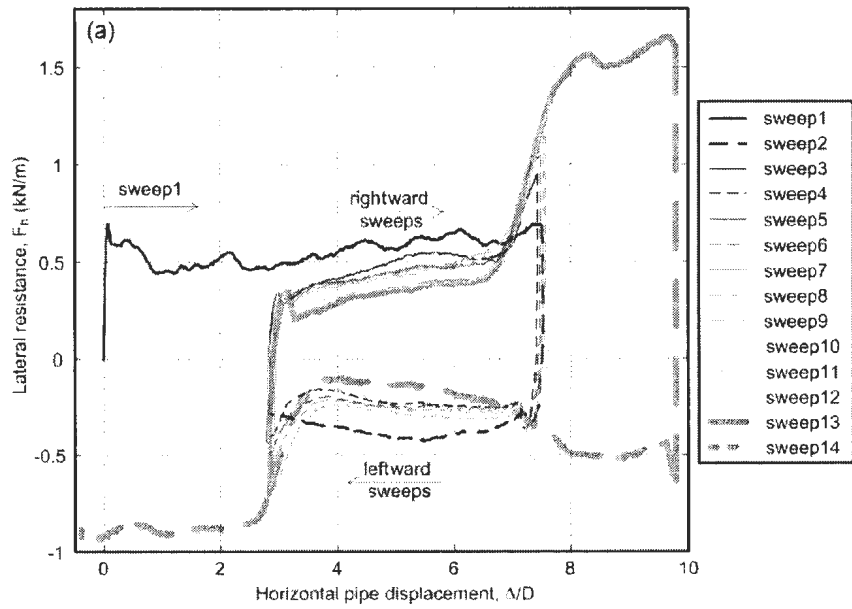


Fig. 2.39 Pipe lateral resistance during steady cyclic lateral movements (Cheuk et al., 2007).

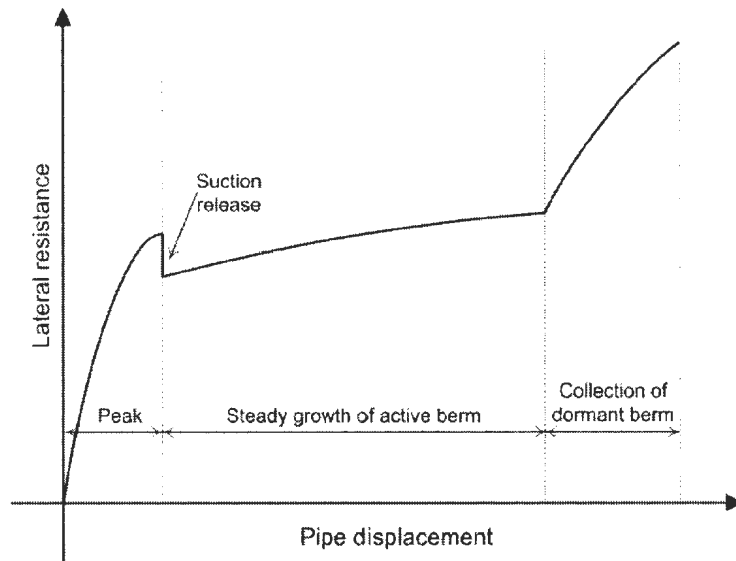


Fig. 2.40 Typical pipe lateral resistance during pipe steady movement (Cheuk et al., 2007).

Dingle et al. (2008) performed the centrifuge tests to quantify the light pipe lateral resistance. Pipe was penetrated into soil at $0.45D$ and displaced laterally. During pipe lateral movement, pipe was free to move in vertical direction. Varying undrained shear strength of soil was considered. Analysis results (Fig. 2.41) showed normalised lateral pipe resistance peak at the very beginning (same as Fig. 2.39) and then to decrease. Three points A, B and C had been selected around the peak lateral resistance and the soil velocity field (using particle image velocity (PIV)) at these locations (A, B, and C) are shown in Fig. 2.42. Lateral breakout resistance occurs when the pipe was about to separate at pipe rear end and soil in front of pipe began to flow along a slip surface (Fig. 2.42).

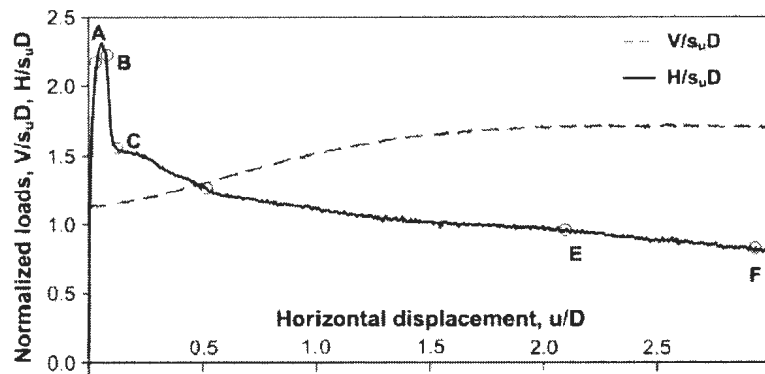


Fig. 2.41 Normalised pipe lateral resistance during pipe lateral movement (Dingle et al., 2008).

However, Dingle et al. (2008) did not propose any guideline to quantify pipe lateral breakout resistance to use in the design. White and Dingle (2011) conducted a number of

centrifuge tests to develop a design guideline. With different soil undrained shear strengths, pipe initial embedments and applied vertical loads (Table 2.4), tests were conducted. Different pipe lateral breakout resistance for different tests were observed (Fig. 2.43). However, all the test results showed a peak horizontal resistance and decreased gradually which was a typical light pipe phenomenon.

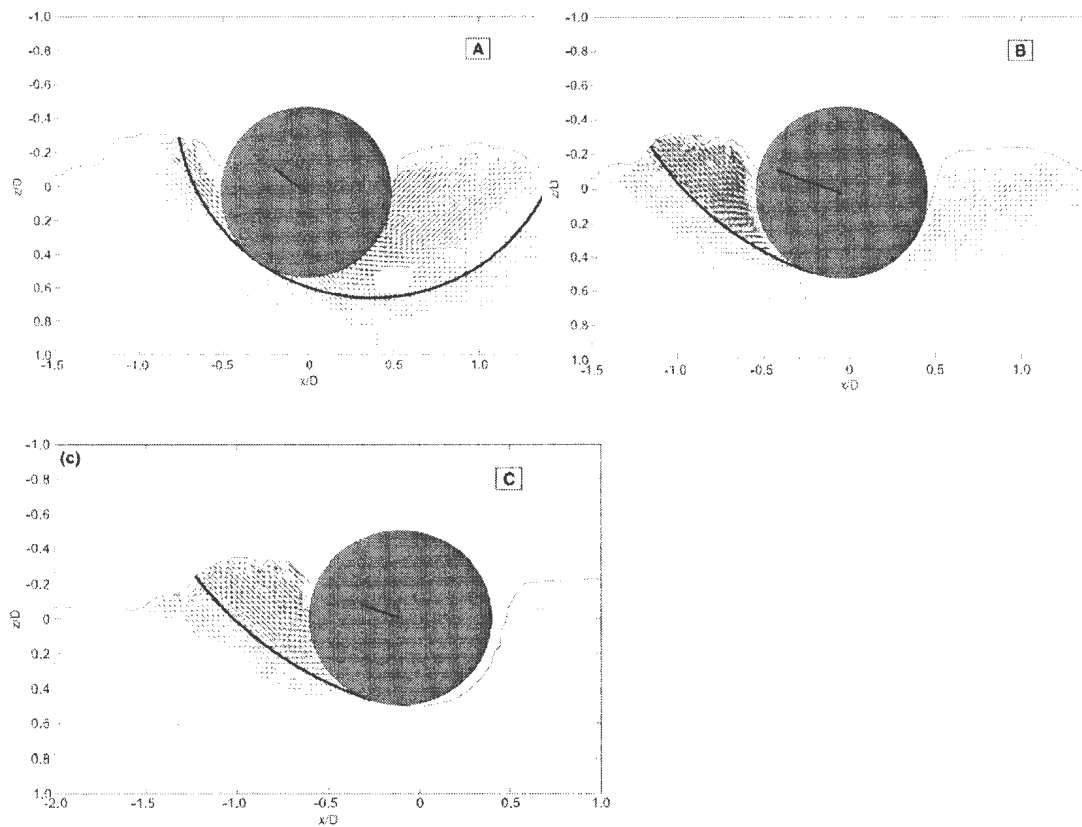


Fig. 2.42 Soil velocity field during pipe lateral breakout (Dingle et al., 2008).

Table 2.4 Parameters used for analysis (White and Dingle, 2011)

Test no	Soil undrained shear strength, kPa	Initial embedment, w/D	Applied Vertical load, kN
L1	$2.3+3.6 \times \text{depth}$	0.52	2.1
L2	$2.3+3.6 \times \text{depth}$	0.46	2.8
L3	$2.3+3.6 \times \text{depth}$	0.25	1.0
L4	$2.3+3.6 \times \text{depth}$	0.18	3.2
L5	$3.0+5.0 \times \text{depth}$	0.02	2.1
L6	$3.0+5.0 \times \text{depth}$	0.05	4.4

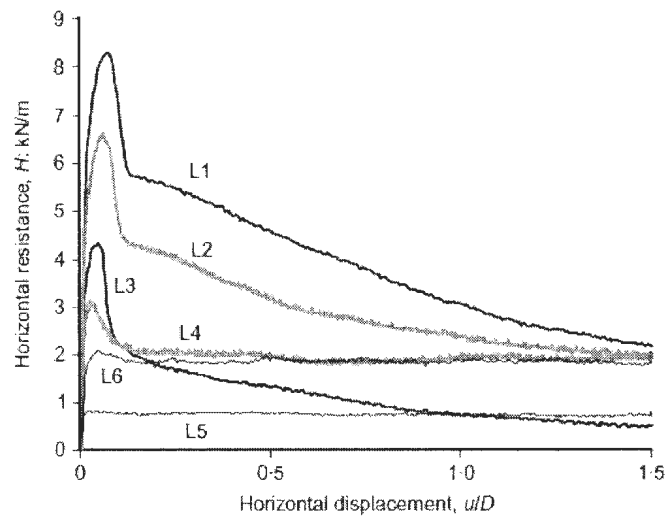


Fig. 2.43 Pipe lateral resistance during lateral movement (White and Dingle, 2011).

One power law equation was proposed using the effective pipe embedment concept.

Effective pipe embedment during lateral travel consists of two parts: (i) pipe embedment

during lateral travel (ii) berm height. During pipe lateral movement, a soil berm is formed in front of the pipe. Formulated soil berm area (in front of pipe) was converted to the berm height by considering the berm area as a rectangular block for an aspect ratio (Fig. 2.44) and was expressed as $h_{berm} = \sqrt{A_{berm}/\eta_e}$. Berm height was added to pipe embedment (during lateral travel) to calculate effective pipe embedment. The formulated soil berm can be extremely remoulded during lateral travel which reduces its undrained shear strength. To account for this issue, formula for berm height calculation was modified and expressed as $h'_{berm} = \frac{h_{berm}}{S_{t,berm}}$ where $S_{t,berm} = \lambda S_t$ indicates the berm sensitivity. Thus, effective pipe embedment was expressed as:

$$\frac{w'}{D} = \frac{w}{D} + \frac{1}{S_{t,berm}D} \sqrt{\frac{A_{berm}}{\eta_e}} \quad (2.8)$$

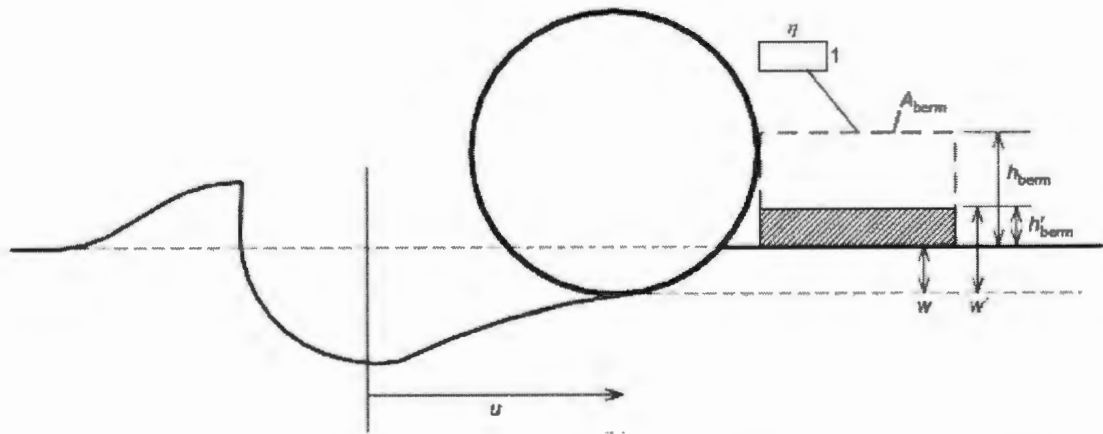


Fig. 2.44 Development of effective embedment using soil berm and softening (White and Dingle, 2011).

White and Dingle (2011) assumed the value of $S_i \times \lambda \times \sqrt{\eta_e}$ as 6.7 to measure its effective embedment. With the help of the above assumption, developed power law relationship for pipe lateral resistance was:

$$\frac{H}{s_{u0}D} = a \left(\frac{w'}{D} \right)^b \quad (2.9)$$

Where $a = 2.8$ and $b = 0.75$.

Pipe lateral resistance with effective embedment are plotted (Fig. 2.45) for both experiments and analytical model. Variation between the developed analytical model and physical experiments are higher at small penetration depths and smaller at higher penetration depths. However, the developed power law equation to quantify the pipe lateral resistance has limitations for its assumption in berm sensitivity and berm area calculation. Again, horizontal pipe resistance is also plotted with pipe embedment during its lateral travel, Fig. 2.46. Comparison between Fig. 2.45 and Fig. 2.46 showed that minor improvement was achieved with effective embedment concept. Note that different authors proposed different value of a and b for the analytical model. Wang et al. (2010) proposed $a=2.3$ and $b=0.9$ (based on numerical investigation), Chatterjee et al. (2011) proposed $a=2.45$ and $b= 0.95$ through numerical analysis and Chatterjee et al. (2012a) proposed $a =2.82$ and $b=0.72$. Wang et al. (2010) and Chatterjee et al. (2012a) deal with both light and heavy pipe whereas Chatterjee et al. (2011) conducted the finite element investigation for light pipe only.

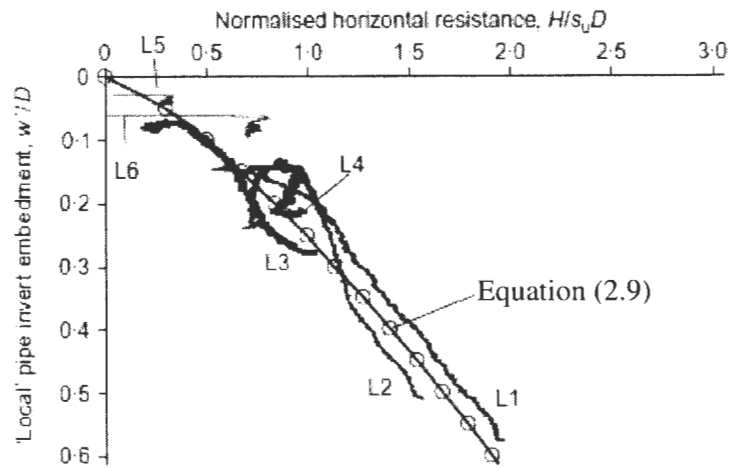


Fig. 2.45 Variation of pipe lateral resistance with effective embedment (White and Dingle, 2011).

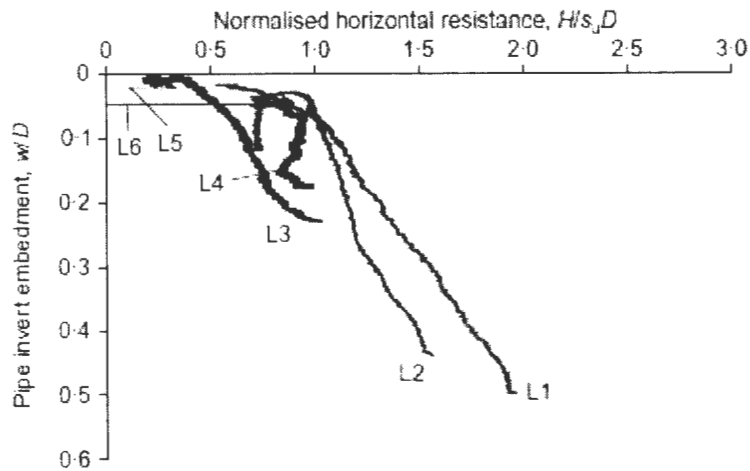


Fig. 2.46 Variation of pipe lateral resistance with embedment (White and Dingle, 2011).

2.5.2.2 Pipe lateral residual resistance

Most of the earlier analyses were performed to quantify the pipe lateral breakout resistance to hydrodynamic loads, such as on-bottom currents. Less attention was paid to the pipe residual resistance. At residual stage, experimental results show higher pipe residual force for higher pipe vertical loads, Fig. 2.47. The classical plasticity theorem determined horizontal to vertical load ratio of 0.39 for a surface foundation with sliding failure (Green, 1954), as shown by the solid line in Fig. 2.47. This classical plasticity theorem under predicts the results (Fig. 2.47). During pipe lateral travel at residual stage, soil (in front of pipe) needs to be lifted into the berm. Therefore, submerged soil unit weight and undrained shear strength of soil is also important for pipe residual resistance (Bruton et al., 2006). Figure 2.48 shows the variation of normalised shear strength ($s_u/\gamma'D$) with equivalent friction factor (h_{res}/v) of experimental results. Based on the experimental observations, Bruton et al. (2006) proposed the following equation for pipe residual resistance calculation:

$$\frac{h_{res}}{v} = 1 - 0.65 \left[1 - e^{\left(\frac{-s_u - 1D}{2\gamma'D} \right)} \right] \quad (2.10)$$

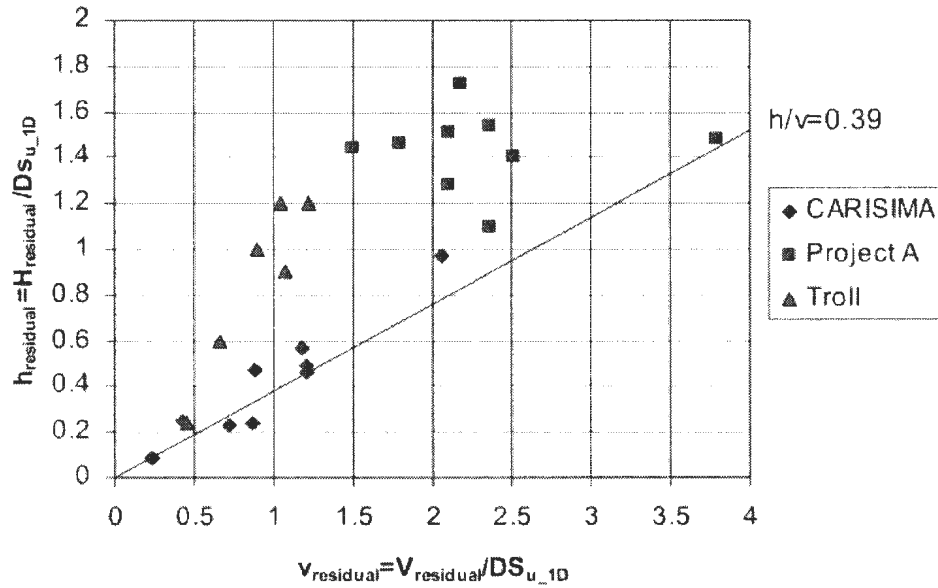


Fig. 2.47 Comparison of normalised residual horizontal and vertical load (Bruton et al., 2006).

To measure $\frac{h_{res}}{v}$, all parameters can be calculated easily except the undrained shear strength. Experimentally, it is very difficult to estimate the soil undrained shear strength at mudline level and Bruton et al. (2006) recommend taking the value of s_u at one (1) pipe diameter. The comparison between test data and the analytical model is also shown in Fig. 2.49, which shows some general trend of these scattered data.. In the analytical model, $-s_u/2\gamma D$ can give guidance to capture the behaviour of lift and shearing the soil ahead of the pipe whereas it does not give any guidance for soil undrained shear strength variation i.e. failure plane consideration for normally consolidated clay. The soil undrained shear strength gradient $ks_u D/s_{um}$ (k is the undrained shear strength gradient, s_u is

the undrained shear strength of soil at any depth and s_{um} is the undrained shear strength of soil at mudline) has an effect on residual frictional resistance as the failure envelope will change with changes in the soil undrained shear strength gradient (Gourvenec et al., 2003).

Cardoso et al. (2010) conducted a number of large scale tests varying the undrained soil shear strength to calculate the pipe lateral resistance. Using a wide range of parameters (soil undrained shear strengths of 1 to 10 kPa, soil undrained shear strength gradient of 2 to 30 kPa/m, pipe diameters of 0.23 to 0.33 m and initial pipe penetration depth of 0.1 to 0.5D), the effect of different parameters on pipe residual resistance were calculated. Analysis shows that pipe residual resistance mainly depends on the dimensionless pipe weight ($S = w_s/s_u D$) and dimensionless weight term $\left(G = \frac{s_u}{\gamma D}\right)$. Based on the experimental database and regression analysis, Cardoso et al. (2010) proposed the equation:

$$\frac{H_{res}}{V} = 0.2 + 0.929 \left(\frac{V}{s_{u,1D} D} \right)^{0.586} \left(\frac{\bar{s}_{u,1D}}{\gamma D} \right)^{-0.479} \quad (2.11)$$

Here, $\bar{s}_{u,1D}$ indicates the mean undrained shear strength of soil between soil surface and at one pipe diameter (i.e. $\bar{s}_{u,1D} = s_{um} + kD/2$). For their project data, a standard deviation of 19% was observed (Fig. 2.49).

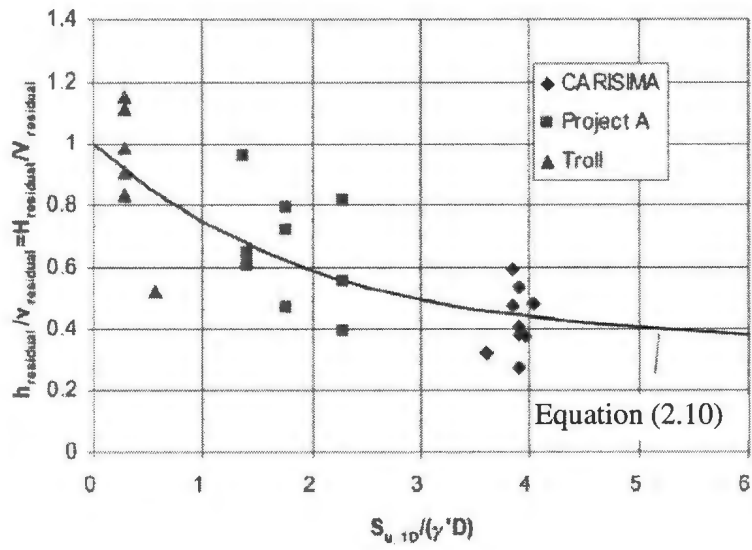


Fig. 2.48 Comparison between model data base and empirical equation (Bruton et al., 2006).

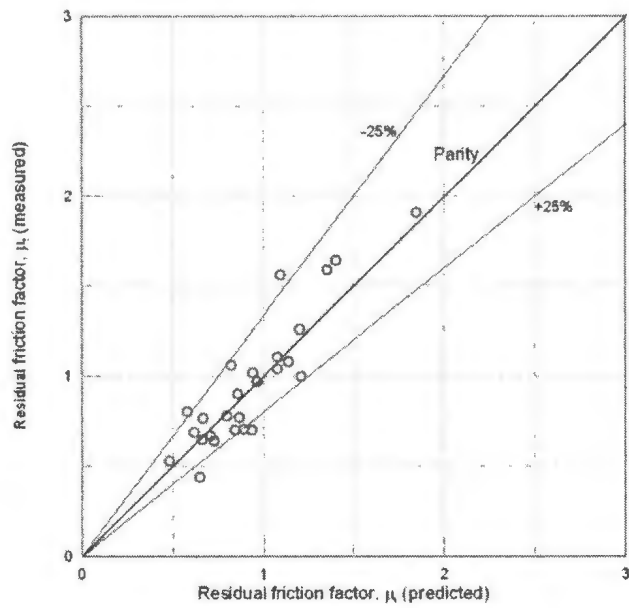


Fig. 2.49 Comparison between measured and predicted equivalent friction factor (Cardoso et al., 2010).

White and Dingle (2011) conducted a total of 6 centrifuge tests. Soil parameters and test conditions are shown in Table 2.4. Figure 2.50 shows that after a lateral pipe movement of approximately $3D$, pipe lateral resistance become constant, which represents the residual resistance.

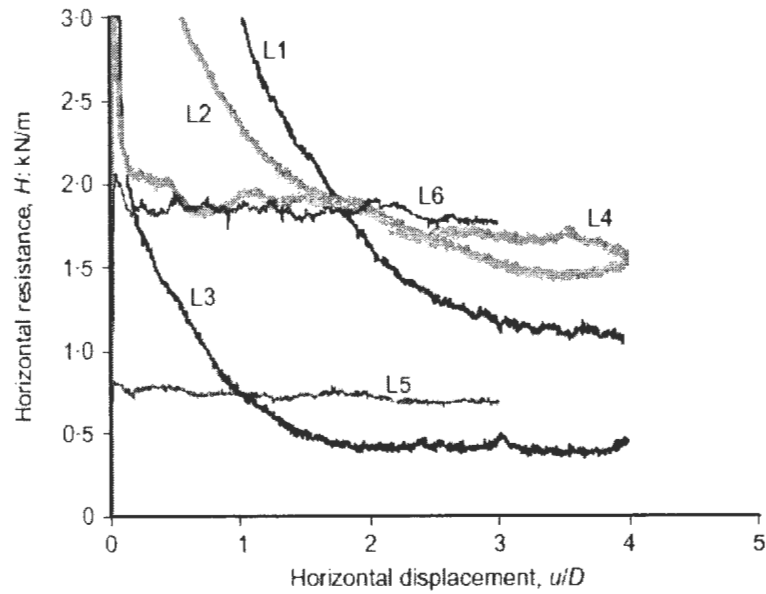


Fig. 2.50 Pipe horizontal resistance during lateral travel (White and Dingle, 2011).

White and Dingle (2011) also proposed the following generalised equation to calculate lateral residual resistance based on their experimental results.

$$\frac{H_{res}}{s_u D} = \frac{V}{s_u D} \left[0.3 + 2 \left(\frac{w}{D} \right)_{init} \frac{1}{\sqrt{R}} \right] \quad (2.12)$$

The comparison between measured and model prediction (Eq. 2.12) is shown in Fig. 2.51.

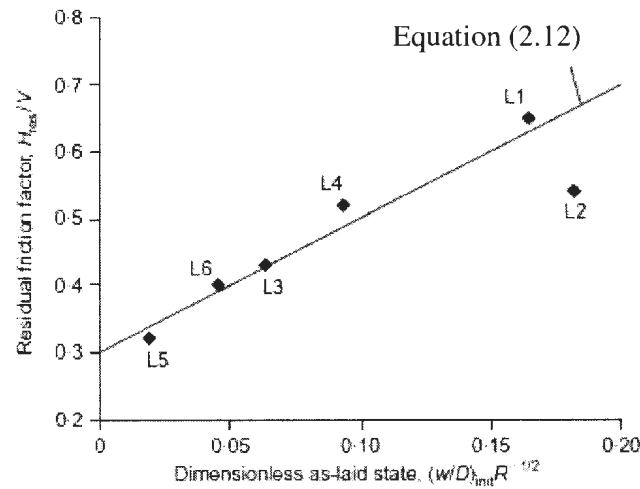


Fig. 2.51 Pipe residual friction factor co-relation (White and Dingle, 2011).

2.5.3 Numerical modelling of pipe lateral resistance

The lateral movement of partially embedded pipelines can also be modelled numerically using small strain or large strain finite element modelling techniques. As it is a large deformation phenomenon the large strain analysis is the most suitable one. Details of pipe lateral movement analysis using small and large strain analysis are described below:

2.5.3.1 Small strain analysis

2.5.3.1.1 Pipe breakout resistance

Lyons et al. (1973) used a finite element approach to model pipe lateral movement for nonlinear stress strain behaviour of soil. Plain strain conditions were used for the analysis.

Mesh size and details of the analysis are shown in Fig. 2.52. An optimum mesh size of 1"

×1" was used in their analysis with fixed and roller boundary conditions as shown. An arbitrary element with low modulus of elasticity was used to model soil/pipe interaction and the pipe (diameter of 9" and 16") was restrained to rotate. Analysis results were compared with physical testing (Fig. 2.53) and a deviation of 5 to 10% is observed between horizontal loads.

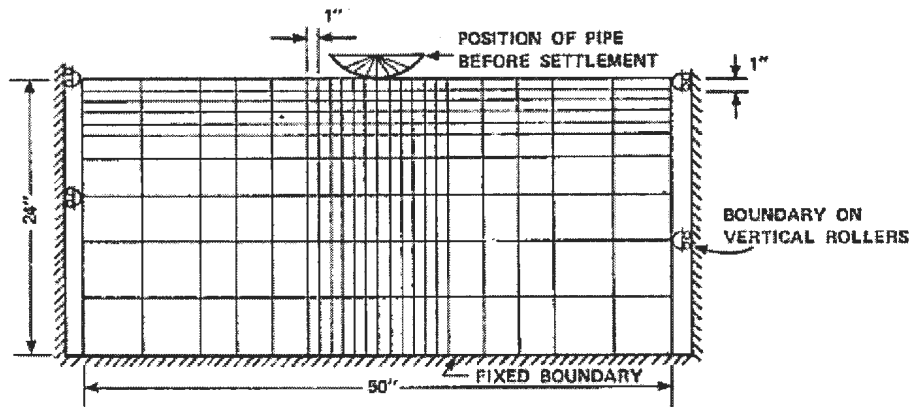


Fig. 2.52 Details of mesh size (Lyons, 1973).

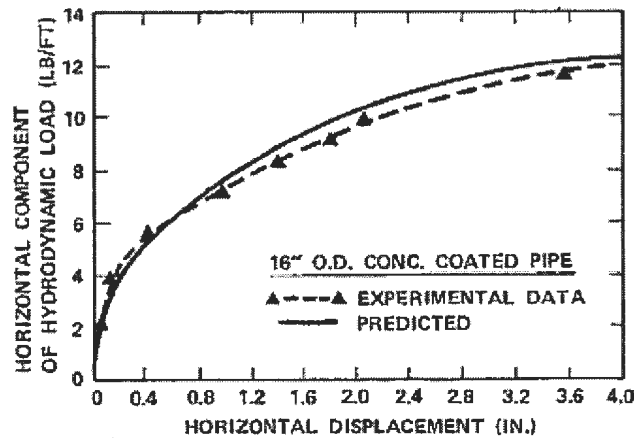


Fig. 2.53 Comparison with numerical and physical experiments (Lyons, 1973).

Although the finite element analysis results showed a good agreement with experimental results, the modelling of soil/pipe interaction behaviour and soil constitutive model used in the analysis are questionable. Later, Merifield et al. (2008) developed a finite element model to investigate the pipe breakout resistance. The pipe was embedded previously and no berm was formed around the shoulders of the pipe (i.e. pipe was at wished in place (WIP) pipe condition). Soil shear strength was uniform and no strain rate and softening effects were considered. The pipe was moved at different angles (Fig. 2.54) for different pipe embedments. This numerical study was limited to a low normalised weight for the pipeline mainly to understand the lateral resistance for a pre-embedded light pipeline. It was observed that during lateral movement, the resultant resistance (resultant of lateral and vertical resistance) had reached almost a constant value within a displacement of 8% of the diameter for both smooth and rough pipe for different as-laid embedments (Fig. 2.55). In this figure R indicates the pipe resultant resistance and Δ indicates the pipe relative displacement. The analysis results are also compared with a theoretical yield envelope which was developed using an upper bound theorem with Martin's mechanism (Fig. 2.30). Comparison with the theoretical yield envelope showed closer agreement with numerical analysis.

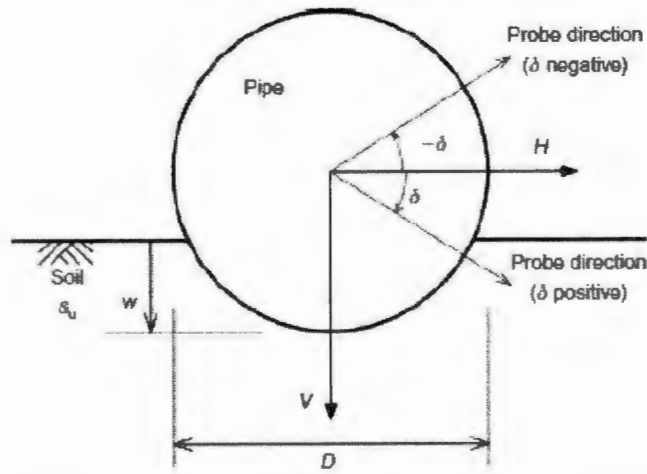


Fig. 2.54 Details of pipe lateral movement (Merifield et al., 2008).

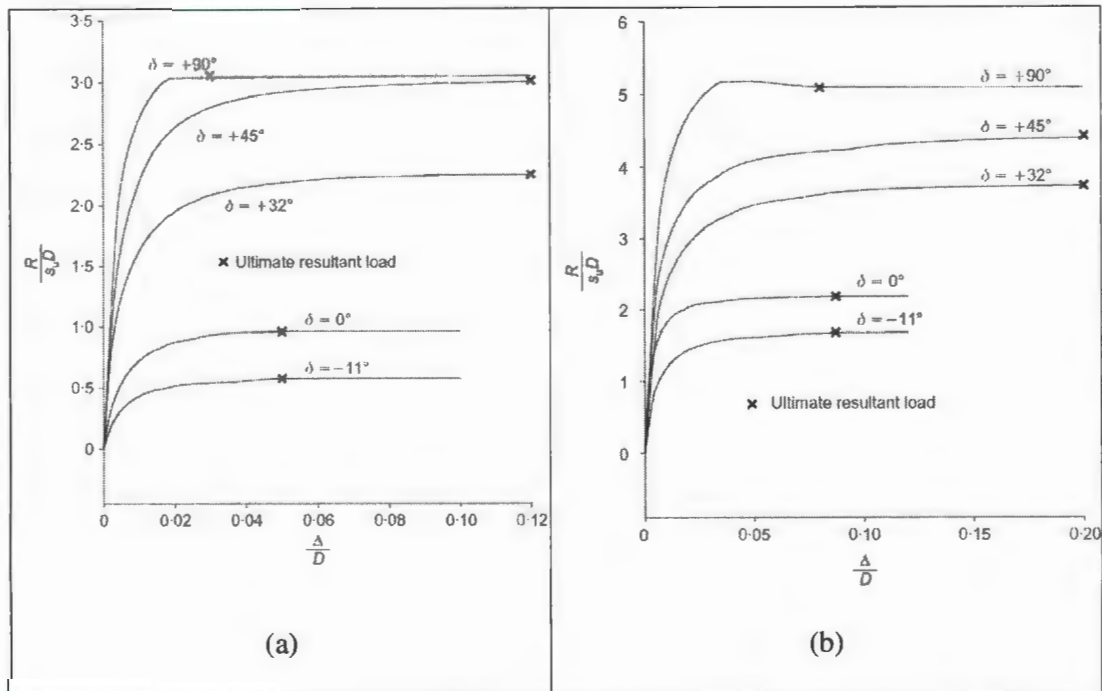


Fig. 2.55 Resultant pipe resistance during relative pipe movement (a) Smooth pipe (b) Rough pipe (Merifield et al., 2008).

2.5.3.1.2 Pipe residual resistance

To calculate pipe lateral residual resistance, a pipe needs to travel at least 3 to 4D. But with small strain analysis, it is very difficult to simulate pipe residual resistance due to mesh distortion and convergence issue. No studies are available in the literature for pipe residual resistance using small strain analysis.

2.5.3.2 Large strain analysis

2.5.3.2.1 Pipe breakout resistance

Merifield et al. (2009) conducted a finite element investigation to calculate the pipe horizontal breakout resistance using the ALE technique. Plain strain condition was used for the analysis. Uniform soil undrained shear strength with Tresca yield criteria was adopted. For both smooth and rough pipe conditions, the horizontal pipe resistance was calculated. Using the concept of soil bearing capacity, an equation was developed to calculate pipe lateral breakout resistance, as shown below:

$$\frac{H}{s_u D} = c\bar{w}^d + \left(\frac{\bar{w}}{2} + 0.15625 \left[\frac{\sin^{-1}(\sqrt{4\bar{w}(1-\bar{w})})}{2\sqrt{\bar{w}(1-\bar{w})}} \right] - (1-2\bar{w}) \right) \left(\frac{\gamma' \bar{w}}{s_u} \right) \quad (2.13)$$

Here, the value of c and d depends on pipe-soil interface. Based on 160 finite element analyses, the values of c and d were back calculated. For smooth pipe, $c = 2.7$ and $d = 0.64$ was proposed whereas for rough pipe, $c = 3.0$ and $d = 0.58$. Also, \bar{w} indicates normalised pipe invert displacement and it was defined as:

$$\bar{w} = \frac{w}{D}$$

As discussed in Section 2.4.3.2, ALE cannot model very large strain behaviour well. Wang et al. (2010) developed a large deformation finite element model in ALE using Remeshing and Interpolation Technique with Small Strain (RITSS) approach. It was claimed that the mesh tangling and convergence issues can be overcome in RITSS. It is mentionable that the adopted numerical tools cannot capture suction behaviour at the pipe rear end during pipe lateral movement initiation and thus breakout resistance can be simulated without suction behaviour at pipe rear end. Based on their numerical analyses, Wang et al. (2010) proposed the following empirical equation to calculate pipe lateral resistance.

$$\frac{H}{s_{u0}D} = a \left(\frac{w'}{D} \right)^b \quad (2.14)$$

where $a=2.3$, $b=0.9$, $w' = w + h'_{berm} = w + \frac{1}{S_{t,berm}} \sqrt{\frac{A_{berm}}{\eta}}$ and η = berm aspect ratio.

The comparison between numerical results and the theoretical yield envelope is shown in Fig. 2.56, developed using the upper bound plasticity theorem with Martin's mechanism. It is mentionable that Wang et al. (2010) used a rate dependent strain softening soil model for their numerical investigation. Comparison was performed with both the rate dependent softening soil constitutive model and without a rate dependent soil constitutive model. Note that for upper bound theorem, a rate dependent softening soil constitutive model was not considered. Chatterjee et al. (2012b) conducted a number of finite element

modelling for pipe lateral resistance using RITSS with the ALE technique. Linearly varying soil shear strength with a rate dependent softening soil model was used and the Tresca yield criterion was adopted. Developed yield envelope for breakout resistance was compared with Merifield et al. (2008), which is shown in Fig. 2.57.

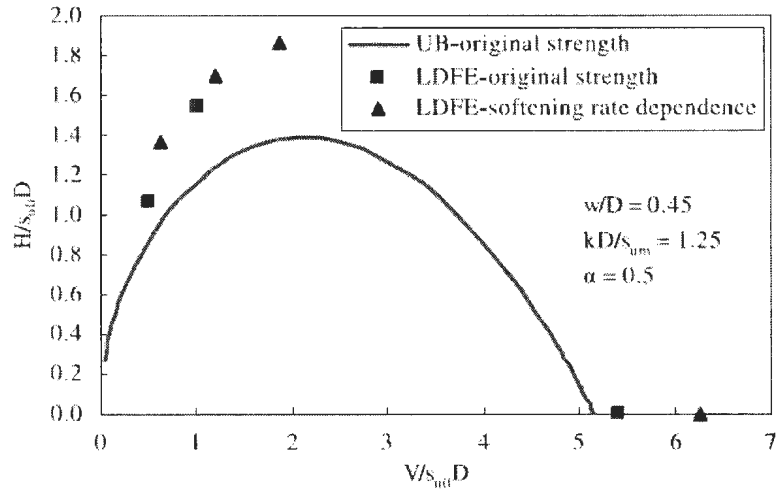


Fig. 2.56 Comparison with yield envelope (Wang et al., 2010).

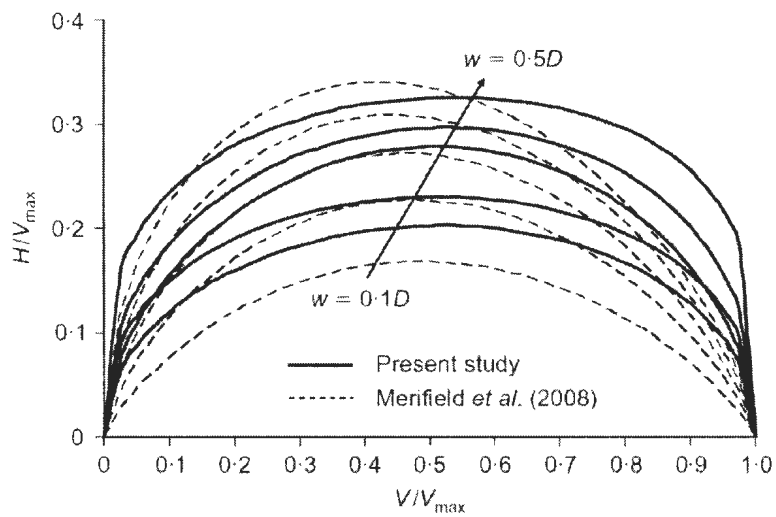


Fig. 2.57 Comparison with yield envelope (Chatterjee et al., 2012b).

2.5.3.2.2 Pipe residual resistance

Limited research is available in the literature for pipe residual resistance using large strain analysis. Wang et al. (2010) conducted a number of finite element investigations for lateral residual resistance. Both light and heavy pipes were considered in their analyses. A strain softening and strain rate dependent soil model was used and the Tresca yield criterion was adopted. Numerical analyses show that the residual resistance for a light pipe develops after a lateral displacement of approximately $2.5D$. The authors suggested that Equation 2.14 could also be used for estimating residual resistance. Note that w' for residual resistance is significantly lower than that for breakout resistance, and therefore residual resistance is less than breakout resistance. Chatterjee et al. (2012b) also shows that the residual resistance for a light pipe develops after a lateral displacement of $2.5D$. It was shown that the higher the initial pipe embedment or applied vertical load the higher the residual friction factor (H_{res}/V). The calculated residual friction factor is also compared with the experimental database (SAFEBUCK phase II and White and Dingle (2011)).

2.6 Conclusion

A comprehensive literature review of the studies on vertical embedment of offshore pipelines into the seabed and subsequent lateral movement during operation period is presented in this chapter. Vertical embedment and lateral movement is a large deformation problem. Experimental, theoretical and numerical studies have been performed in the past to model this behaviour. Finite element modeling of such large

deformation problems is very complicated and challenging. Although some researchers attempted to model this behaviour using traditional finite element method in a Lagrangian framework in a form of “pseudo” large deformation problem, their results are somehow questionable as they could not simulate the whole process together. Later researchers used the Arbitrary Lagrangian Eulerian (ALE) approach with remeshing technique to overcome some of these issues. The finite element modelling techniques in a Lagrangian framework has been significantly advanced over the last few years. The research presented in the following chapters is based on such a FE modelling technique to simulate the large deformation behaviour of partially embedded pipelines in deep sea.

Chapter 3

Finite Element Modeling of Vertical Penetration of Offshore Pipelines using Coupled Eulerian Lagrangian Approach

Co-Authorship: Chapter 3 is prepared according to the Guidelines for Manuscript-Format Theses in the Faculty of Engineering and Applied Science at Memorial University. This part of the research has been published as: Dutta, S., Hawlader, B. and Phillips, R. (2012) “Finite Element Modeling of Vertical Penetration of Offshore Pipelines using Coupled Eulerian Lagrangian Approach,” 22nd International Offshore (Ocean) and Polar Engineering Conference & Exhibition, Rodos Palace Hotel, Rhodes (Rodos), Greece, June 17–22, 2012.

Most of the research work presented in this chapter was conducted by the first author. He also prepared the draft manuscript. The other two authors mainly supervised the research and reviewed the manuscript.

3.1 Abstract

Subsea pipelines are the preferred mode of transporting hydrocarbon in both shallow and deep water. In deepwater, pipelines are usually laid on the seabed. A portion of the pipe diameter penetrates into the seabed because of the effects of several factors including

wave action and vessel motions during installation and pipeline self weight. Embedment of the pipeline has a major influence on lateral buckling and thermal expansion during operation. Conventional finite element method in Lagrangian framework cannot be used to model such large deformation behavior as occurs in subsea pipeline penetration. In this study, finite element analyses using Coupled Eulerian Lagrangian technique is presented. The pipeline has been modeled in Lagrangian and the soil has been modeled in Eulerian framework. Comparison with other solutions and test results are also presented.

3.2 Introduction

Offshore pipelines are typically operated under high temperature and pressure to ease the liquid hydrocarbon flow through the pipe and to reduce wax solidification. High temperature and pressure can generate axial stress along the pipeline which might cause lateral buckling of the pipeline if insufficient resistance to prevent the movement of the pipeline is available. The pipelines are often laid on the seabed in the deep sea which penetrate into the seabed due to static load resulted from initial stress concentration from pipe catenary shape and submerged pipeweight. However, because of some other actions such as dynamic motion of the pipeline at the touch down zone due to vessel movement, the vertical penetration can increase up to 2 to 10 times of static embedment of pipelines (Westgate et al., 2010a). Previous studies show that vertical pipe penetration/embedment has a significant impact on lateral resistance (Karal, 1977; Lyons, 1973) and therefore on lateral buckling during operation.

Small et al. (1971) present a method to calculate pipe penetration using the concept of bearing capacity of shallow foundations. Since then a number of studies have been performed to better understand the mechanism of pipe embedment which includes theoretical works (e.g. Karal, 1977, Randolph and Houlsby, 1984, Murff et al., 1989), experimental work (e.g. Verley and Lund, 1995), centrifuge modeling (e.g. Dingle et al., 2008, Cheuk and White, 2011) and finite element modeling (Merifield et al., 2008, 2009, Wang et al., 2010).

The finite element (FE) technique has been widely used for modeling various aspects of geotechnical engineering. However, offshore pipe embedment is fundamentally a large deformation problem. Therefore, conventional finite element method cannot be used for this problem as it suffers numerical instability at large strain. Various techniques have been proposed in the past to overcome numerical difficulties in large strain finite element modeling, which include updated Lagrangian, updated Eulerian, pure Eulerian, mesh-free and Arbitrary Lagrangian Eulerian. Recently, Wang et al. (2010) simulated pipe embedment using remeshing and interpolation technique with small strain (RITSS) which is essentially an Arbitrary Lagrangian Eulerian (ALE) approach.

The main purpose of this study is to present modeling of offshore pipe embedment using a more advanced finite element tool based on Coupled Eulerian Lagrangian (CEL). In CEL Eulerian material flows through the fixed mesh and therefore there is no meshing

issue at large deformation. The analyses have been performed using ABAQUS FE software.

3.3 Problem Definition

Figure 3.1 shows the idealized condition of vertical penetration of offshore pipelines modeled in this study. A pipe of diameter D has been penetrated into the seabed at a given velocity to a desired depth. The pipe does not roll during the vertical penetration. The depth of penetration (w) represents the depth below the original seabed to the bottom of the pipe. A soil berm will be formed with penetration of the pipe into the seabed. The berm formation is symmetric on both sides of the pipe in this case because the pipe moved only in the vertical direction due to the idealized condition.

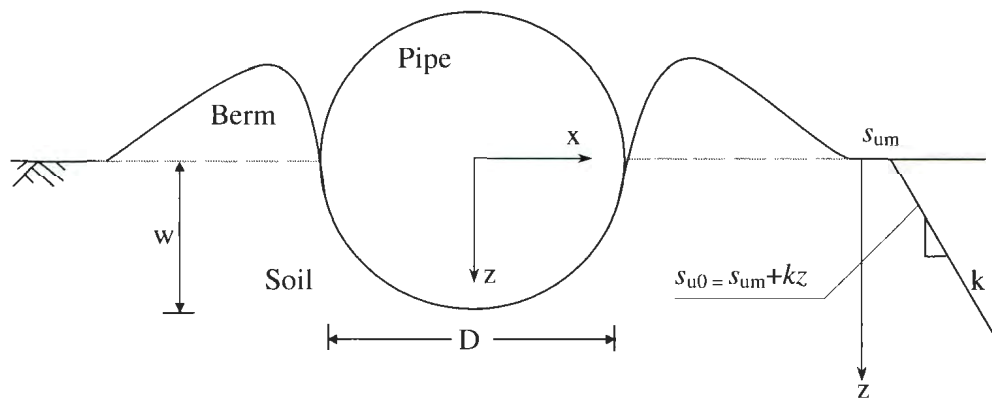


Fig. 3.1 Problem definition

The pipe was penetrated into a clay seabed. As the penetration typically occurs in a short period of time and the permeability of the clay is low, the undrained shear strength (s_{u0})

governs the design. The undrained shear strength of clay is a function of effective stress (σ'_0) and overconsolidation ratio (OCR). To account for these effects a linear variation of s_{u0} in the form of $s_{u0} = s_{um} + kz$ has been used, where s_{um} is the undrained shear strength of clay at the mudline, k is the strength gradient and z is the depth of the soil element below seabed.

3.4 Finite Element Model Formulation

ABAQUS 6.10-EF1 finite element software has been used in this study for numerical modeling. Coupled Eulerian Lagrangian (CEL) approach has been used in the analysis. Figure 3.2 shows the finite element model used in this study. The finite element model consists of three parts: (i) pipeline, (ii) soil and (iii) voids to accommodate displaced soil mass. The pipeline is modeled as Lagrangian elements while the soil has been modeled using Eulerian elements. The pipeline is modeled as rigid body since the deformation is negligible in comparison with soil, which also makes the model computationally more efficient. Pipe is modeled using shell element and element type of S4R. The soil layer is modeled using Eulerian element EC3D8R, which is an 8-noded linear brick, multi-material, reduced integration with hourglass control.

The pipe is penetrated into the clay layer (Eulerian materials) to a desired depth and a berm is formed from displaced soil. One of the key features of CEL is that the space is required to be defined to accommodate the displaced soil—the berm in this case. A void space is created above the clay layer using the “volume fraction” tool in Eulerian element.

Soil and void spaces are created in Eulerian domain using Eulerian Volume Fraction (EVF). For void space EVF is zero (i.e. no Eulerian material, soil in this case). On the other hand, EVF is unity in clay layer, meaning that these elements are filled with Eulerian material.

The bottom of the model (Fig. 3.2) is restrained from any vertical movement, while all the vertical faces are restrained from any lateral movement using roller supports. All components of velocity at each Eulerian node on the bottom or vertical faces are defined as zero so that no Eulerian material moves outside the domain. The top of the seabed is free to move and no velocity boundary condition is applied that allows this surface to move freely and Eulerian materials could move into the voids. The pipe was moved downward using a velocity boundary condition applied at all faces of the Eulerian domain.

The pipeline is modeled in plane strain condition. Although in Coupled Eulerian Lagrangian (CEL) technique only 3D model can be generated, the plane strain condition has been created using one element depth along the axial direction of the pipe. It also makes the numerical model computationally less expensive than a full 3D model.

One of the limitations with ABAQUS CEL is that the Eulerian material might penetrate through Lagrangian element. A Lagrangian mesh two times finer than the Eulerian mesh (Brown et al., 2001) was used to avoid this problem in numerical analysis. Another

limitation in ABAQUS FE software is that the linear variation of undrained shear strength with depth (see Fig. 3.1) cannot be defined as an input. In this study, the increase in s_{u0} with depth has been incorporated using the user subroutine.

The pipe-soil interface plays an important role in modeling partially embedded pipelines. General contact algorithm is used to define soil-pipe interaction properties. In this study, analyses are performed for both smooth (frictionless) and rough conditions.

For convenience, the numerical analysis is divided into three steps. The first step is the geostatic step. During geostatic step the pipe is kept $\frac{1}{2}D$ above the seabed in order to avoid any pipe penetration or interaction with seabed due to gravity. In the second step, the pipe is moved downward at given velocity to the seabed. As this movement occurs only through the void, no vertical reaction force is developed. In the third step, the pipe is penetrated vertically through the soil at a given velocity using amplitude options in ABAQUS FE software.

3.5 Parameter Selection

Table 3.1 shows the geometry and mechanical properties of the soil and pipe. A steel pipe of 0.8 m diameter has been modeled in this study. To model the soil an Eulerian domain of 8 m \times 5 m \times 0.04 m (width \times height \times thickness) is used (Fig. 3.2). The soil is modeled as an elastic-perfectly plastic material. Field investigation shows that most of the sediments near the seabed in deep sea are normally consolidated to lightly

overconsolidated clays (Quiros et al., 2003, Cheuk and White, 2011). The soil parameters for liner variation of s_{u0} are obtained from Dingle et al. (2008) and Cheuk and White (2011). Submerged unit weight of soil (γ') is taken as 6.5 kN/m^3 and undrained elastic modulus as $E_u = 500s_{u0}$.

Table 3.1 Geometry and parameters used in the analyses

Pipe:	
Pipe diameter, D	800 mm
Depth of penetration, w	360 mm
<i>Soil (Clay)</i>	
Undrained modulus of elasticity, E_u	$500s_u$
Poisson's ratio, ν_u	0.49
Undrained shear strength at mudline, s_{um}	2.3 kPa
Gradient of shear strength increase, k	3.6 kPa/m
Submerged unit weight of soil, γ'	6.5 kN/m^3

The pipe is penetrated vertically to the maximum depth of 360 mm ($=0.45D$) at a speed of $0.015D$ per second. These values are typical values and also compare centrifuge test of Dingle et al. (2008).

3.6 Model Validation and Results

The numerical model is used to understand phenomena of vertical penetration of offshore pipelines, which are presented in the following sections.

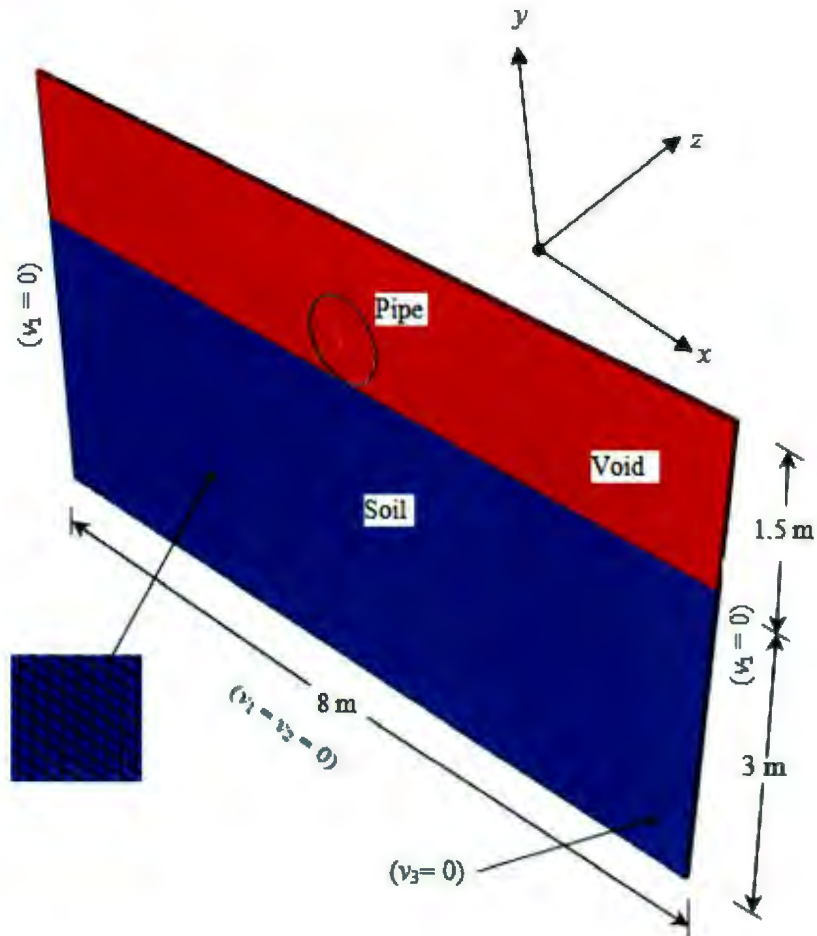


Fig. 3.2 Finite element model used in this study

3.7 Mesh Sensitivity

Mesh size has a significant impact on model performance. In general, finer mesh yields more accurate results but are computationally expensive. One of the key parameters

required in the design of a partially embedded offshore pipeline is the vertical reaction force (V). Therefore, the effect of mesh size on V is examined in this section to find optimum mesh size. Figure 3.3 shows the variation of normalized reaction force ($V/s_{u0(i)}D$) with normalized depth of embedment (w/D) for three different mesh sizes, where $s_{u0(i)}$ is the undrained shear strength of clay at the invert of the pipe. Other parameters used in the analysis are listed in Table 3.1. The largest mesh ($0.25D$) gives erratic results, and calculated V is significantly higher than other two especially for initial penetration. However, for other two mesh sizes the calculated values gives smooth variation of V with depth. Hence a mesh size of $0.05D$ (i.e. $0.04 \text{ m} \times 0.04 \text{ m}$) is adopted for further analysis.

3.8 Comparison with Centrifuge Test Results

Dingle et al. (2008) performed a series of centrifuge tests to simulate the behavior of a section of partially embedded pipeline. A model pipe of 0.8 m prototype diameter was penetrated in a clay bed having geotechnical properties similar to the values listed in Table 3.1. In the present study, numerical simulation has been performed for both smooth and rough soil-pipe interface conditions. Figure 3.4 shows the comparison between numerical prediction and centrifuge test results.

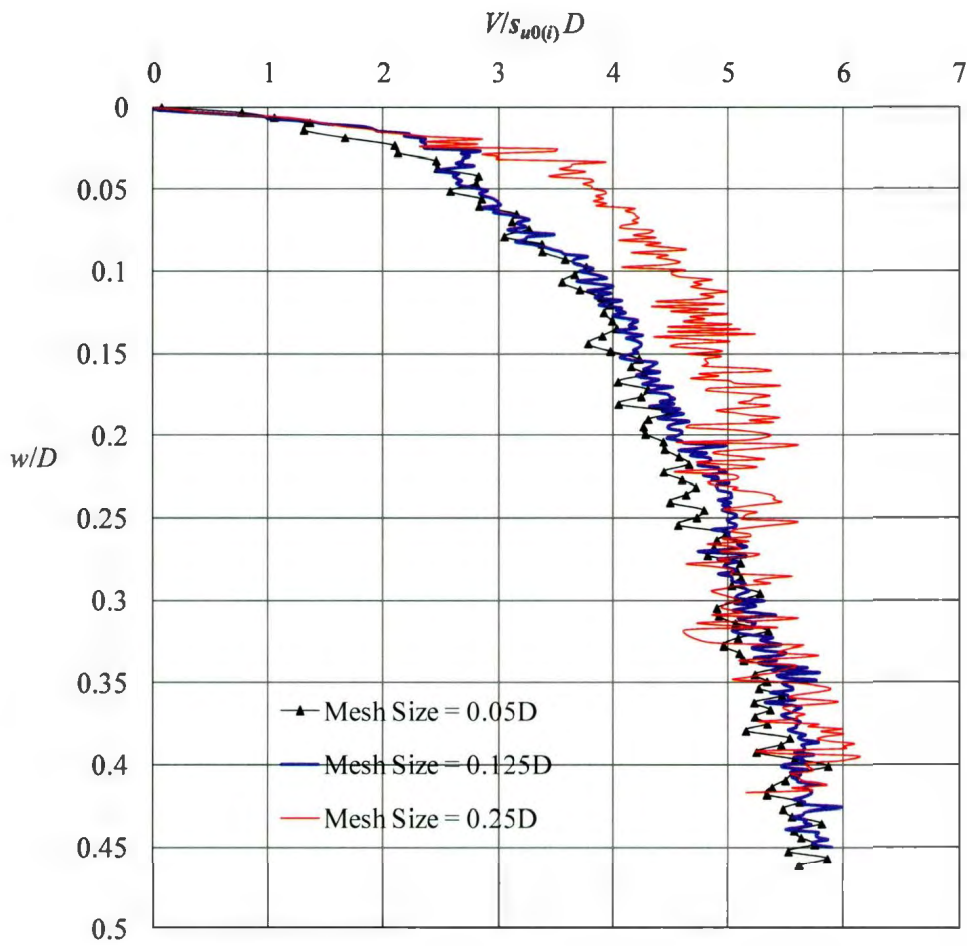


Fig. 3.3 Effect of mesh size on vertical reaction

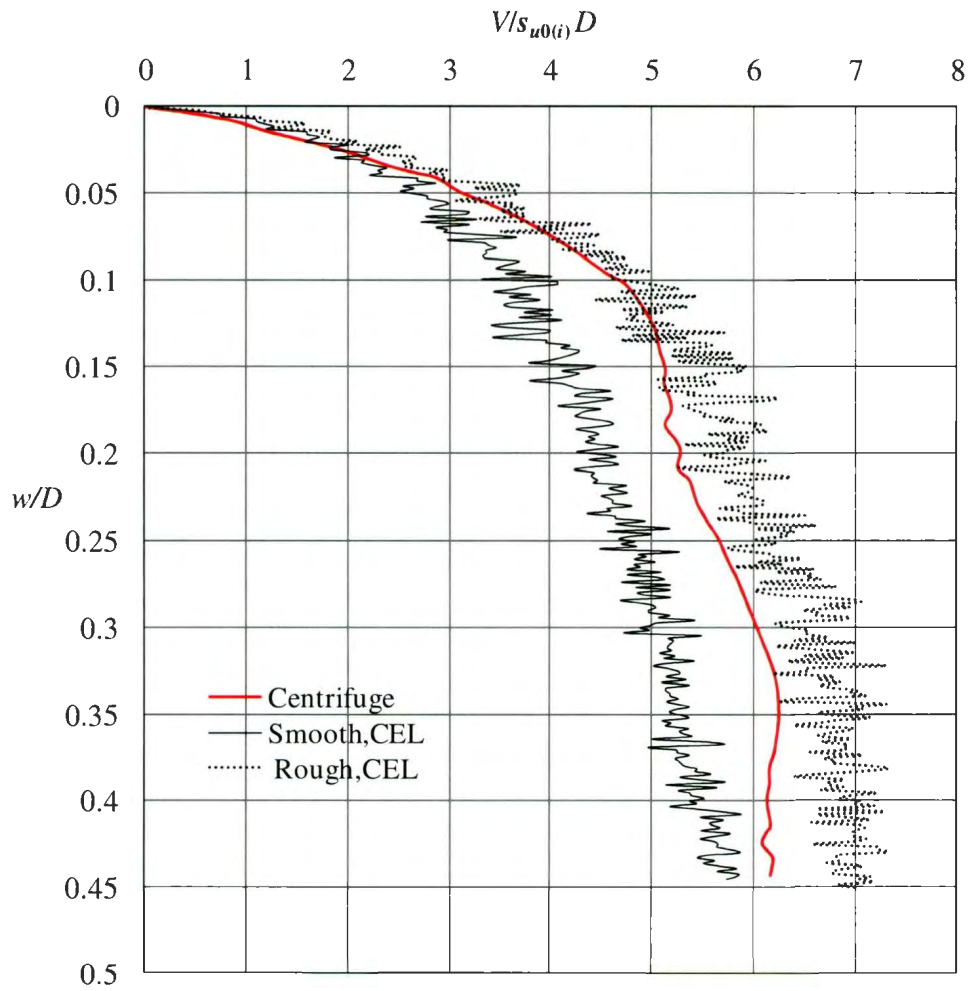


Fig. 3.4 Comparison between finite element and centrifuge test results

The centrifuge test result is in between the rough and smooth conditions. A roughness coefficient between rough and smooth conditions might give a better comparison. However, it is to be noted here that not only the value of roughness coefficient but also other factors such as the variation of undrained shear strength with strain and strain rate should be considered for better modeling.

3.9 Soil Deformation around the Pipe

With penetration the soil around the pipe, especially the soil near the invert of the pipe, is significantly displaced. This type of large deformation behavior of soil can be simulated well using CEL approach as used in this study. Figure 3.5 shows the velocity vectors of the soil around the pipe at two depths of embedment ($w/D = 0.18$ and 0.25) for smooth and rough interface conditions. The numerical prediction has been compared with centrifuge test results (Dingle et al., 2008). In centrifuge, the images were captured using a digital camera and conducted PIV photogrammetric analyses to obtain velocity fields. The velocity distribution obtained from the present study is very similar to the velocity fields obtained in centrifuge tests using image capture technique. Figure 3.5 also shows that the soil particle movement is higher only in the failure zone near the pipe and outside that zone the particle velocity is reduced. That means, the vertical resistance V mainly depends upon the shear strength of the soil in this failure zone.

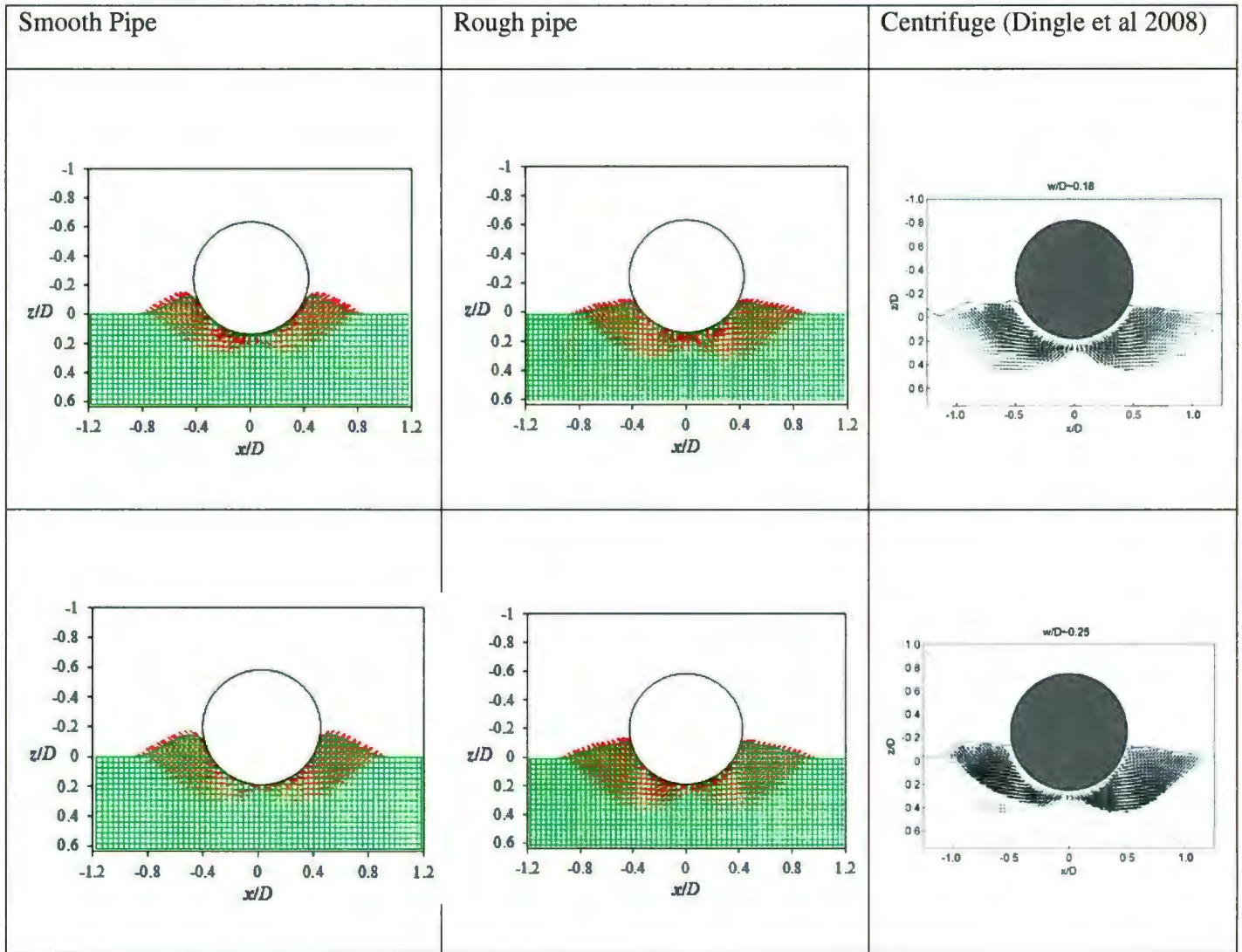


Fig. 3.5 Predicted and observed velocity vectors at different depth of penetration

3.10 Strain in Soil Mass

Figure 3.6 shows the variation of equivalent plastic strain ($\epsilon^{pl} = \sqrt{\frac{2}{3}} \epsilon^{pl}$, where ϵ^{pl} is the plastic strain) around the pipe at $w/D=0.45$. As shown, significant shear strain

developed near the pipe. The maximum equivalent plastic strain in case of rough pipe is higher than that of smooth pipe.

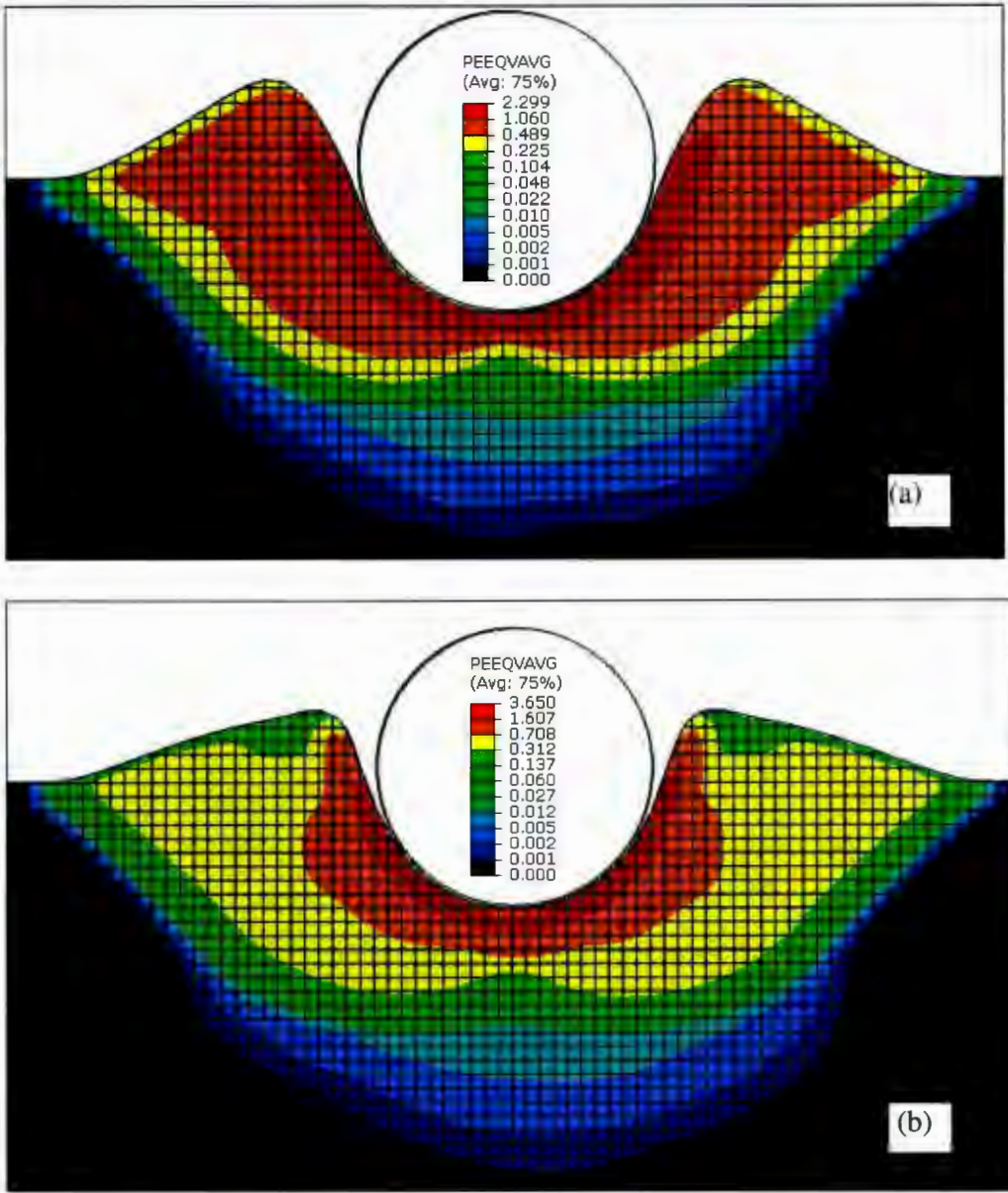


Fig. 3.6 Equivalent plastic strain around the pipe at $w/D=0.45$: (a) smooth (b) rough

3.11 Berm Development Mechanism

Figure 3.7 shows a typical image of pipe penetration observed in the centrifuge tests (Dingle et al., 2008). The size of the soil berm formed on both sides of the pipe depends on soil properties, depth of penetration and soil-pipe interface behavior.



Fig. 3.7 Vertical penetration and berm formation (Dingle et al., 2008)

Figure 3.8 shows the predicted berm size using the finite element model presented above. The height of the berm for smooth pipe is slightly higher than that of rough pipe. On the other hand, the lateral extent of the berm is higher for rough pipe. The predicted berm size using the numerical model compares well with centrifuge test (Dingle et al., 2008) results for the cases analyzed in this study.

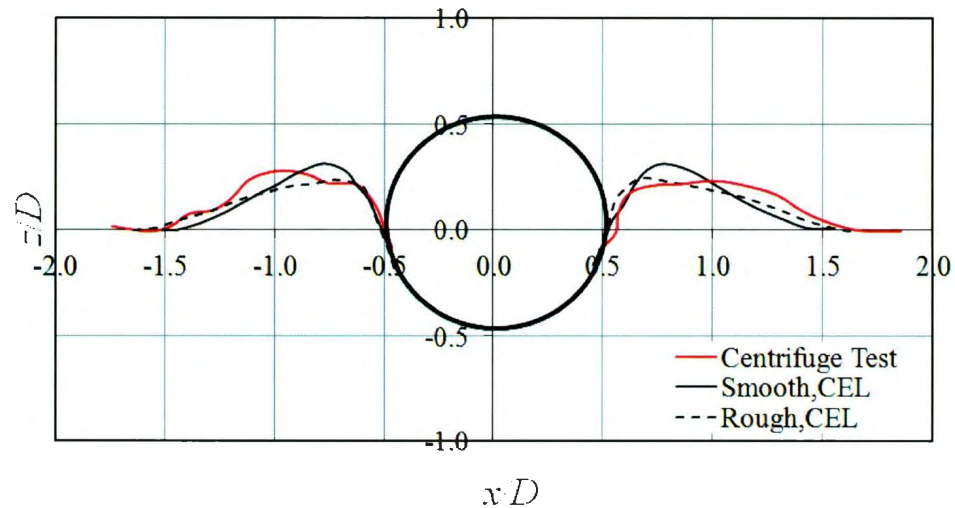


Fig. 3.8 Predicted and observed berm size at $w/D=0.45$

3.12 Conclusions

The process of vertical penetration of on-bottom offshore pipelines in deep sea is analyzed in this study. Offshore pipeline penetration in seabed is a large deformation problem. Coupled Eulerian Lagrangian (CEL) approach, recently incorporated in ABAQUS FE software, is used for numerical modeling of this process. Comparison with available model test results using a geotechnical centrifuge shows that ABAQUS CEL can successfully model such very large deformation problems. These analyses provide some valuable insights into soil failure and berm formation mechanism.

Although the present study shows the capability of CEL for modeling offshore pipeline embedment, the research with advanced soil constitutive model for various loading conditions is in progress.

3.13 Acknowledgements

The work presented in this paper has been funded by MITACS, C--CORE and NSERC Discovery grant. The authors also express their sincerest thanks to Mr. John Barrett at C-CORE for his valuable suggestions in finite element analysis.

3.14 References

ABAQUS Version 6.10-EF1 Documentation.

Brown, KH, Burns, SP and Christon, MA (2001). "Coupled Eulerian Methods for Earth Penetrating Weapon Applications," A report prepared by Sandia National Laboratory.

Cheuk, CY and White, DJ (2011). "Modeling the Dynamic Embedment of Seabed Pipelines," *Geotechnique* 61(1): 39-57.

Dingle, HRC, White, DJ & Gaudin, C (2008). "Mechanisms of Pipe Embedment and Lateral Breakout on Soft Clay," *Canadian Geotechnical Journal*, 45(5): 636-652.

Karal, K (1977). "Lateral Stability of Submarine Pipeline," *Proceedings of the 9th Offshore Technology Conference, Houston, USA.* OTC 2967.

Lyons, CG (1973). "Soil Resistance to Lateral Sliding of Marine Pipelines," Proceedings of the 6th Offshore Technology Conference, Houston, USA. OTC 1876.

Merifield, R, White, DJ, and Randolph, MF (2008). "The Ultimate Undrained Resistance of Partially Embedded Pipelines," *Geotechnique* 58(6): 461-470.

Merifield, RS, White, DJ and Randolph, MF (2009). "Effect of Surface Heave on Response of Partially Embedded Pipelines on Clay," *Journal of Geotechnical and Geoenvironmental Engineering*, 135(6): 819-829.

Murff, JD, Wagner, DA and Randolph, MF (1989). "Pipe Penetration in Cohesive Soil," *Geotechnique* 39(2): 213-229.

Quiros, WG and Little, LR (2003). "Deepwater Soil Properties and Their Impact on the Geotechnical Program," Offshore Technology Conference, OTC 15262.

Randolph, MF and Houslby, GT (1984). "The Limiting Pressure on a Circular Pile Loaded Laterally in Cohesive Soil," *Geotechnique* 34(4): 613-623.

Small, SW, Tamburello, RD and Piasecky, PJ (1971). "Submarine Pipeline Support by Marine Sediments," Offshore Technology Conference, OTC 1357:309-318.

Verley, R and Lund, KM (1995). "A Soil Resistance Model for Pipelines Placed on Clay Soils," Proceedings of the International Conference on Offshore Mechanics and Arctic Engineering, Vol.5. Copenhagen, Denmark: Pipeline Technology, p.225-232.

Wang, D, White, DJ and Randolph, MF (2010). "Large Deformation Finite Element Analysis of Pipe Penetration and Large Amplitude Lateral Displacement," *Canadian Geotechnical Journal*, 47: 842-856.

Westgate, ZJ, Randolph, MF, White, DJ and Li, S (2010). "The Influence of Sea State on As Laid Pipeline Embedment: A case study," *Applied Ocean Research*, 32(3): 321-331.

Chapter 4

Strain Softening and Rate Effects on Soil Shear Strength in Modelling of Vertical Penetration of Offshore Pipelines

Co-Authorship: Chapter 4 is prepared according to the Guidelines for Manuscript-Format Theses in the Faculty of Engineering and Applied Science at Memorial University. This part of the research has been accepted for publication as: Dutta, S., Hawlader, B. and Phillips, R. (2012) "Strain Softening and Rate Effects on Soil Shear Strength in Modelling of Vertical Penetration of Offshore Pipelines," 9th International Pipeline Conference, IPC2012, September 24–28, 2012, Calgary, Alberta, Canada.

Most of the research work presented in this chapter was conducted by the first author. He also prepared the draft manuscript. The other two authors mainly supervised the research and reviewed the manuscript.

4.1 Abstract

Offshore pipelines play a vital role in the transportation of hydrocarbon. In deep seas, pipelines laid on the seabed usually penetrate into the soil a certain amount. These pipelines might experience significant lateral movement during the operational period. The resistance to lateral movement depends on vertical penetration and berm formation around the pipe. Vertical penetration is a large deformation problem. Finite element

modeling of vertical penetration of offshore pipelines in soft clay seabed in deep water is presented in this study. The modeling was performed using ABAQUS finite element software. Soil was modeled in an Eulerian framework and the pipe in a Lagrangian framework. Strain softening behavior and strain rate effects on undrained shear strength of clay was incorporated in ABAQUS FE software using user subroutines written in FORTRAN. The variation of undrained shear strength with depth is also considered. The results are compared with centrifuge test results and also with available solutions.

Keywords: Pipeline, Strain rate, Strain softening, Large deformation analysis.

4.2 Introduction

Demand for offshore oil and gas development has increased significantly over the last several decades. Industry is moving from shallow to deep water in search of oil and gas to meet the global demand for energy. One of the key components in offshore oil and gas development is pipelines. In deep sea, pipelines are often laid on the seabed. However, because of some other actions such as laying effects, hydrodynamic force and weight of the pipe and its contents, pipelines often penetrate partially into the seabed. Offshore pipelines are typically operated under high temperature and pressure which is required to ease the flow through the pipe and to reduce the wax formation. However, during maintenance and emergency shutdown the internal pressure and temperature are reduced. This causes cyclic lateral movement of the pipeline. High temperature and pressure can

generate axial stress along the pipeline which might cause lateral buckling of the pipeline if sufficient resistance to prevent the movement of the pipeline is not available. The vertical penetration/embedment of pipeline and formation of berms during penetration have a significant impact on lateral resistance.

Various models have been proposed for static pipeline penetration in the seabed. At first, the pipeline was modeled as a strip footing and vertical resistance was taken as the bearing capacity [16]. Since then, various attempts have been made to understand the mechanism of pipe embedment which includes theoretical works [e.g. 8, 12, 14], experimental work [e.g. 18], centrifuge modeling [e.g. 4, 6] and finite element modeling [2, 3, 9, 10, 17, 19]. One of the key issues in finite element modeling of pipe penetration is that it is fundamentally a large deformation problem and therefore typical finite element modeling in Lagrangian framework is not suitable. Another important issue is the modeling of soil behavior at large strain. With penetration, the soil around the pipeline undergoes significant plastic shear strain which could soften the soil element. Moreover, the pipelines usually penetrate the soil at much higher shear strain rates in the soil elements near the pipe as compared to the shear strain rate typically used in laboratory tests. Therefore, for successful modeling the strain-softening and strain rate effects on shear strength should be considered.

The main purpose of this study is to present modeling of offshore pipe embedment using a more advanced finite element tool based on Coupled Eulerian Lagrangian (CEL)

approach. In CEL, Eulerian material flows through the fixed mesh and therefore there is no mesh tangling issue at large deformation. The analyses are performed using ABAQUS FE software. The modeling is done in an undrained condition. The undrained shear strength of the soil is varied as a function of accumulated plastic shear strain and shear strain rate.

4.3 Problem Definition

Large deformation finite element (LDFE) is performed to have an insight into the soil behavior during pipe vertical penetration and its effects on vertical resistance during penetration. An offshore pipeline of diameter D is penetrated vertically at a constant velocity through the seabed to a certain depth as shown in Fig.4.1. It is assumed that the pipeline is infinitely long and hence the plane strain condition is used in the simulation. Soil is displaced during pipe vertical penetration and the berm is formed by the displaced soil mass. In normally consolidated clays, the insitu undrained shear strength (s_{u0}) increases near linearly with depth as $s_{u0} = s_{um} + kz$ where s_{um} is the undrained shear strength of clay at the mudline, k is the strength gradient and z is the depth of the soil element below seabed. The undrained shear strength is updated during the analyses as a function of strain rate and accumulated plastic shear strain as discussed in the following sections. von Mises yield criterion is adopted.

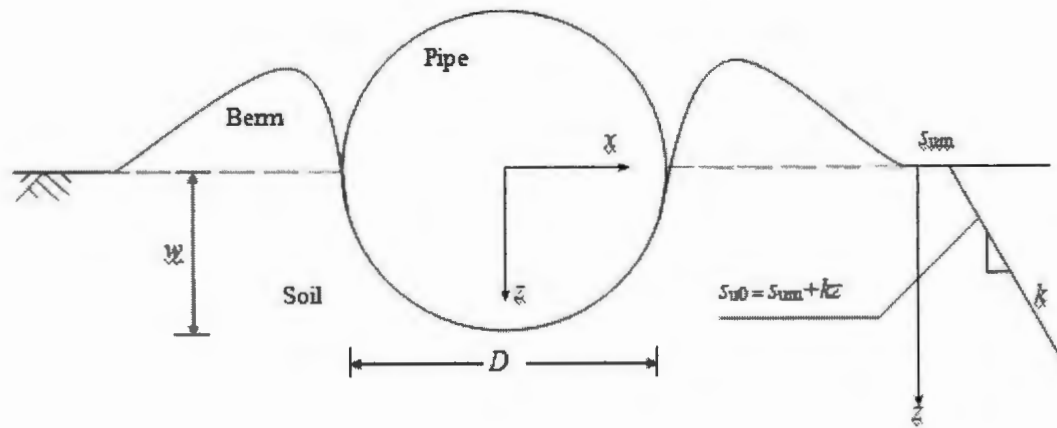


Fig. 4.1 Problem definition

4.4 Strain Rate and Strain Softening Effects on Undrained Shear Strength of Clay

In general, deep sea sediments are normally consolidated soft clay [4, 13]. Undrained shear strength of clay depends on the rate of shearing. The undrained shear strength degradation depends upon the plastic shear strain magnitude. T-bar or spherical ball penetrometer can be used to capture the effects of strain rate and softening on undrained shear strength of clay [7]. In this study, the following empirical model proposed by Einav and Randolph (2005) and Zhou and Randolph (2009) has been used.

$$s_u = \left[1 + \mu \log \left\{ \frac{\max(\dot{\gamma}, \dot{\gamma}_{ref})}{\dot{\gamma}_{ref}} \right\} \right] \left[\delta_{rem} + (1 - \delta_{rem}) e^{-3\xi/\xi_n} \right] s_{u0} \quad (4.1)$$

$$= [f_1] [f_2] s_{u0}$$

Here f_1 in the first square bracket represents the strain rate effect while f_2 in the second one represents the strain-softening effect; s_{u0} is the insitu shear strength at or below the

reference shear strain rate ($\dot{\gamma}_{ref}$) and prior to any softening; μ is the rate of undrained strength increase per log cycle; δ_{rem} is the ratio of remoulded to insitu shear strength which is the inverse of remoulded sensitivity S_t ; ξ is the accumulated absolute plastic shear strain; and ξ_{95} is the value of ξ at which soil has undergone 95% reduction in shear strength due to remolding.

4.5 Finite Element Model

ABAQUS 6.10 EF-1 is used to perform the large deformation finite element (LDFE) analysis of vertical penetration of offshore pipelines. Note that, conventional finite element technique in Lagrangian approach cannot handle large deformation problem due to convergence issues and mesh distortions. These issues are solved in the recently developed novel approach in Coupled Eulerian Lagrangian (CEL) technique. In CEL, the mesh is fixed and material can flow through the mesh. Thus, CEL can overcome the problems associated with mesh tangling and convergence and therefore it is adopted in the present study.

For finite element modeling, the pipe is modeled using Lagrangian framework whereas the soil is modeled in an Eulerian framework. The pipeline is modeled as a rigid body since the deformation is negligible in comparison with soil, which also makes the model computationally more efficient. The pipe is modeled using shell element and element type of S4R. The soil layer is modeled using Eulerian element EC3D8R, which is an 8-noded linear brick, multi-material, reduced integration with hourglass control.

The pipe is penetrated into the clay layer (Eulerian materials) to a desired depth and a berm is formed from displaced soil. One of the key features of CEL is that the space is required to be defined to accommodate the displaced soil—the berm in this case. Soil and void spaces are created in Eulerian domain using Eulerian Volume Fraction (EVF). For void space EVF is zero (i.e. no Eulerian material, soil in this case). On the other hand, EVF is unity in clay layer, meaning that these elements are filled with Eulerian material.

Velocity boundary conditions are provided at all faces of the Eulerian domain (Fig.4.2) to make sure that Eulerian materials are within the domain and cannot move outside. However, at seabed-void interface, no boundary condition is provided so that the soil can flow to the void. That means, the bottom of the model (Fig. 4.2) is restrained from any vertical movement, while all the vertical faces are restrained from any lateral movement.

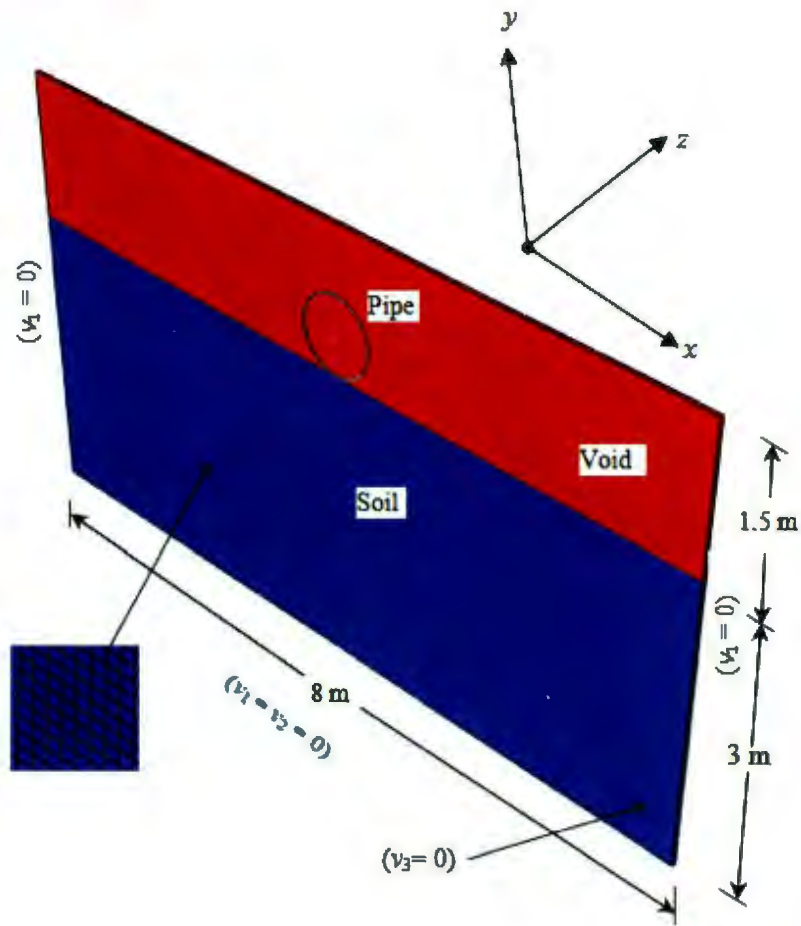


Fig. 4.2 Finite element model used in this study

A displacement boundary condition is applied at the reference point of the pipe to move it vertically downward and penetrated into the soil to a desired depth. As CEL can generate only 3D model, plane strain condition is simulated by considering single element along the axial direction of the pipe. It makes the model computationally less expensive.

One of the limitations of ABAQUS FE software is that it cannot incorporate the linear variation of initial undrained shear strength of clay (s_{u0}) with depth as shown in Fig. 4.1

using graphical user interface or from input file. Moreover, ABAQUS does not have any direct option for modeling the soil behavior using a strain-softening and strain-rate dependent soil constitutive model as shown in Eq.4.1. In this study, the soil model is implemented using a user subroutine. The subroutine is written in FORTRAN. The accumulated plastic shear strain is read in each time increment and the values of f_1 and f_2 in Eq. 4.1 are calculated. Then the value of s_u is calculated, which is returned as an input parameter for numerical analysis.

The total analysis is divided into three time steps to capture the soil behavior accurately during pipe vertical penetration. First step is the geostatic step. In geostatic step, pipe is located $\frac{1}{2} D$ above the sea bed to avoid any interaction with seabed. In the second step, the pipe is moved downward vertically to the seabed. In the third step, the pipe is further moved vertically through the seabed. The pipe is penetrated vertically to the maximum depth of embedment of $0.45D$ at a velocity of $0.015D/s$ which is same as the centrifuge test [6].

4.6 Parameter Selection

Table 4.1 shows the geometry and mechanical properties of soil and pipe. As shown in Fig. 4.2, a domain of $8m \times 4.5m \times 0.04m$ (length \times height \times thickness) is considered in finite element analysis. The pipe is placed at mid-length to avoid any boundary effect. The soil is modeled as an elastic-perfectly plastic, strain softening and strain rate dependent

material. The soil parameters used in this study are obtained from Dingle et al. (2008) and Cheuk and White (2011).

Table 4.1 Geometry and parameters used in the analyses

Pipe	
Pipe diameter, D	800 mm
Depth of penetration, w	360 mm
<i>Soil (Clay)</i>	
Undrained modulus of elasticity, E_u	$500s_u$
Poisson's ratio, ν_u	0.49
Undrained shear strength at mudline, s_{um}	2.3 kPa
Gradient of shear strength increase, k	3.6 kPa/m
Submerged unit weight of soil, γ	6.5 kN/m^3
Rate of shear strength increase, μ	0.1
Reference shear strain rate, $\dot{\gamma}_{ref}$	$3 \times 10^{-6} /s$
Remoulded soil sensitivity, S_r	3.2
Accumulate absolute plastic shear strain for 95% degradation of soil strength, ξ_{95}	10

4.7 Model Validation and Results

The finite element model is used to calculate the vertical resistance during the penetration of pipeline. As the vertical resistance depends on the mobilized value of s_u , the effects of strain rate and strain softening on s_u is also investigated.

4.7.1 Mesh sensitivity

Mesh size has a significant impact on finite element modeling. Often a finer mesh yields more accurate results but computational time is higher. In general, computational time in CEL is higher than the time required in typical finite element analysis using Lagrangian framework. The optimum mesh size is selected after conducting the analyses for a number of different mesh sizes. For example the calculation using three mesh sizes are shown in Fig. 4.3. In these analyses, the effects of strain softening or strain rate on undrained shear strength are not considered, but the strength does increase linearly with depth (Fig. 4.1). In this study, this condition is referred to as “ideal soil.” Figure 4.3 shows the variation of normalized reaction force ($V/s_{u0(i)}D$) with normalized depth of embedment (w/D), where $s_{u0(i)}$ is the undrained shear strength of clay at the invert of the pipe. Other parameters used in the analysis are listed in Table 4.1. The largest mesh ($0.25D$) gives erratic results, and calculated V is significantly higher than the other two cases especially for initial penetration. However, for the other two mesh sizes the calculated values give a smooth variation of V with depth. Hence a mesh size of $0.05D$ (i.e. $0.04 \text{ m} \times 0.04 \text{ m}$) is adopted for further analysis.

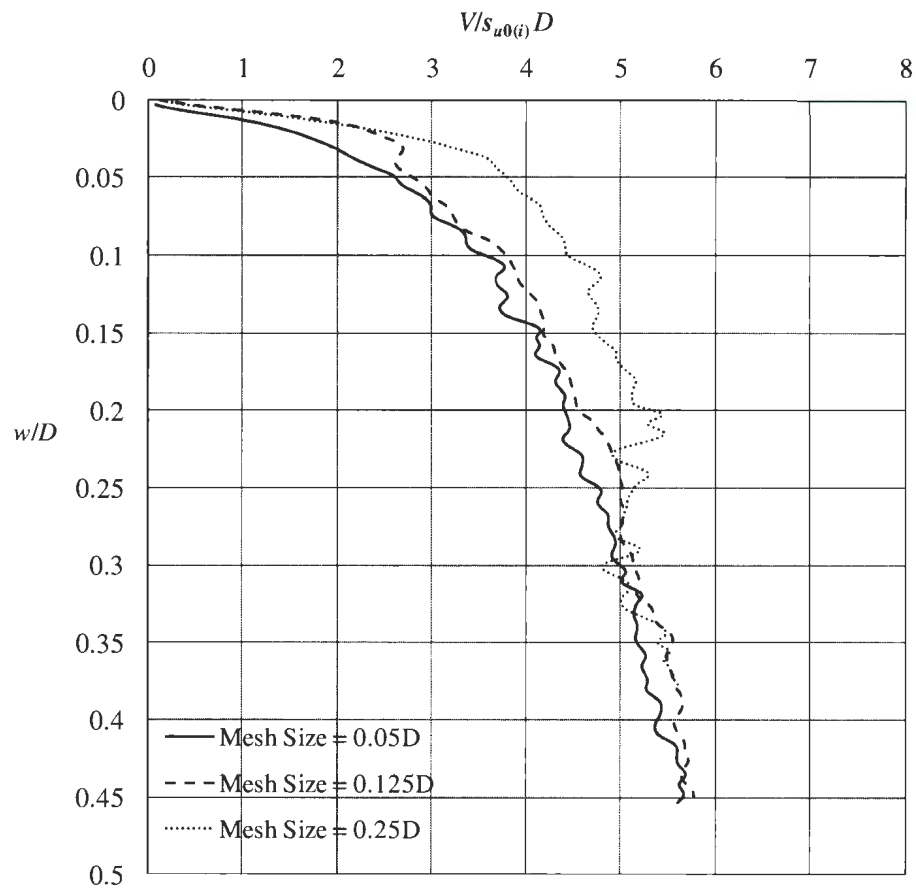


Fig. 4.3 Effect of mesh size on pipe vertical penetration resistance for smooth pipe-soil interface

4.7.2 Comparison with existing models

In the past, both static and dynamic penetrations of offshore pipelines have been investigated. In the present study, static penetration of the pipe is modeled. Several mathematical models are available in the literature for estimating vertical penetration

resistance. Some of them are based on model tests results [18] while some of them are developed from analytical or finite element modeling [e.g. 9, 10, 15, 19]. Finite element analysis of offshore pipeline embedment in pure Lagrangian framework with some limited success was presented by Aubeny et al. (2005) and Bransby et al. (2008). Merifield et al. (2009) conducted a series of large deformation finite element analysis using Arbitrary Lagrangian Eulerian (ALE) approach for uniform undrained shear strength of clay and proposed analytical solutions for estimating vertical resistance based on the numerical results. Tho et al. (2009) first demonstrated the use of Eulerian technique for modeling pipe embedment in seabed with an uniform undrained shear strength profile. Morrow and Bransby (2010) showed the effects of various undrained shear strength profiles of the seabed on vertical penetration resistance using FLAC 6.0 finite difference software. None of these previous studies [3, 11, 17] had considered strain softening or strain rate effects. Wang et al. (2010) conducted two-dimensional large strain finite element modeling using remeshing and interpolation technique with small strain (RITSS).

In order to show the performance of the present model, the calculated vertical penetration resistance has been compared with four recent studies namely Randolph et al. (2008), Merifield et al. (2009), Tho et al. (2009) and Wang et al. (2010). Based on an upper bound plasticity solution, Randolph et al. (2008) proposed a model to estimate vertical penetration resistance. The soil behavior is modeled as isotropic rigid plastic material with an undrained shear strength, which is uniform or proportional to depth.

Figure 4.4 shows the comparison between the present model for ideal soil (i.e. s_u proportional to depth) and the other four models. Analyses are performed both for smooth (Fig. 4.4a) and rough (Fig. 4.4b) pipe-soil interface conditions. As shown, the calculated vertical resistance at a given depth of penetration using the present model is higher than the values obtained from previous models. However, the use of Tresca criterion gives closer results to the previous studies. An average undrained shear strength of 3 kPa was used for Merifield et al. (2009).

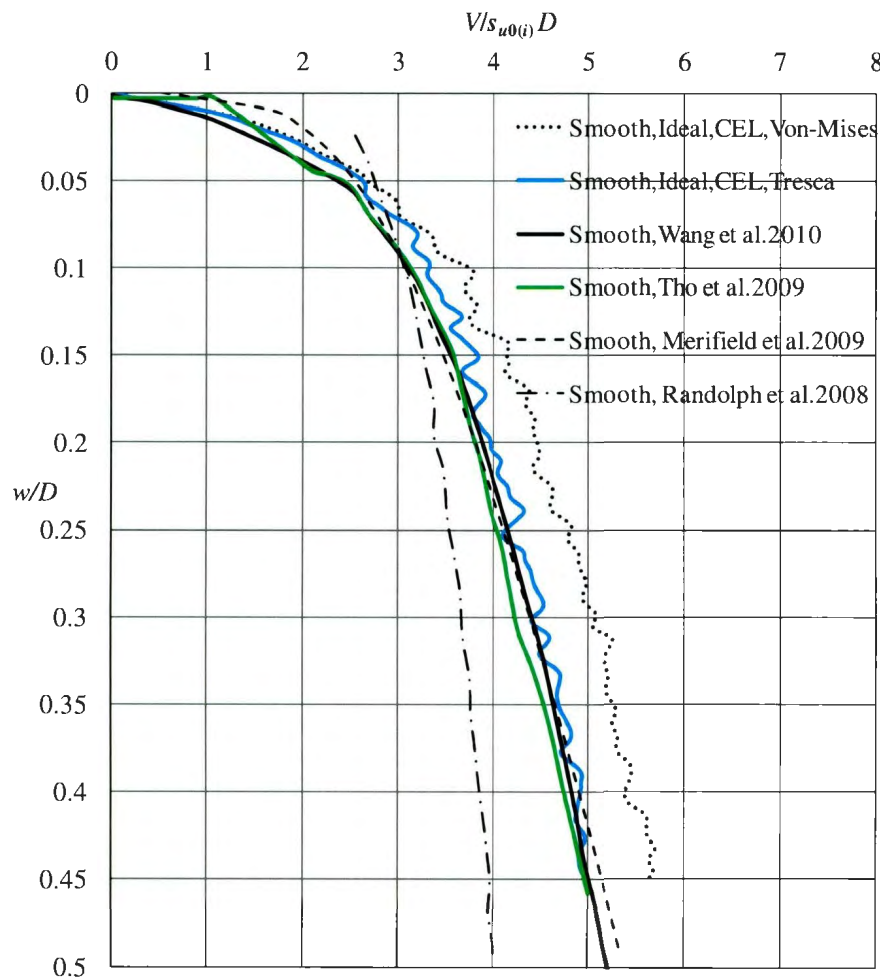


Fig. 4.4(a) Comparison with previous solutions for smooth pipe-soil interface

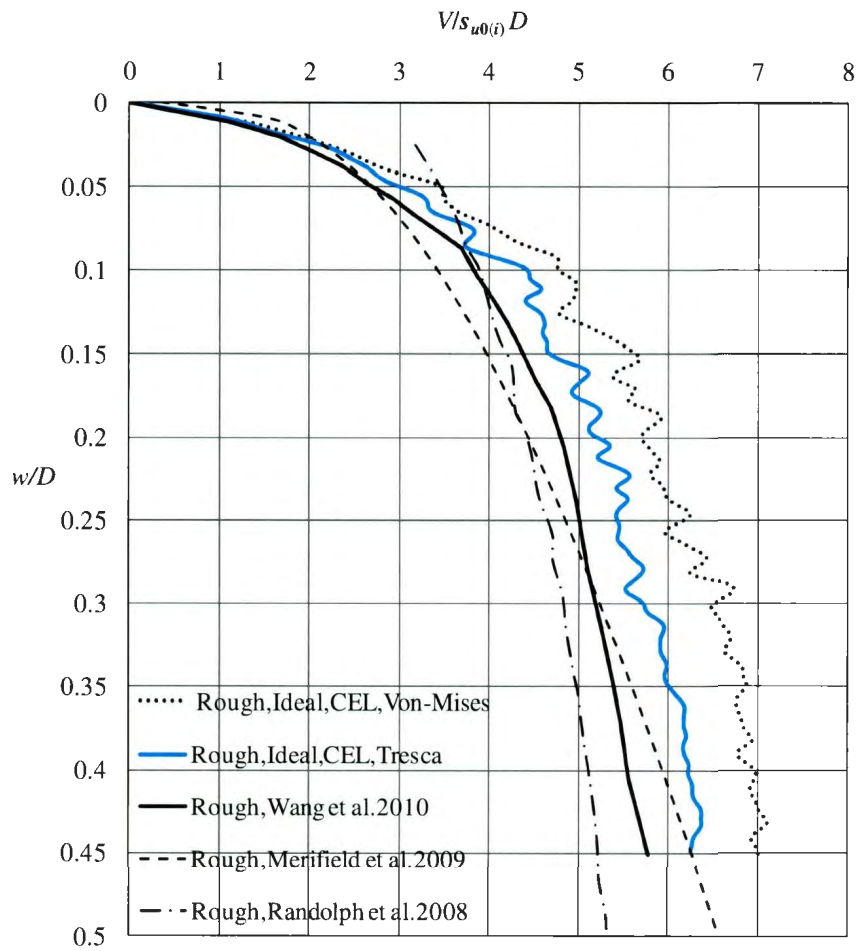


Fig. 4.4(b) Comparison with previous solutions for rough pipe-soil interface

4.8 Effect of Strain Softening and Strain Rate

The results presented above are for ideal soil, that means without any strain rate or strain softening effects. In the following sections the effects of strain softening and strain rate are presented.

4.8.1 Comparison with centrifuge test results

Dingle et al. (2008) performed a series of centrifuge tests to simulate the behavior of a section of partially embedded pipeline. A model pipe of 0.8 m prototype diameter was penetrated into a soft clay bed. Figure 4.5 shows the comparison between numerical prediction and centrifuge test results. The soil parameters used in the analyses are shown in Table 4.1. As shown in Fig. 4.5, the centrifuge test result is between the calculated values using smooth and rough pipe-soil interface conditions. It is to be noted here that the authors also compared the centrifuge test results using ideal soil conditions [5]. For comparison the reaction vs. penetration curves for ideal soil condition are also shown in this figure. As shown in Eq. 4.1, the strain rate in general increases but softening effect reduces the shear strength of the soil. The combined effects of these two govern the vertical resistance. The strain rate and strain softening parameters used in this study effectively increase the shear strength. Therefore, penetration resistance is increased when strain rate and strain softening effects are considered.

4.8.2 Plastic strain in soil mass

Equivalent plastic shear strain around the pipe at the depth of penetration of $0.45D$ is shown in Fig. 4.6 for both smooth and rough pipe-soil interface conditions. The strain contour interval is in logarithmic scale. As shown, significant plastic shear strain is developed near the pipe, which decreases with distance from the pipe. The maximum equivalent plastic shear strain in the case of rough pipe is higher than that of smooth pipe.

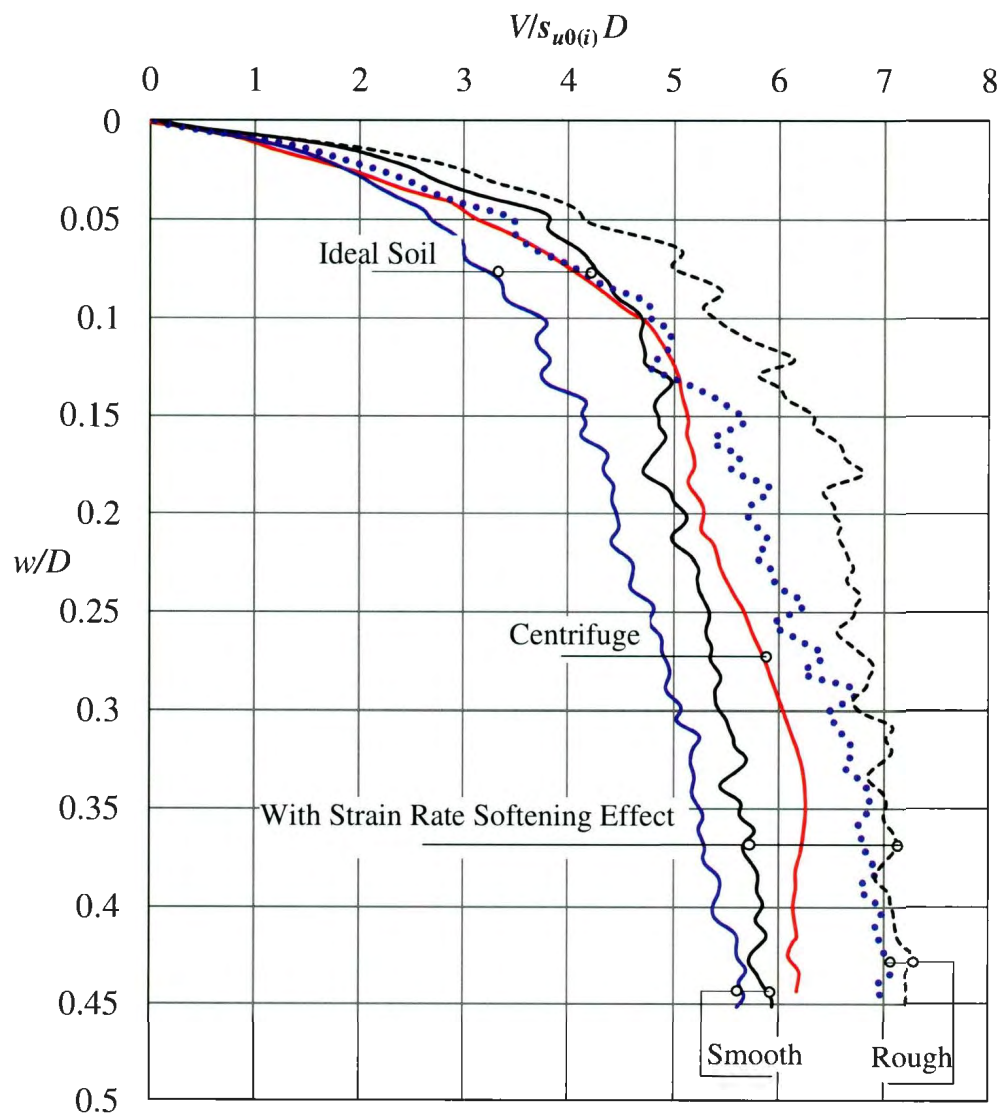


Fig. 4.5 Comparison between finite element and centrifuge test results

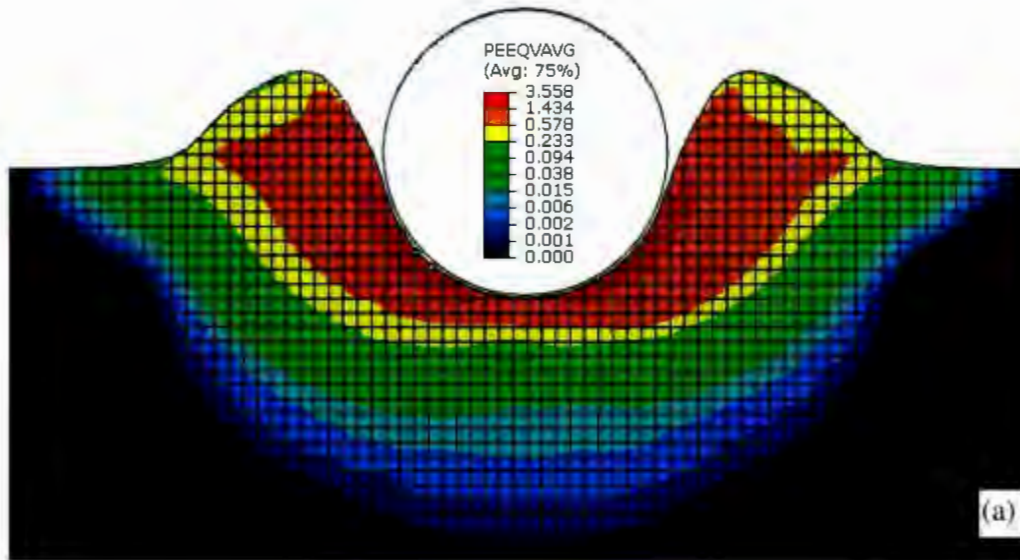


Fig. 4.6(a) Equivalent plastic shear strain around the pipe at $w/D = 0.45$ for smooth pipe-soil interface

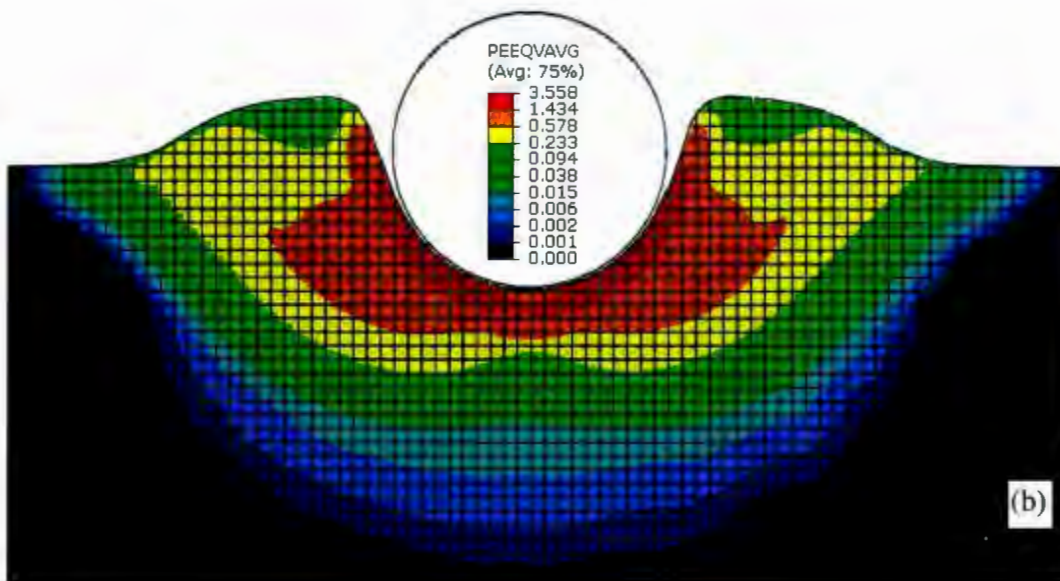


Fig. 4.6(b) Equivalent plastic shear strain around the pipe at $w/D = 0.45$ for rough pipe-soil interface

4.9 Parametric Study

Equation 4.1 shows that mainly three parameters (μ , S_r and ξ_{95}) define the effects of strain softening and strain rate. The effect of these parameters on vertical penetration resistance is examined in this section. In the parametric study only one of these three parameters is varied keeping other soil parameters the same as ideal soil condition.

4.9.1 Effect of μ

As shown in Eq. 4.1 the strain rate effect on shear strength mainly depends on the value of μ , which is typically varied between 0.05 and 0.2 [7]. Figure 4.7 shows the normalized vertical resistance with normalized depth of penetration of the pipe for three different values of μ (0, 0.1 and 0.2) with no softening effects. Note that, $\mu=0$ means no strain rate effect on undrained shear strength. As shown, the higher the value of μ , the higher the vertical resistance as the mobilized undrained shear strength is increased.

4.9.2 Effect of S_r

Figure 4.8 shows the effect of remoulded sensitivity (S_r) on vertical penetration resistance with no strain rate effects. Three different values of S_r (1, 3.2 and 4) are considered. As shown, the $V/s_{u0(i)}D$ vs. w/D curve shifts to the left with an increase in S_r . Figure 4.8 also shows that the calculated vertical resistance is not very sensitive to the value of S_r . This is because of the fact that the undrained shear strength reduced significantly only in a small zone of soil near the pipe where large plastic shear strain is developed.

4.9.3 Effect of ξ_{95}

Figure 4.9 shows the effect of accumulated plastic shear strain on vertical penetration resistance with no strain rate effects. Einav and Randolph (2005) suggested that ξ_{95} could vary between 10 and 50 (1000% to 5000%). Figure 4.9 shows the variation of $V/s_{u0(i)}D$ with w/D . As expected, vertical reaction is higher for higher value of ξ_{95} .

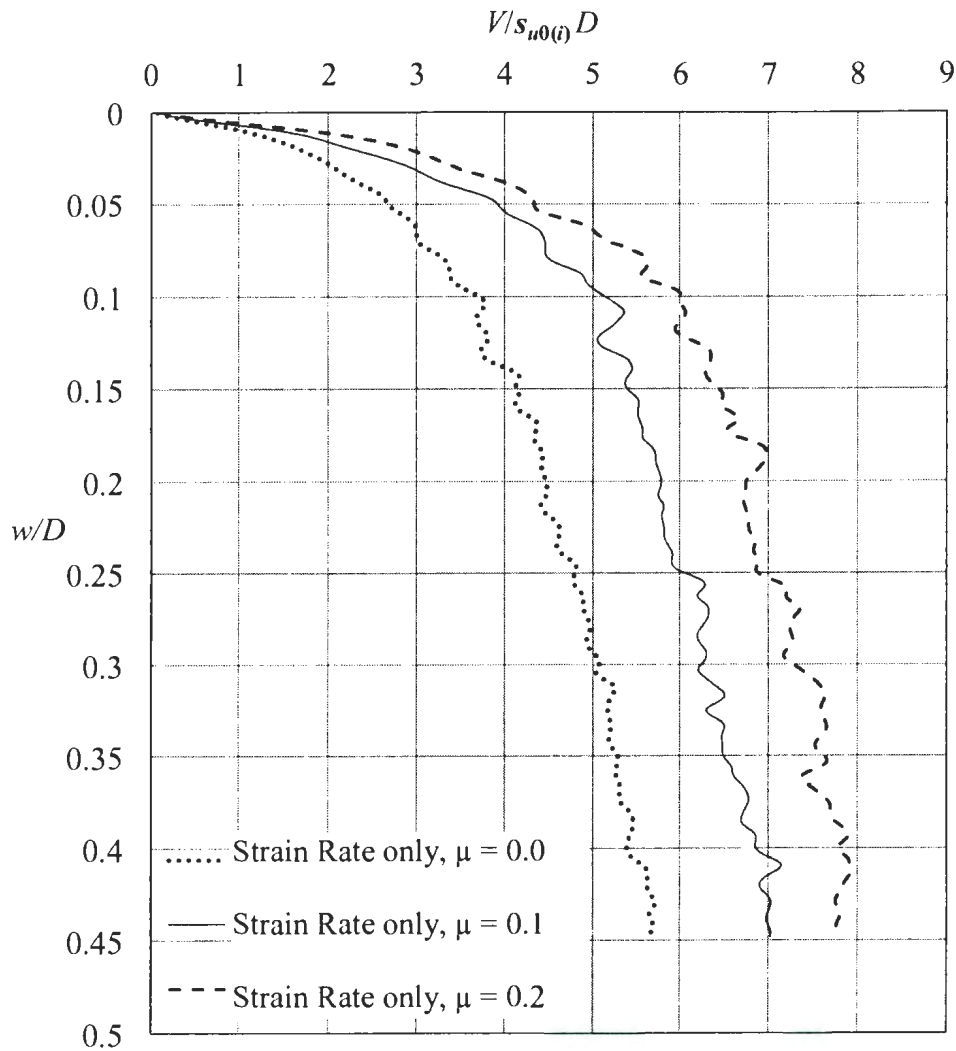


Fig. 4.7 Effect of strain rate parameter, μ for smooth pipe-soil interface

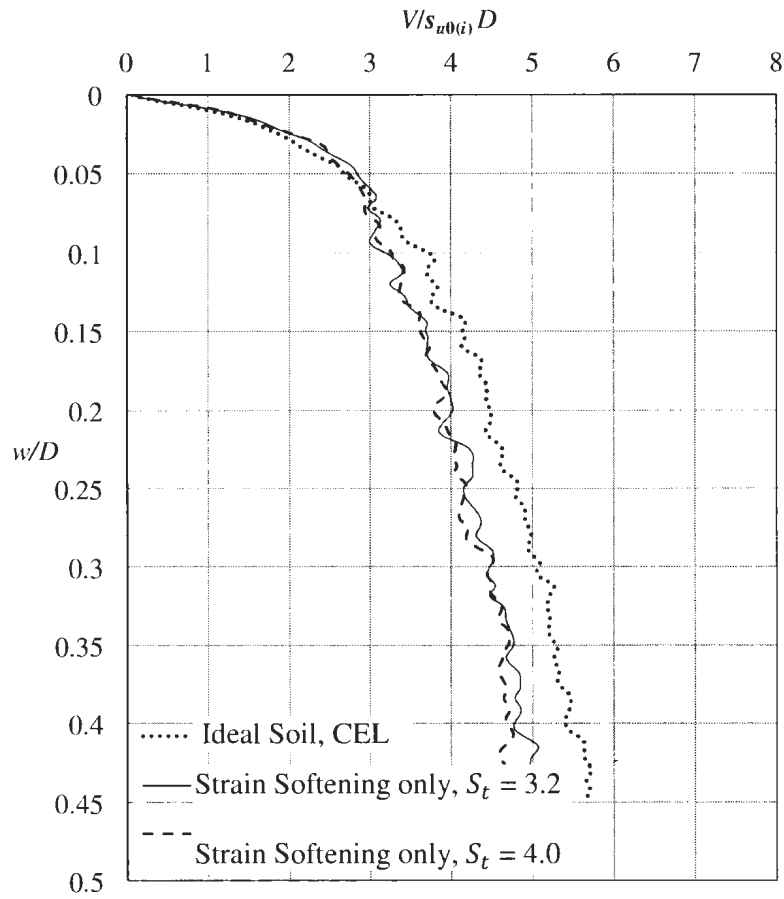


Fig. 4.8. Effect of remoulded sensitivity, S_t for smooth pipe-soil interface.

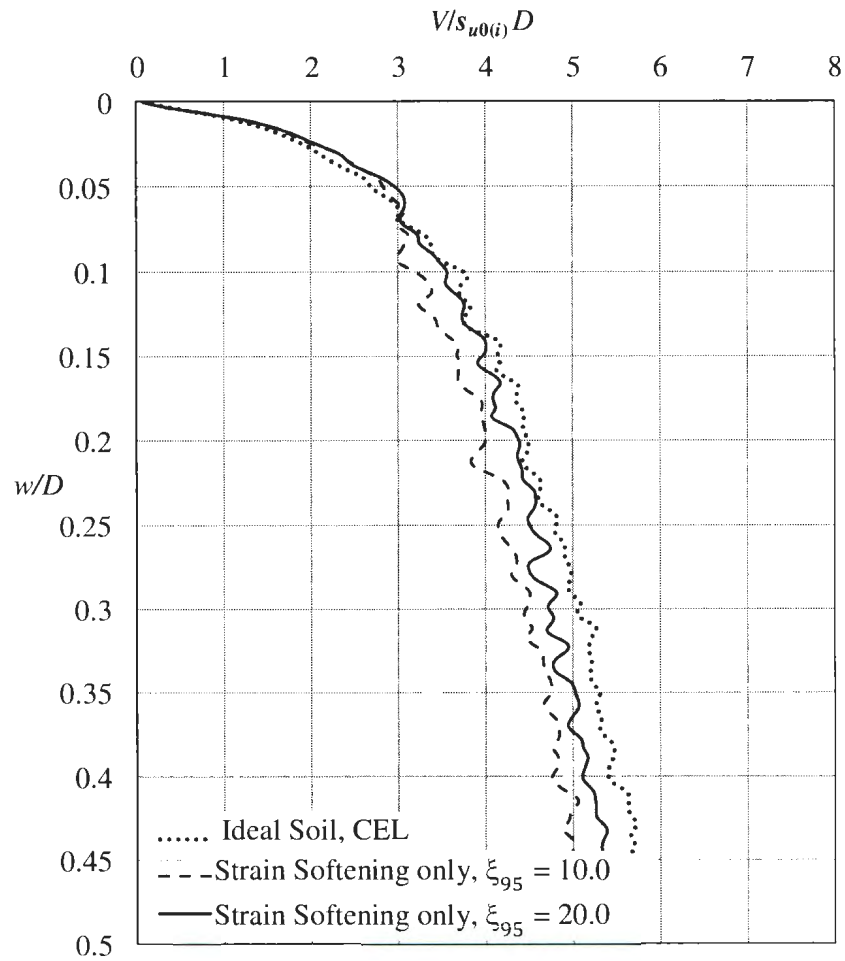


Fig. 4.9. Effect of strain softening parameter, ξ_{95} for smooth pipe-soil interface

4.10 Conclusion

Large deformation finite element (LDFE) is adopted to analyze the vertical penetration of offshore pipelines at seabed. The Coupled Eulerian Lagrangian (CEL) method currently available in ABAQUS finite element software was used for the numerical analysis. A strain rate and plastic shear strain dependent model of undrained shear strength is implemented into ABAQUS using a user subroutine. The current CEL analysis with

strain rate and strain softening effects shows higher penetration resistance compared to ideal soil with a linear variation of undrained shear strength and also to the previous studies. Further calibration of the model and its application to offshore pipeline design is in progress. The analyses also indicates that the strain rate effect on vertical penetration resistance is more significant than remoulded sensitivity or strain softening parameter (ξ).

4.11. Acknowledgments

The work presented in this paper has been funded by MITACS, C-CORE and NSERC Discovery grant. The authors also express their sincerest thanks to Mr. John Barrett at C-CORE for his valuable suggestions in finite element analysis.

4.12. References

- [1] ABAQUS Version 6.10-EF1 Documentation.
- [2] Aubeny, C. P., Shi, H., and Murff, J. D., 2005, "Collapse Loads for a Cylinder Embedded in Trench in Cohesive Soil," *International Journal of Geomechanics*, 5(4), pp. 320-325.
- [3] Bransby, M.F., Zajac, P., and Amman, S., 2008, "Finite Element Analysis of the Vertical Penetration of On-bottom Pipelines in Clay," 18th International Offshore and Polar Engineering Conference, Vancouver, BC, Canada, pp.245-249.

- [4] Cheuk, C. Y., and White, D. J., 2011, "Modeling the Dynamic Embedment of Seabed Pipelines," *Géotechnique* 61(1), pp. 39-57.
- [5] Dutta, S., Hawlader, B., and Phillips, R., 2012, "Finite Element Modeling of Vertical Penetration of Offshore Pipelines using Coupled Eulerian Lagrangian Approach," Proceedings of 22nd Int. Off. and Polar Engineering Conference & Exhibition, Rhodes, Greece, June 17–22, 2012(2012-TPC-0626).
- [6] Dingle, H. R. C., White, D. J., and Gaudin, C., 2008, "Mechanisms of Pipe Embedment and Lateral Breakout on Soft Clay," *Canadian Geotechnical Journal*, 45(5), pp. 636-652.
- [7] Einav, I., and Randolph, M. F., 2005, "Combining Upper Bound and Strain Path Methods for Evaluating Penetration Resistance". *International Journal for Numerical Methods in Engineering*, Vol. 63, No. 14, pp. 1991-2016.
- [8] Karal, K., 1977, "Lateral Stability of Submarine Pipeline," Proceedings of the 9th Offshore Technology Conference, Houston, USA.OTC 2967.
- [9] Merifield, R., White, D. J., and Randolph, M. F., 2008, "The Ultimate Undrained Resistance of Partially Embedded Pipelines," *Géotechnique* 58(6), pp. 461-470.
- [10] Merifield, R. S., White, D. J., and Randolph, M. F., 2009, "Effect of Surface Heave on Response of Partially Embedded Pipelines on Clay," *Journal of Geotechnical and Geoenvironmental Engineering*, 135(6), pp. 819-829.
- [11] Morrow, D.R., and Bransby, M.F., 2010, "Pipe-Soil Interaction on Clay with a Variable Shear Strength Profile," *Frontiers in Offshore Geotechnics II*, pp.821-826.

- [12] Murff, J. D., Wagner, D. A., and Randolph, M. F., 1989, "Pipe Penetration in Cohesive Soil," *Géotechnique* 39(2), pp. 213-229.
- [13] Quiros, W. G., and Little, L. R., 2003, "Deepwater Soil Properties and Their Impact on the Geotechnical Program," Offshore Technology Conference, OTC 15262.
- [14] Randolph, M. F., and Houslby, G. T., 1984, "The Limiting Pressure on a Circular Pile Loaded Laterally in Cohesive Soil," *Géotechnique* 34(4), pp. 613-623.
- [15] Randolph, M. F., and White, D. J., 2008, .Technical note. "Upper Bound Yield Envelopes for Pipelines at Shallow Embedment in Clay," *Géotechnique* 58(4), pp. 297-301.
- [16] Small, S. W., Tamburello, R. D., and Piaseckyj, P. J., 1971, "Submarine Pipeline Support by Marine Sediments," Offshore Technology Conference, OTC 1357, pp.309-318.
- [17] Tho, K.K., Leung, C.F., Chow, Y.K., and Swanddiwudhipong, S., 2009, "Application of Eulerian Finite Element Technique for Analysis of Spudcan and Pipeline Penetration into the Seabed," 12th Jack Up Conference, City University, London.
- [18] Verley, R., and Lund, K. M., 1995, "A Soil Resistance Model for Pipelines Placed on Clay Soils," Proceedings of the International Conference on Offshore Mechanics and Arctic Engineering, Vol.5. Copenhagen, Denmark: Pipeline Technology, pp.225-232.
- [19] Wang, D., White, D. J., and Randolph, M. F., 2010, "Large Deformation Finite Element Analysis of Pipe Penetration and Large Amplitude Lateral Displacement," *Canadian Geotechnical Journal*, 47, pp. 842-856.

Chapter 5

Lateral Movement of Partially Embedded Offshore Pipelines

5.1 Introduction

After successful installation of partially embedded pipelines in deep water, pipelines might experience problems regarding lateral stability. Lateral instability of pipelines occurs due to wave induced pressure (during severe storms), lay tension or pipeline internal temperature and pressure changes in oil and gas. For deep water pipeline, wave induced instability of pipelines is not significant (White and Cheuk, 2008). Lay tension from steel catenary shape formation during installation remains in the pipelines after installation. However, it cannot significantly affect lateral buckling of the pipeline under high temperature and pressure during the operational period (Bruton et al., 2008). Therefore, the lateral instability occurs mainly due to internal pressure and temperature changes. The lateral movement of the pipeline is mainly opposed by the resistance from soil and therefore the understanding of soil/pipe interaction is important. However, the modeling of such complex soil/pipe interaction problems is extremely difficult (Bruton et al., 2006).

Mitigation procedures for the pipeline lateral buckling includes snake lay, buried pipelines and sleeper systems. The choice of the appropriate techniques largely depends on the site specific data and the operational requirements. The current practice for a partially embedded pipeline is the controlled lateral buckling as discussed in Section 2.5

of Chapter 2. However, the estimation of pipe feed for buckle formation is very uncertain. In this chapter, numerical investigations are presented for light pipes under various conditions for lateral loading. The numerical results have been also compared with physical model test results.

5.2 Comparison between Numerical and Centrifuge Models

Dingle et al. (2008) conducted one centrifuge test to simulate the soil/pipe interaction behavior during lateral movement. The test was conducted in a seabed with a linearly varying undrained shear strength profile. Pipe was embedded to $0.45D$ and moved laterally. White and Dingle (2011) extended the work of Dingle et al. (2008) by conducting six more centrifuge tests (L1 to L6) for different initial embedment and applied vertical loads. In the centrifuge tests, Dingle et al. (2008) displaced the pipe laterally up to $3D$ whereas White and Dingle (2011) moved the pipe laterally up to $4D$. Residual friction factor between as-laid pipelines and seabed during pipe lateral movements was investigated. The test conditions including undrained shear strength profiles, applied vertical loads and initial depths of embedment are shown in Table 5.1.

The experimental works of Dingle et al. (2008) and six cases of White and Dingle (2011) are simulated in the present study using Coupled Eulerian Lagrangian (CEL) finite element technique. The roughness of the pipe surface has significant effects on both vertical and horizontal resistance. The maximum shear resistance at the pipe/soil interface in undrained loading is generally expressed as $\tau_{\max}=\alpha s_u$, where α is constant and a value

of $\alpha=0$ means fully smooth condition. Although this function is available in ABAQUS, it does not work properly in ABAQUS CEL. Therefore, analyses have been performed only for smooth and no-slip (rough) soil/pipeline interface conditions.

Table 5.1 Centrifuge test conditions (White and Dingle, 2011; Dingle et al., 2008).

Test	Initial Undrained shear strength of soil, kPa	Applied Vertical load, kN/m	Initial Embedment, $(w/D)_{int}$
D1	2.3+3.6×depth	3.39	0.45
L1	2.3+3.6×depth	2.1	0.52
L2	2.3+3.6×depth	2.8	0.46
L3	2.3+3.6×depth	1.0	0.25
L4	2.3+3.6×depth	3.2	0.18
L5	3.0+5.0×depth	2.1	0.02
L6	3.0+5.0×depth	4.4	0.05

Note:
D1: Test conducted by Dingle et al. (2008);
L1 to L6: Tests conducted by White and Dingle 2011;
depth: distance from mudline.

5.2.1 Vertical penetration

As shown in Table 5.1, the undrained shear strength profile of soil is the same in centrifuge tests by Dingle et al. (2008) and the L1 to L4 tests of White and Dingle (2011). However, the applied vertical loads and initial depths of embedment are different. The

rate of vertical penetration of the pipe was also the same for all these tests ($0.015D/s$). As the soil profile and rate of penetration is the same in these five tests, only one simulation is shown in the present study for a vertical penetration up to the maximum embedment of $0.52D$. The normalised vertical resistance with vertical embedment is shown in Fig. 5.1. The only vertical penetration resistance curve from a centrifuge test available in the literature is from Dingle et al. (2008), which is also shown in Fig. 5.1. The arrows on the right vertical axis show the depth of embedment from where lateral movement started. Other parameters used in the analysis are listed in Table 4.1. The strain-rate and strain softening model described in Section 4.4 is used to represent the undrained shear strength behaviour of soil. Vertical embedment for Cases-L5 and L6 are very small and are not shown.

5.2.2 Lateral movement

The seven centrifuge tests listed in Table 5.1 are simulated for pipe lateral displacement. The strain softening and strain-rate dependent soil model implemented in ABAQUS discussed in Section 4.4 is used. The other soil parameters are listed in Table 4.1. After penetration of the pipe to the desired depth the lateral displacement is applied under applied vertical load. For example, in Test L2 the pipe is penetrated vertically into the soil to a depth of $0.46D$, a vertical load of 2.8 kN/m is applied and then moved laterally under this applied vertical load giving a displacement boundary condition to the pipe. Figures 5.2 to 5.8 show the comparison between numerical and physical modelling results.

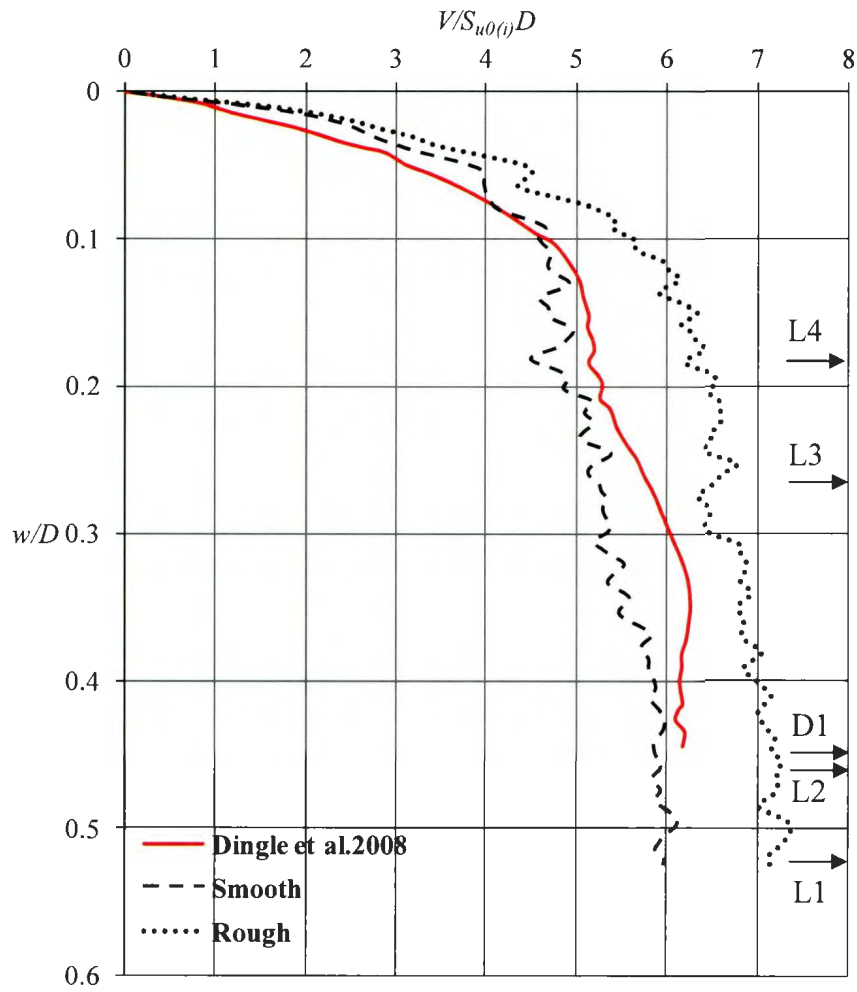


Fig. 5.1 Variation of pipe vertical penetration resistance with embedment depth.

5.2.2.1 Load displacement curves

Figures 5.2(a) to 5.8(a) show the developed lateral force (H) per unit length of the pipe with normalized lateral displacement (U_1/D). The lateral force increases first with lateral displacement and reaches a peak and then decreases gradually almost to a constant

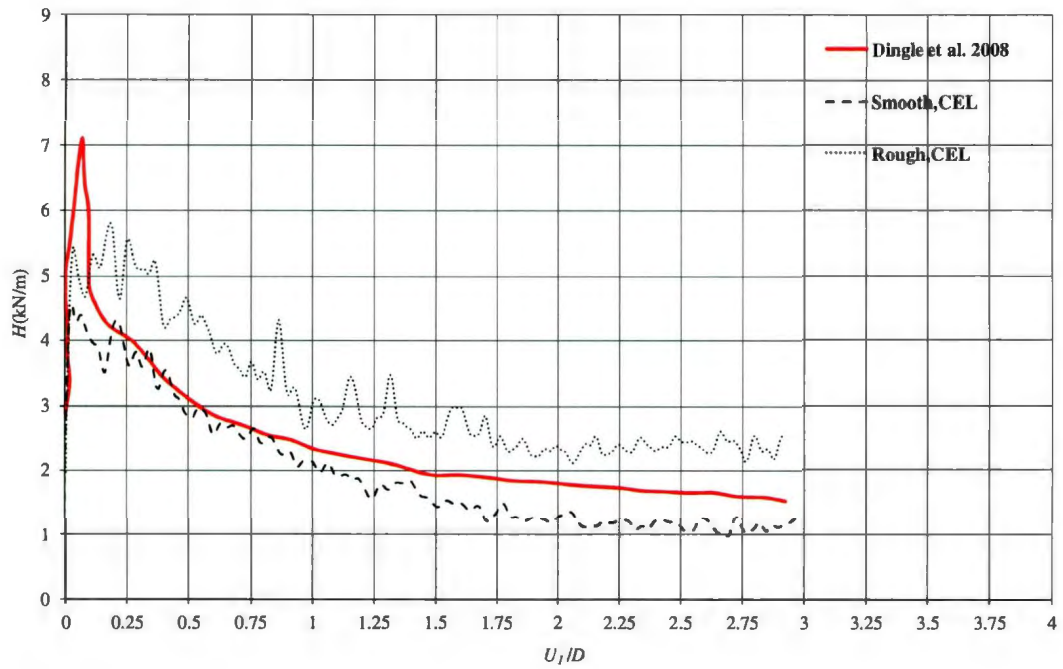


Fig. 5.2 (a) Pipe resistance during lateral movement (Case-D1: Dingle et al., 2008).

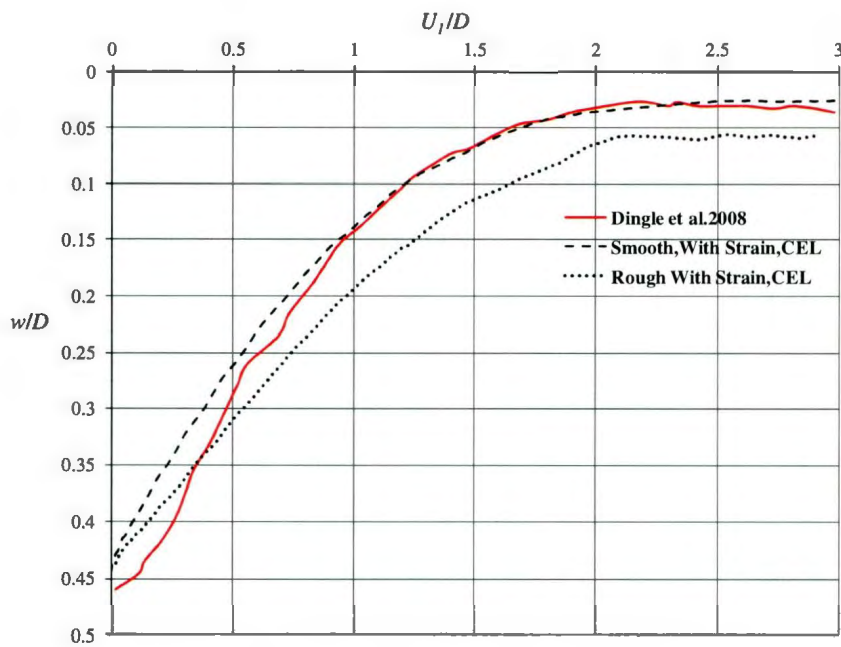


Fig. 5.2(b) Pipe invert trajectory (Case-D1: Dingle et al., 2008).

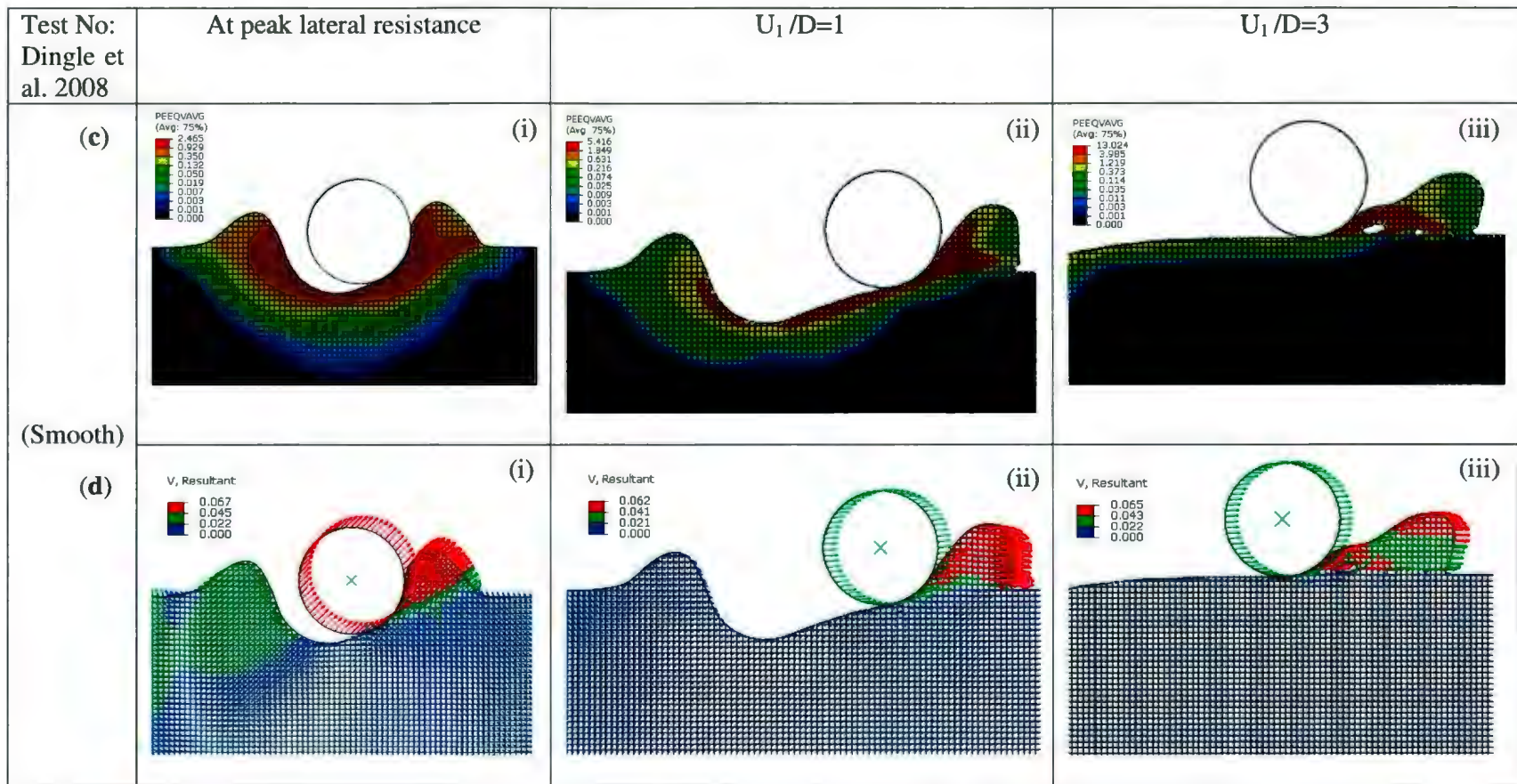


Fig. 5.2 (c) Equivalent plastic strain around pipeline and (d) Velocity field during pipe lateral movement at (i) breakout point (ii) lateral displacement of one pipe diameter (iii) lateral displacement of three pipe diameter.

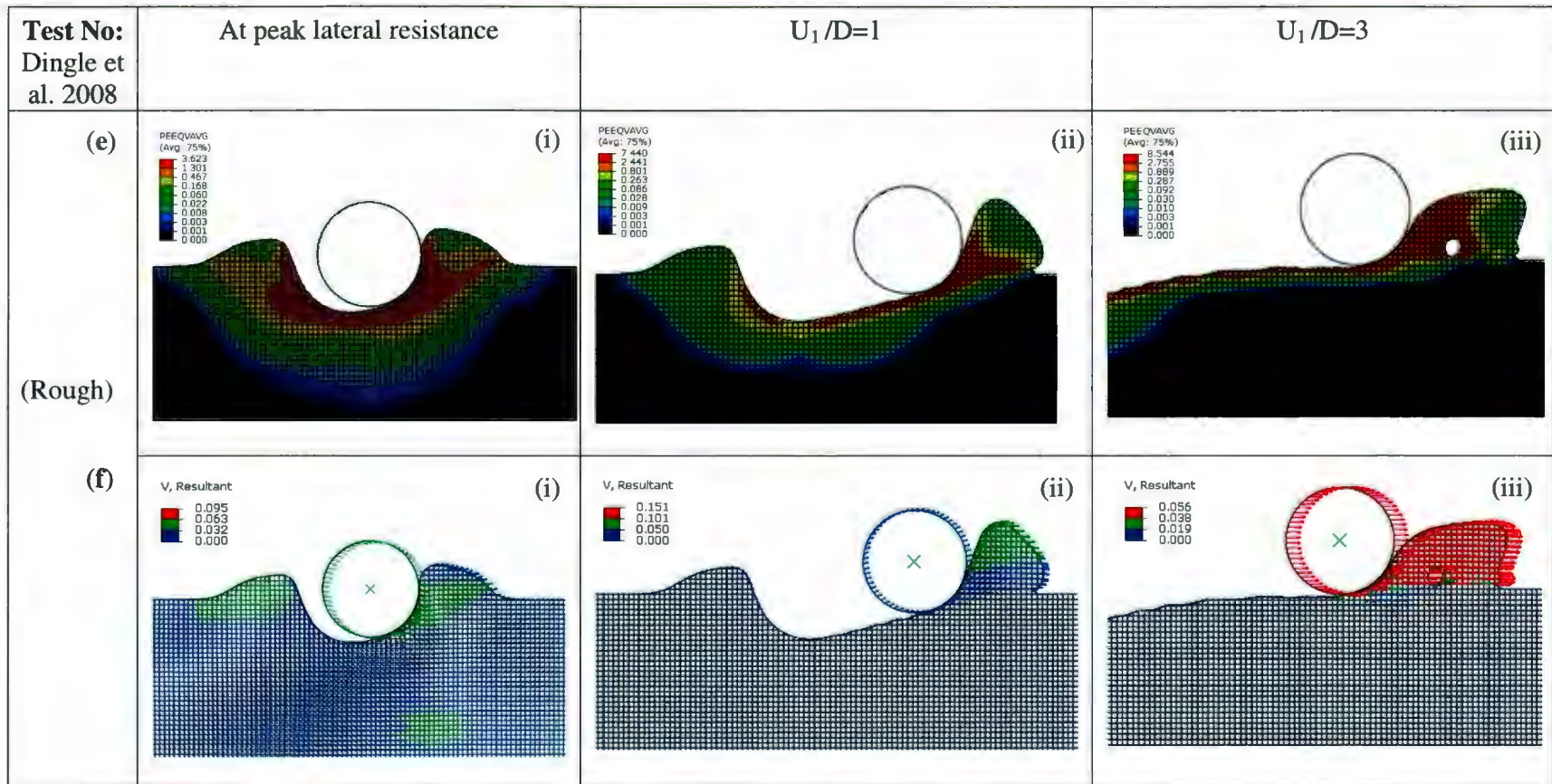


Fig. 5.2 (e) Equivalent plastic strain around pipeline and (f) Velocity field during pipe lateral movement at (i) breakout point (ii) lateral displacement of one pipe diameter (iii) lateral displacement of three pipe diameter.

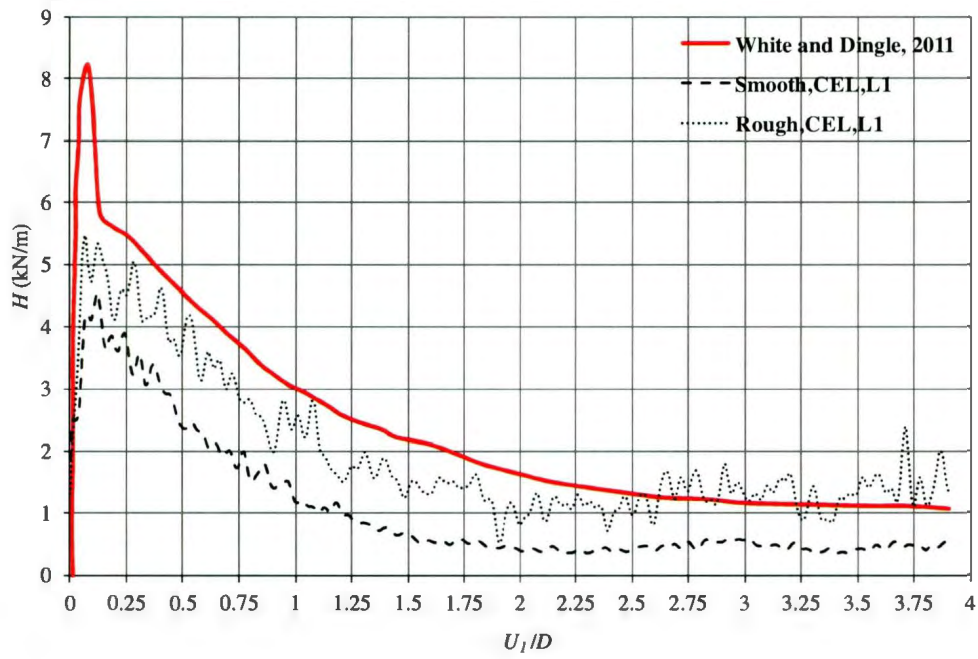


Fig. 5.3(a) Pipe resistance during lateral movement (Case-L1).

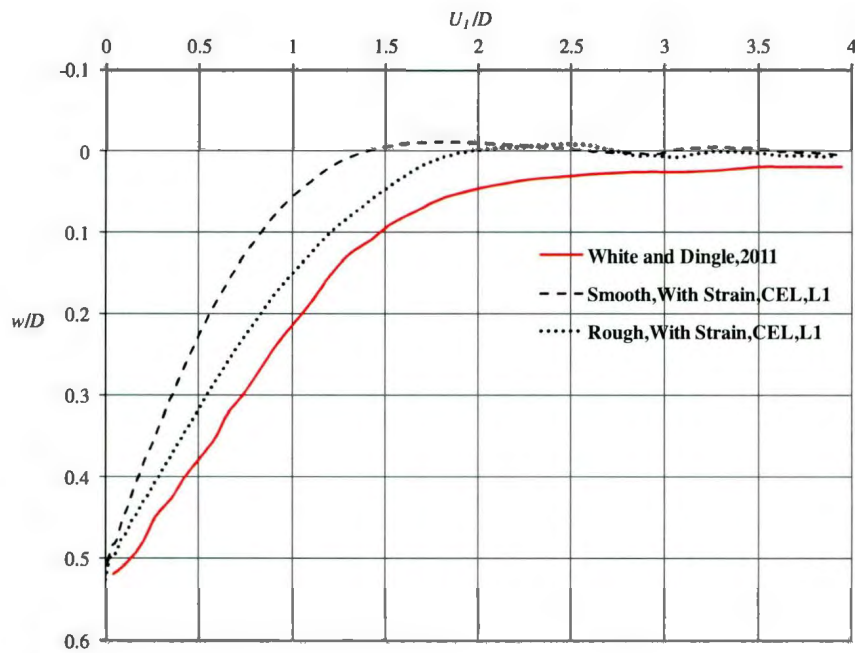


Fig. 5.3(b) Pipe invert trajectory (Case-L1).

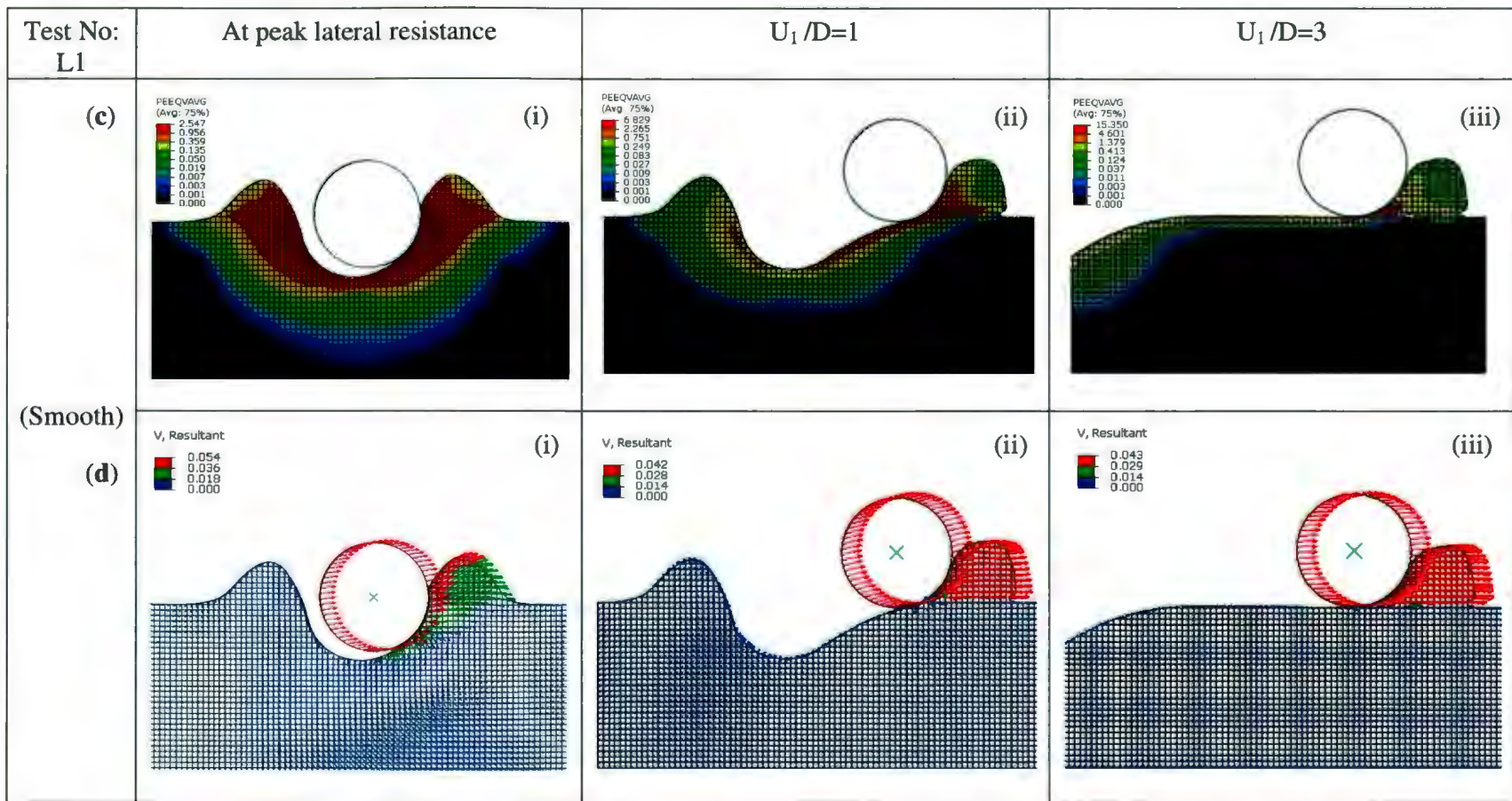


Fig. 5.3 (c) Equivalent plastic strain around pipeline and (d) Velocity field during pipe lateral movement at (i) breakout point (ii) lateral displacement of one pipe diameter (iii) lateral displacement of three pipe diameter.

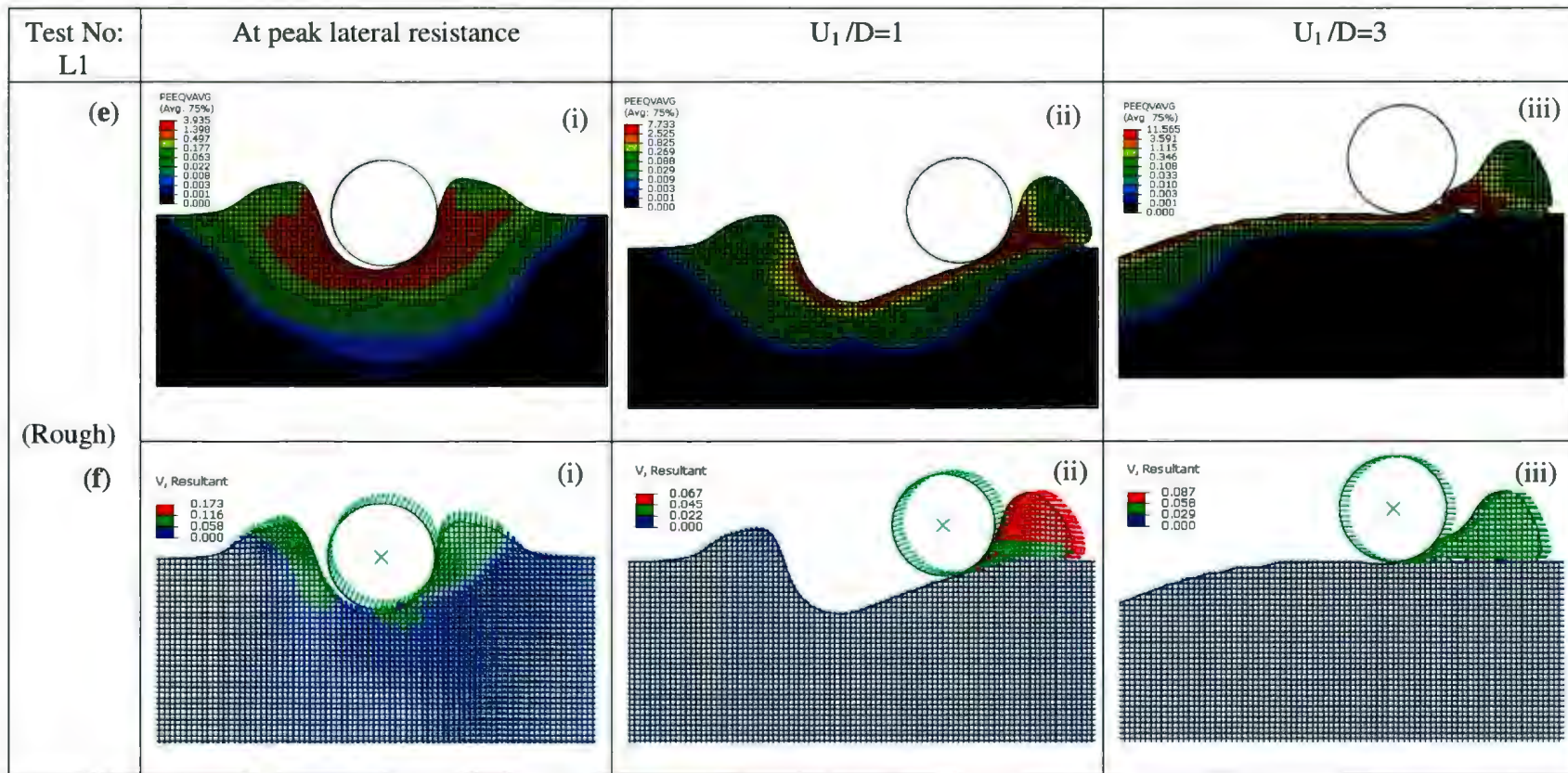


Fig. 5.3 (e) Equivalent plastic strain around pipeline and (f) Velocity field during pipe lateral movement at (i) breakout point (ii) lateral displacement of one pipe diameter (iii) lateral displacement of three pipe diameter.

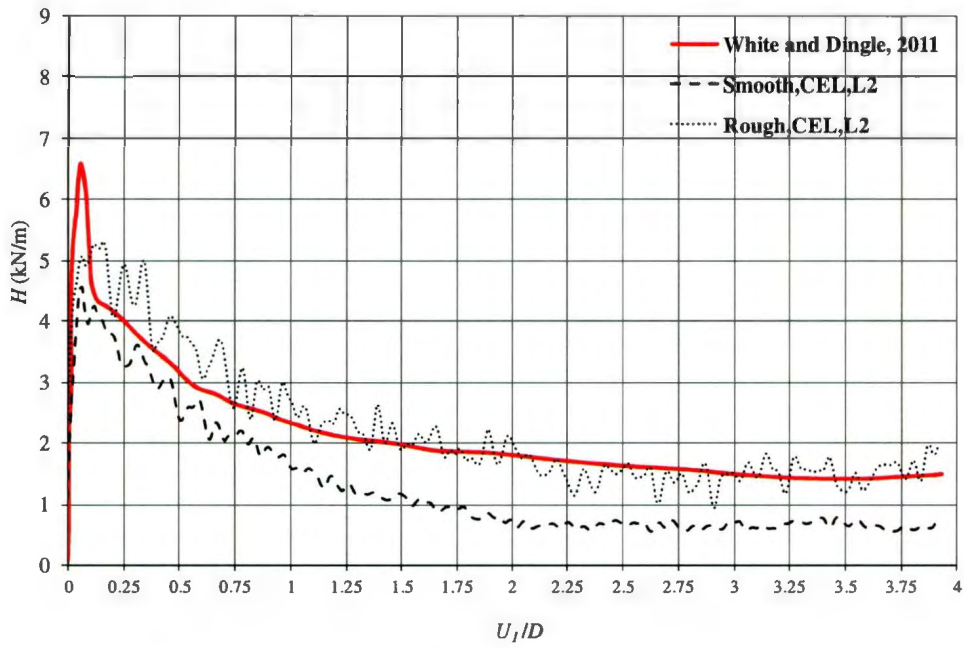


Fig. 5.4(a) Pipe resistance during lateral movement (Case-L2).

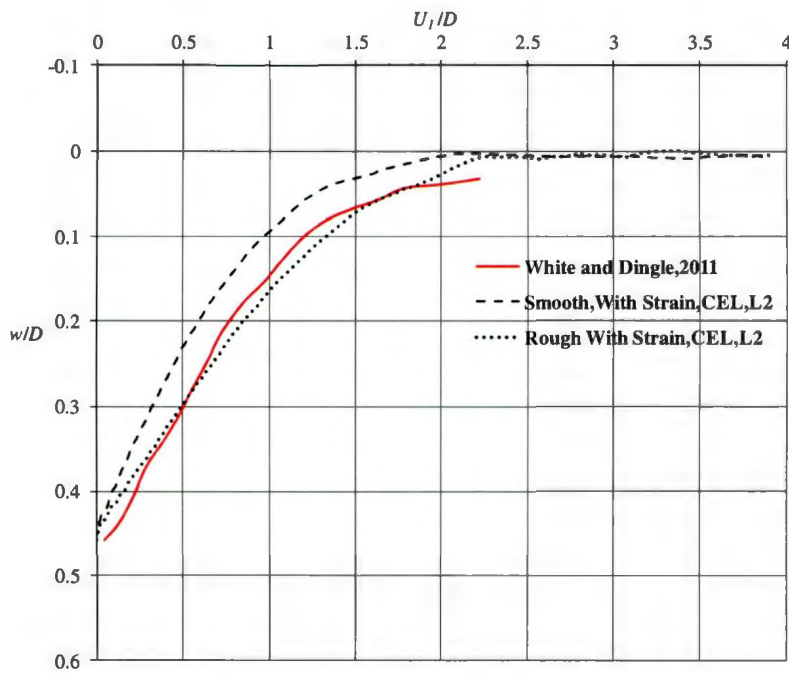


Fig. 5.4(b) Pipe invert trajectory (Case-L2).

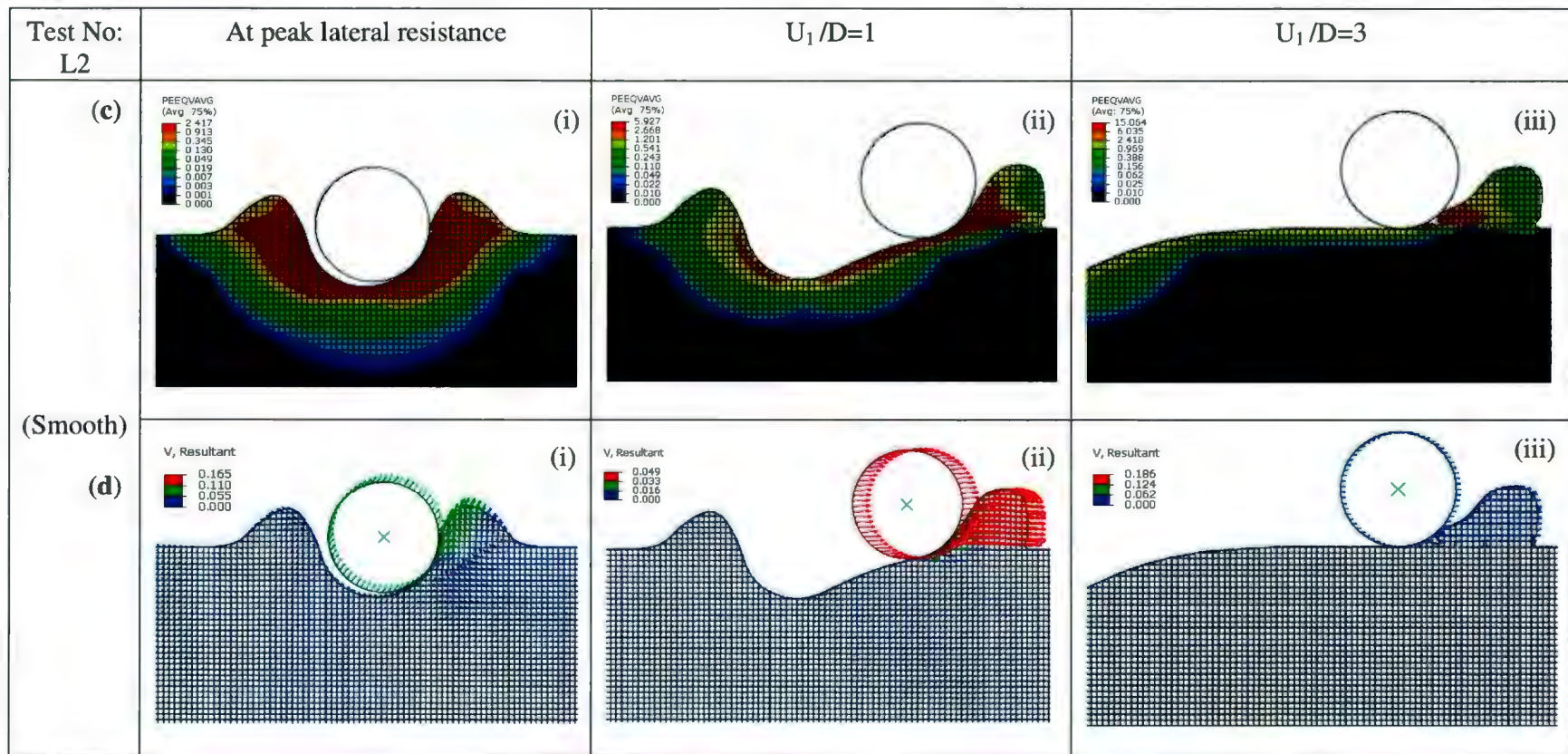


Fig. 5.4 (c) Equivalent plastic strain around pipeline and (d) Velocity field during pipe lateral movement at (i) breakout point (ii) lateral displacement of one pipe diameter (iii) lateral displacement of three pipe diameter.

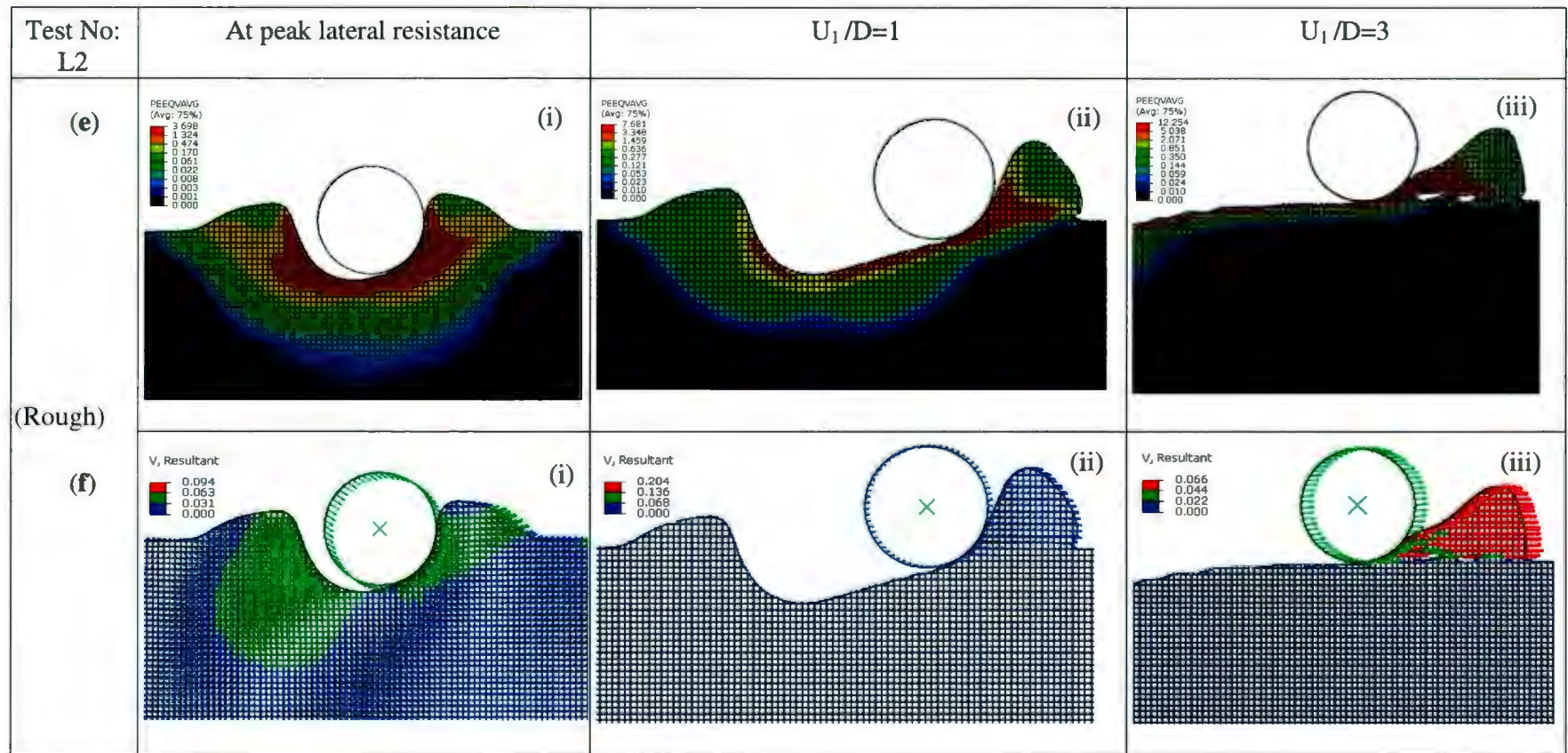


Fig. 5.4 (e) Equivalent plastic strain around pipeline and (f) Velocity field during pipe lateral movement at (i) breakout point (ii) lateral displacement of one pipe diameter (iii) lateral displacement of three pipe diameter.

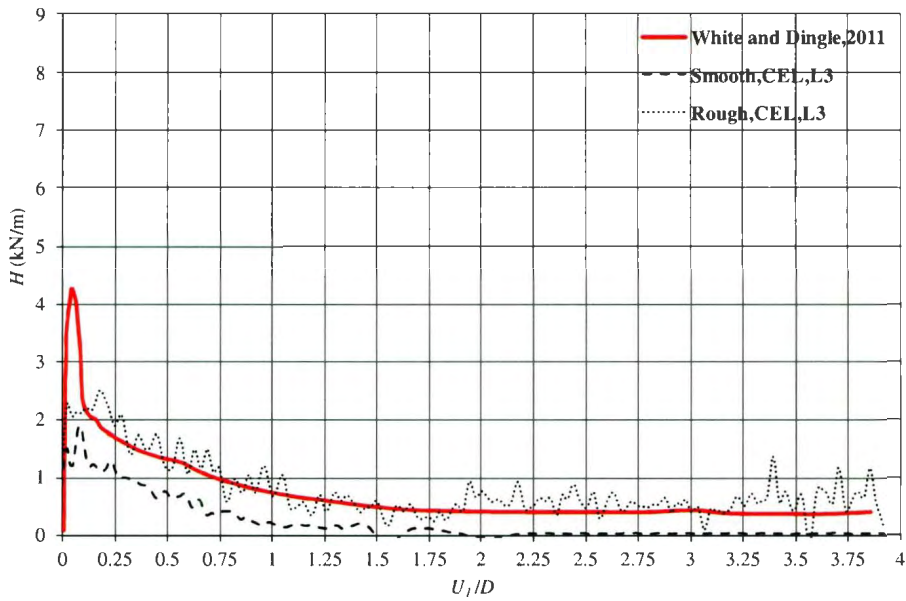


Fig. 5.5(a) Pipe resistance during lateral movement (Case-L3).

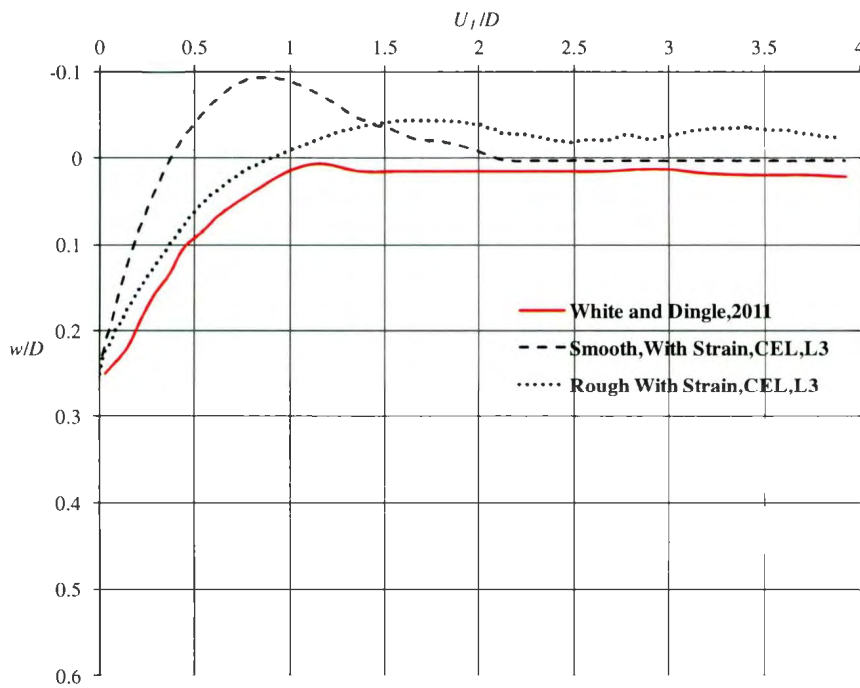


Fig. 5.5(b) Pipe invert trajectory (Case-L3).

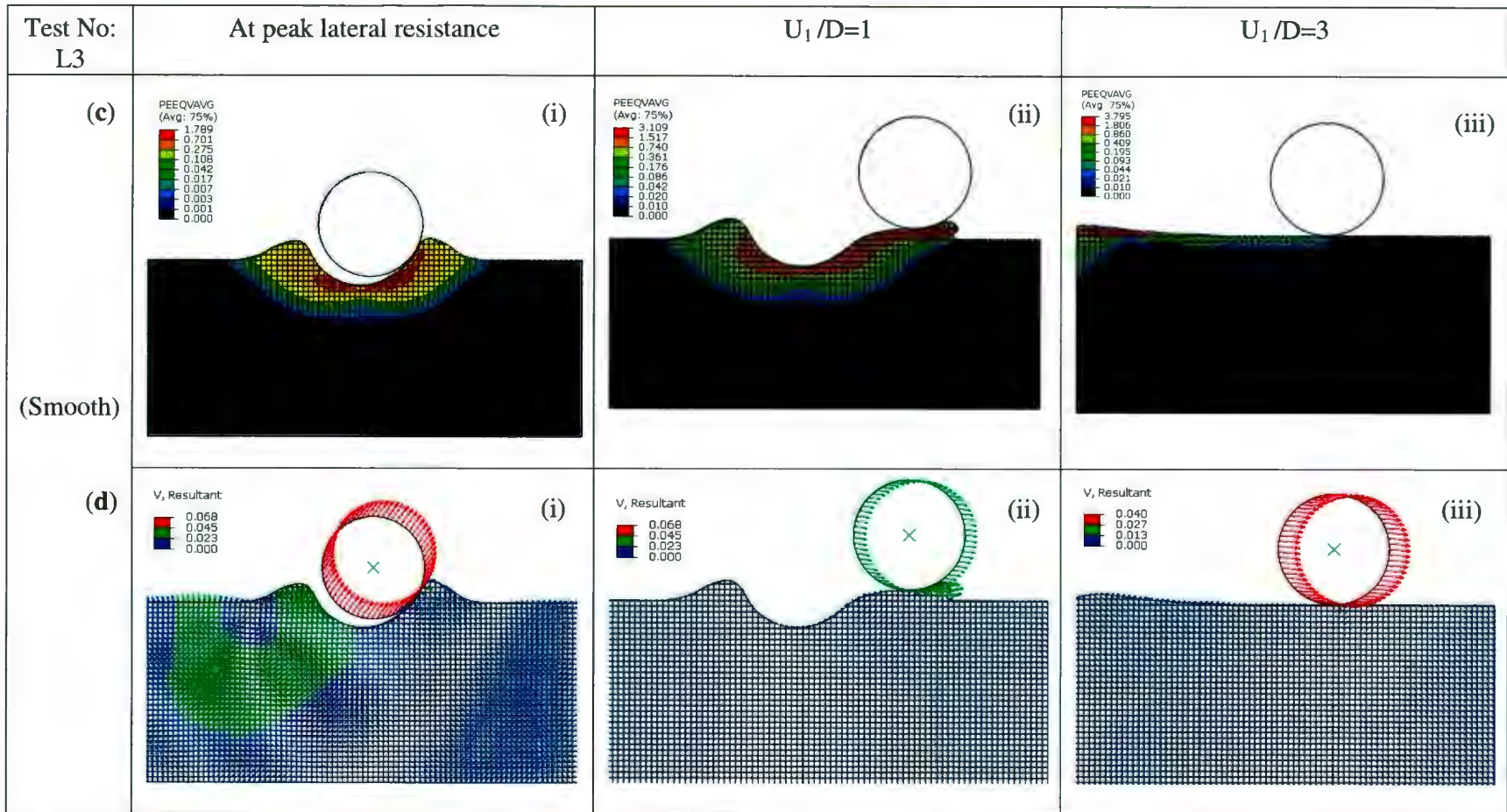


Fig. 5.5 (c) Equivalent plastic strain around pipeline and (d) Velocity field during pipe lateral movement at (i) breakout point (ii) lateral displacement of one pipe diameter (iii) lateral displacement of three pipe diameter.

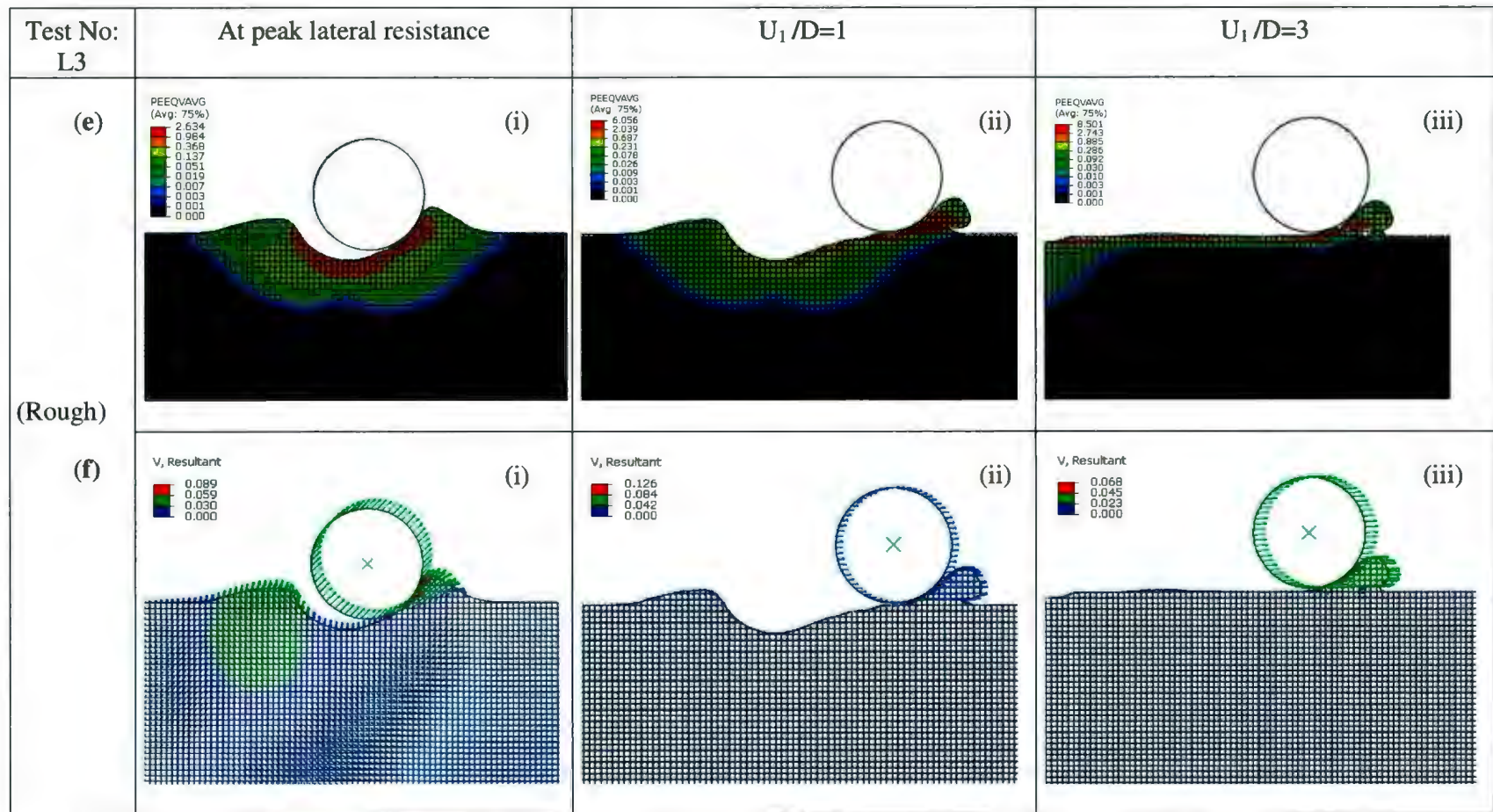


Fig. 5.5 (e) Equivalent plastic strain around pipeline and (f) Velocity field during pipe lateral movement at (i) breakout point (ii) lateral displacement of one pipe diameter (iii) lateral displacement of three pipe diameter.

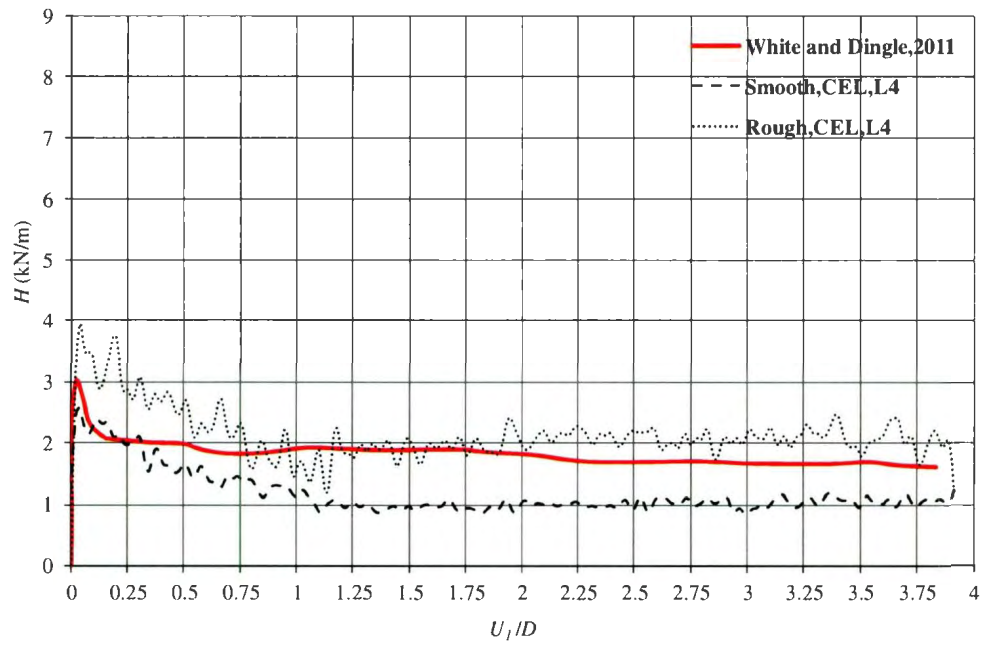


Fig. 5.6(a) Pipe resistance during lateral movement (Case-L4)

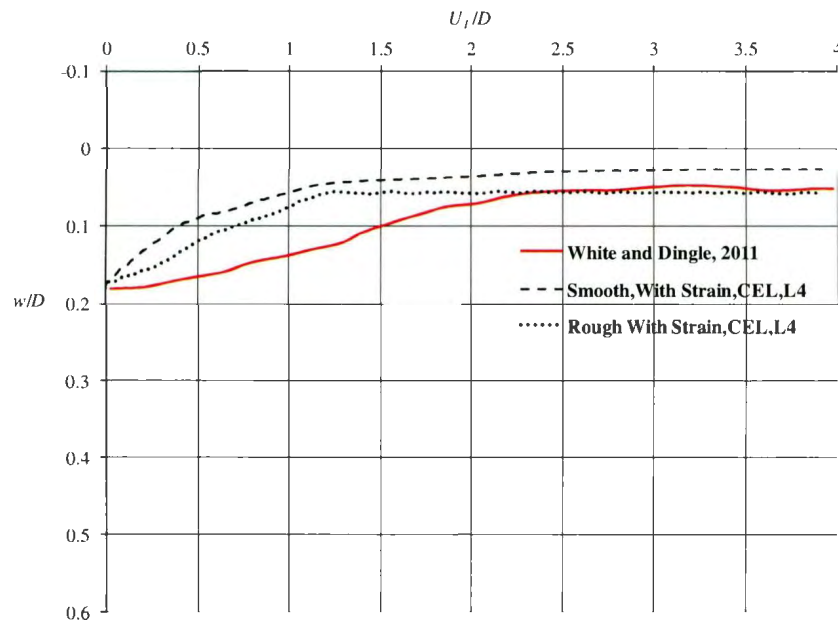


Fig. 5.6(b) Pipe invert trajectory (Case-L4)

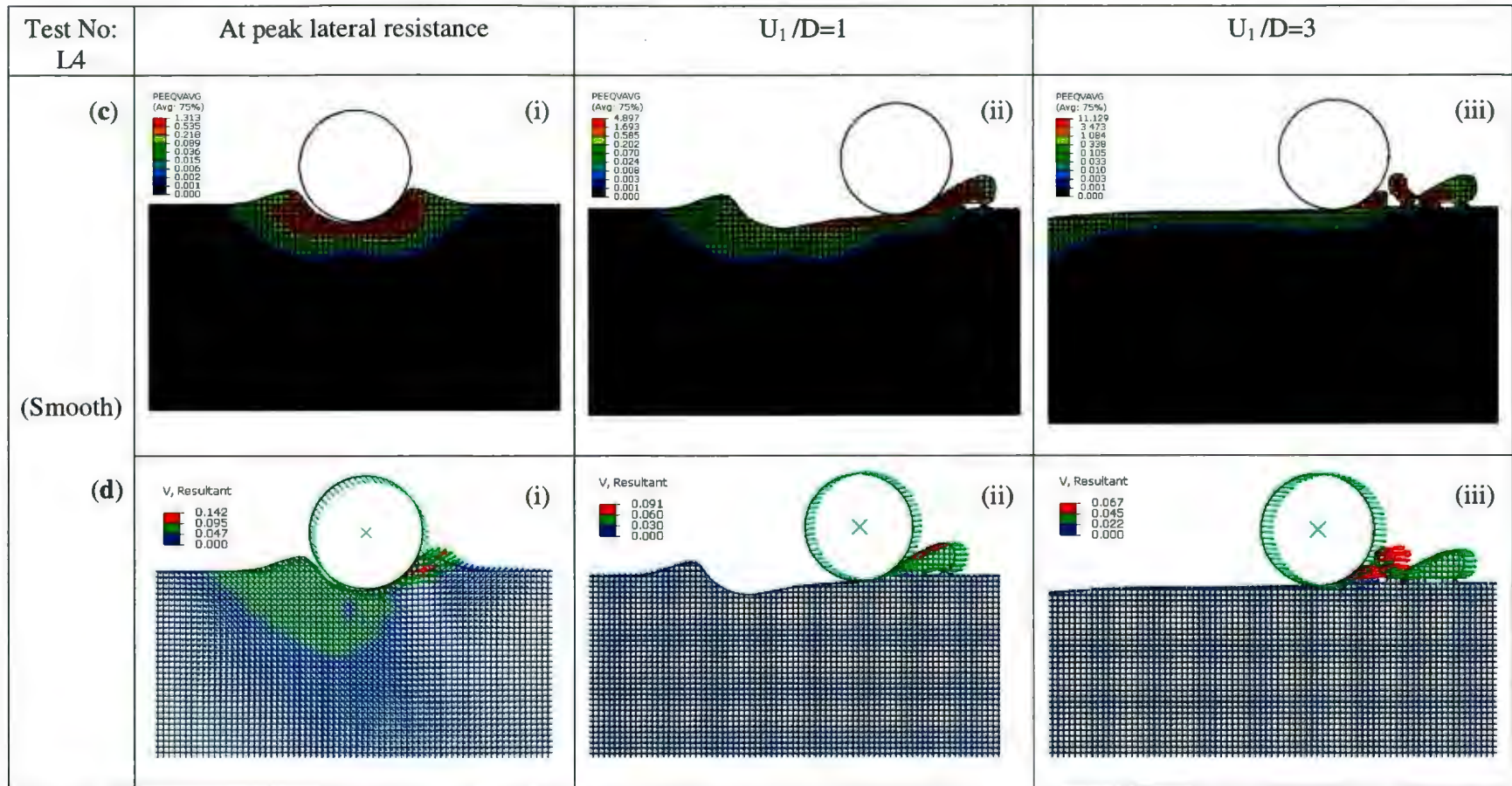


Fig. 5.6 (c) Equivalent plastic strain around pipeline and (d) Velocity field during pipe lateral movement at (i) breakout point (ii) lateral displacement of one pipe diameter (iii) lateral displacement of three pipe diameter.

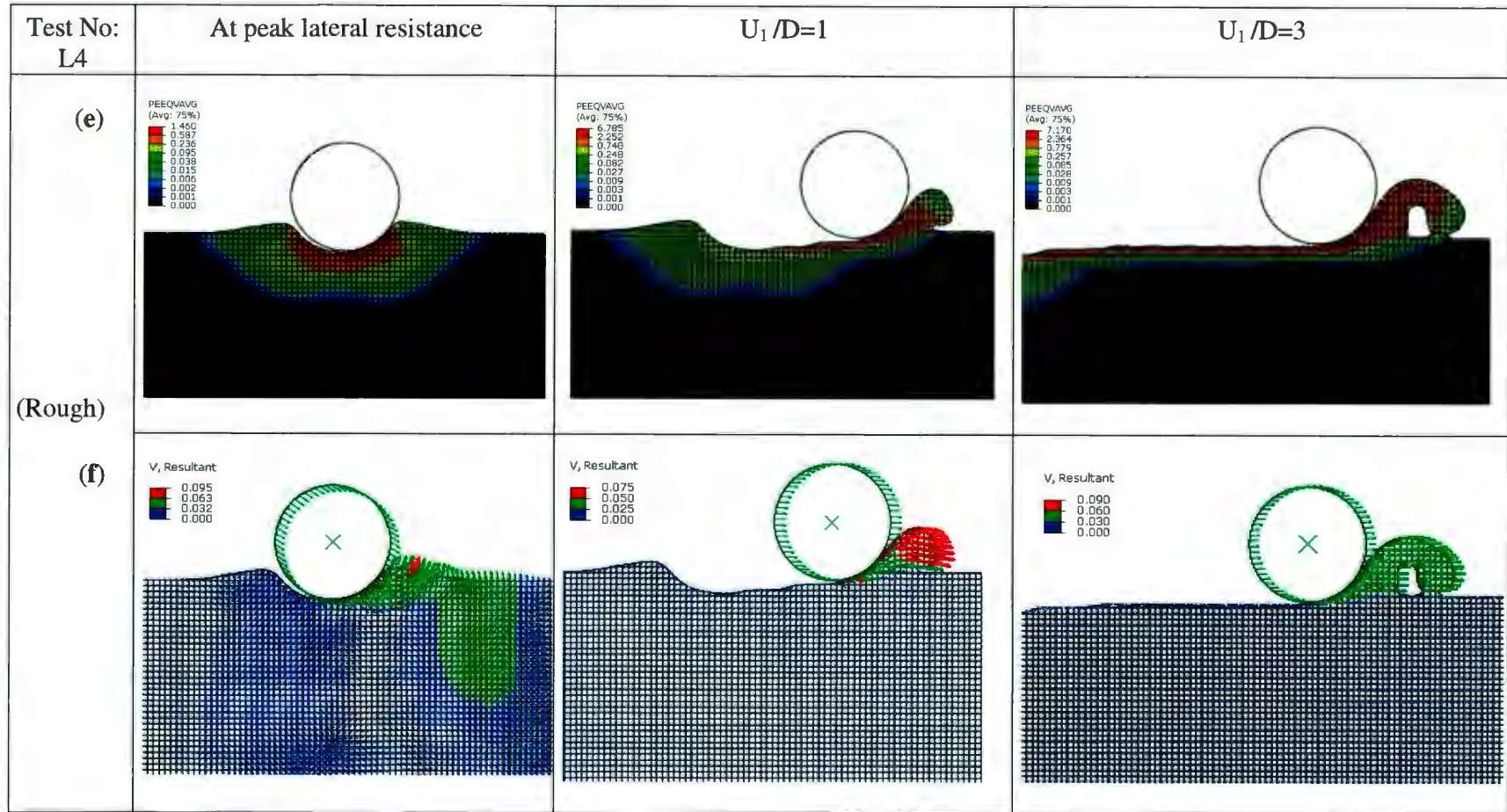


Fig. 5.6 (e) Equivalent plastic strain around pipeline and (f) Velocity field during pipe lateral movement at (i) breakout point (ii) lateral displacement of one pipe diameter (iii) lateral displacement of three pipe diameter.

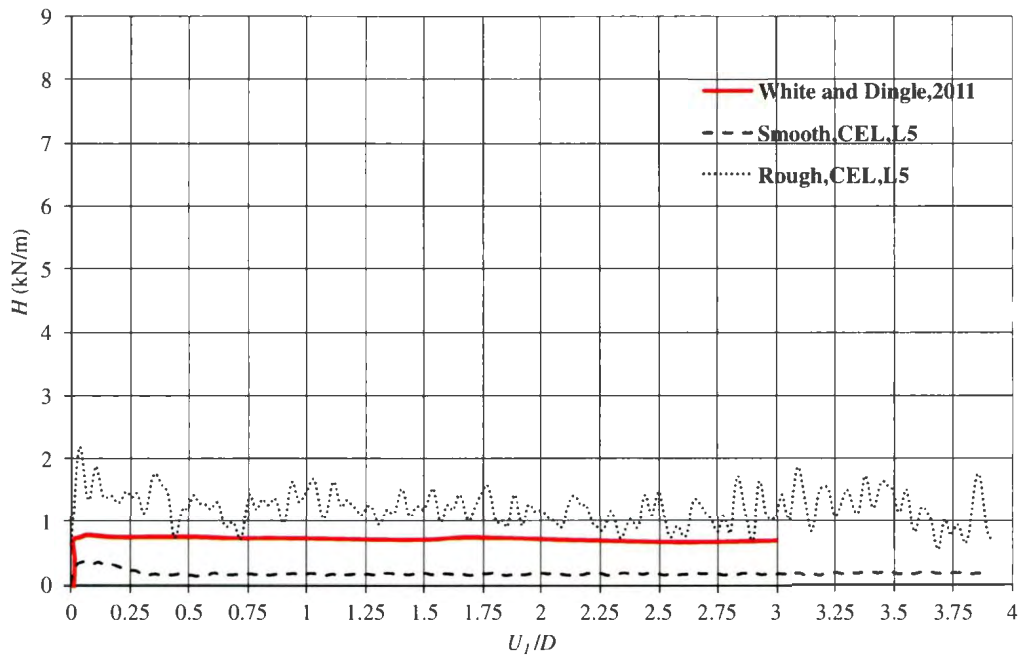


Fig. 5.7(a) Pipe resistance during lateral movement (Case-L5).

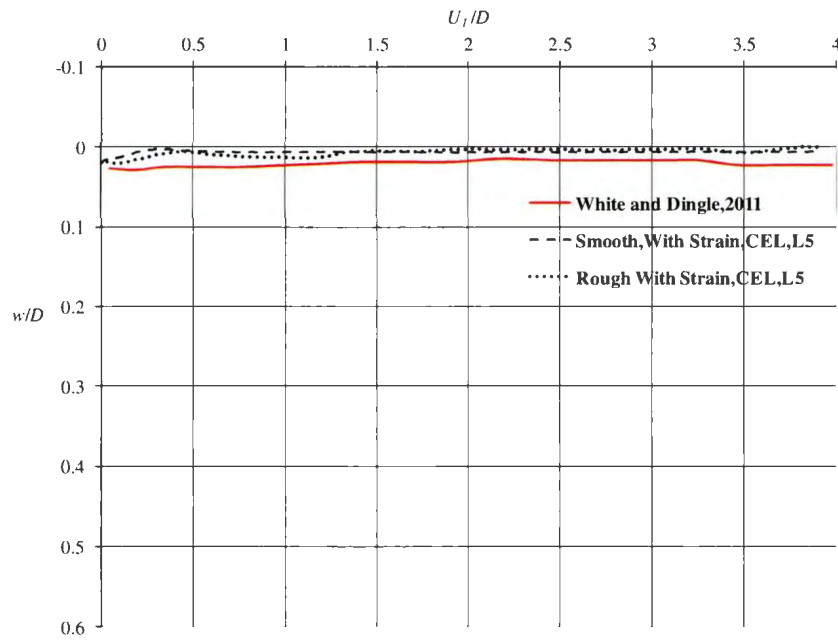


Fig. 5.7(b) Pipe invert trajectory (Case-L5).

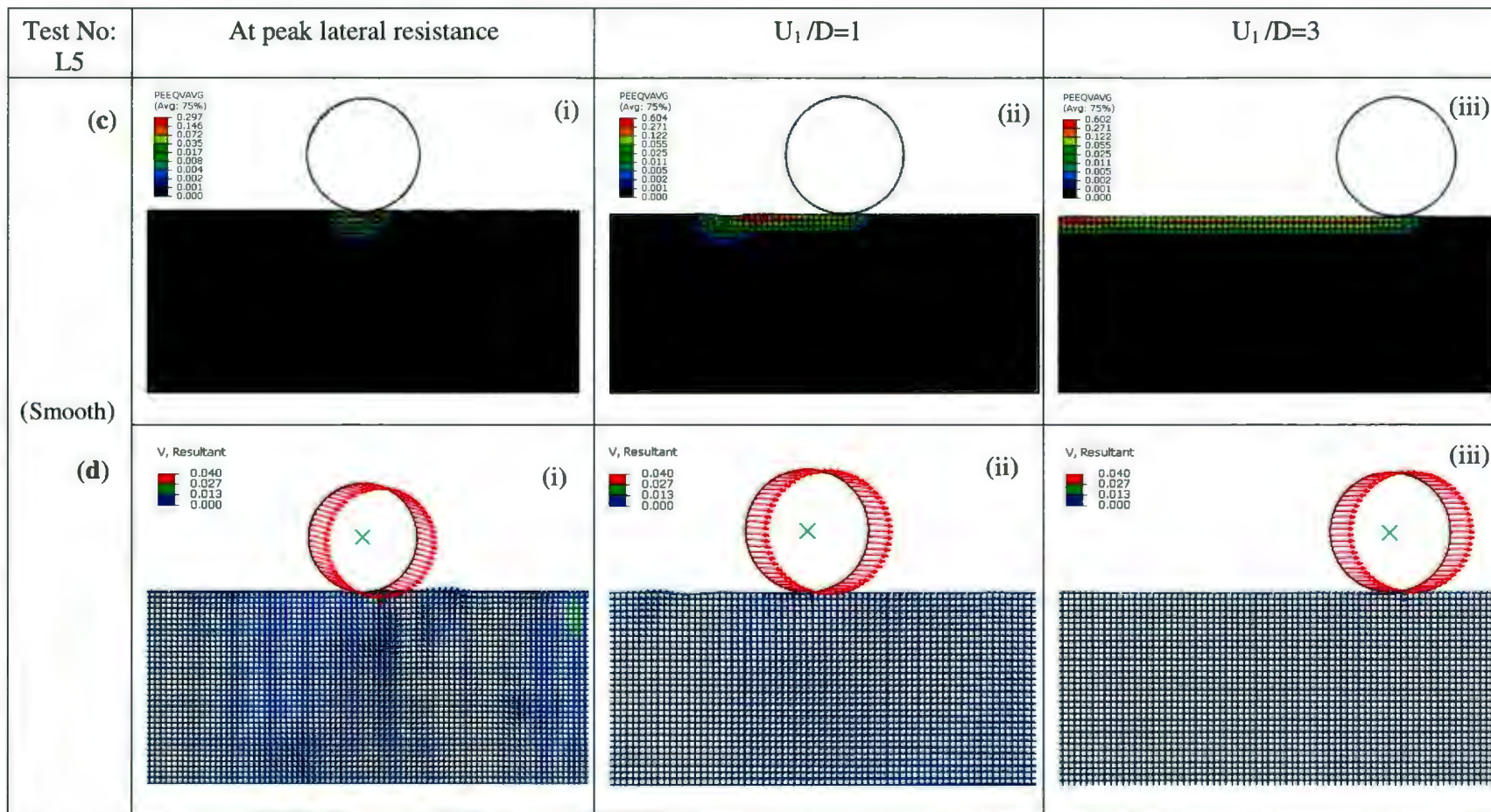


Fig. 5.7 (c) Equivalent plastic strain around pipeline and (d) Velocity field during pipe lateral movement at (i) breakout point (ii) lateral displacement of one pipe diameter (iii) lateral displacement of three pipe diameter.

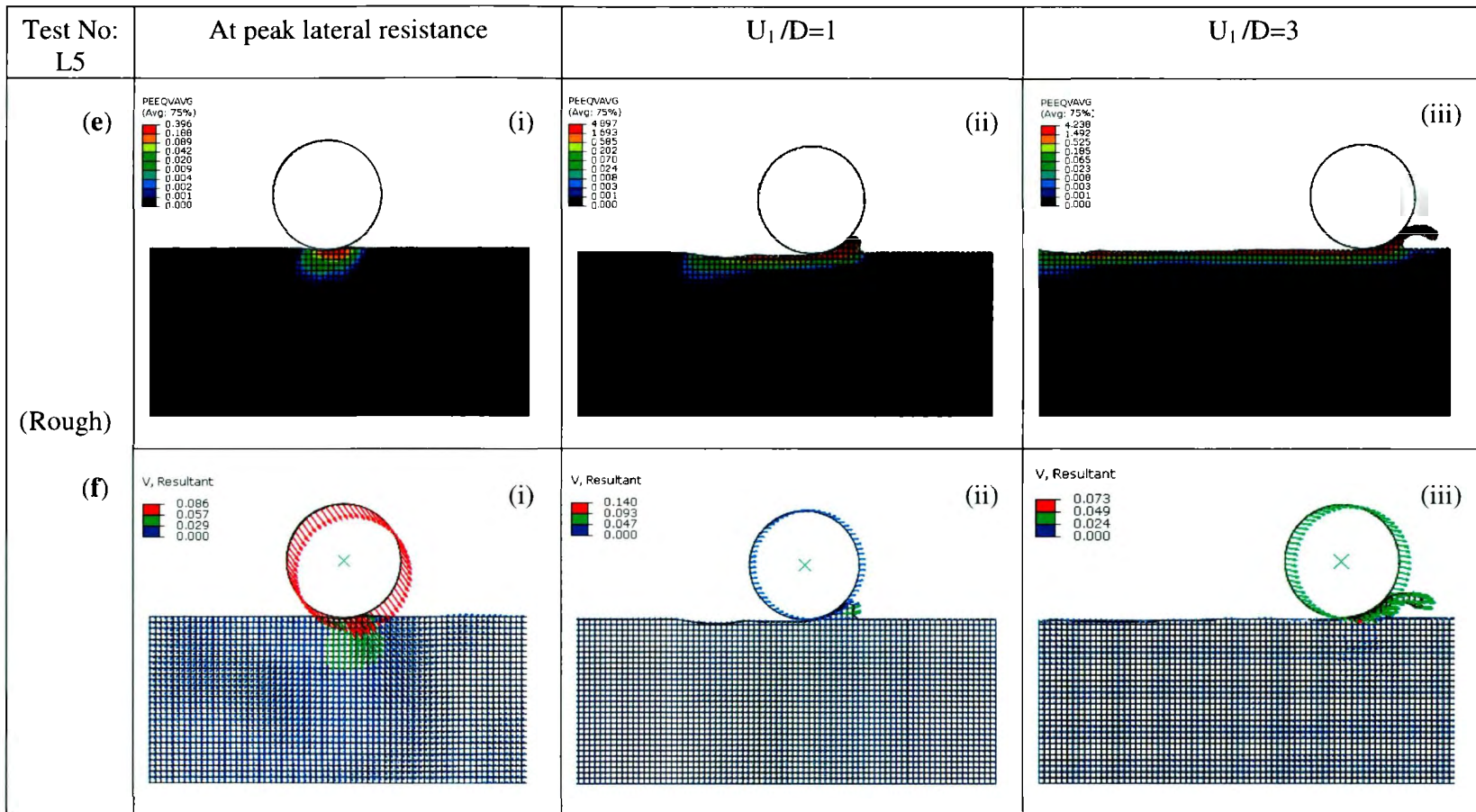


Fig. 5.7 (e) Equivalent plastic strain around pipeline and (f) Velocity field during pipe lateral movement at (i) breakout point (ii) lateral displacement of one pipe diameter (iii) lateral displacement of three pipe diameter.

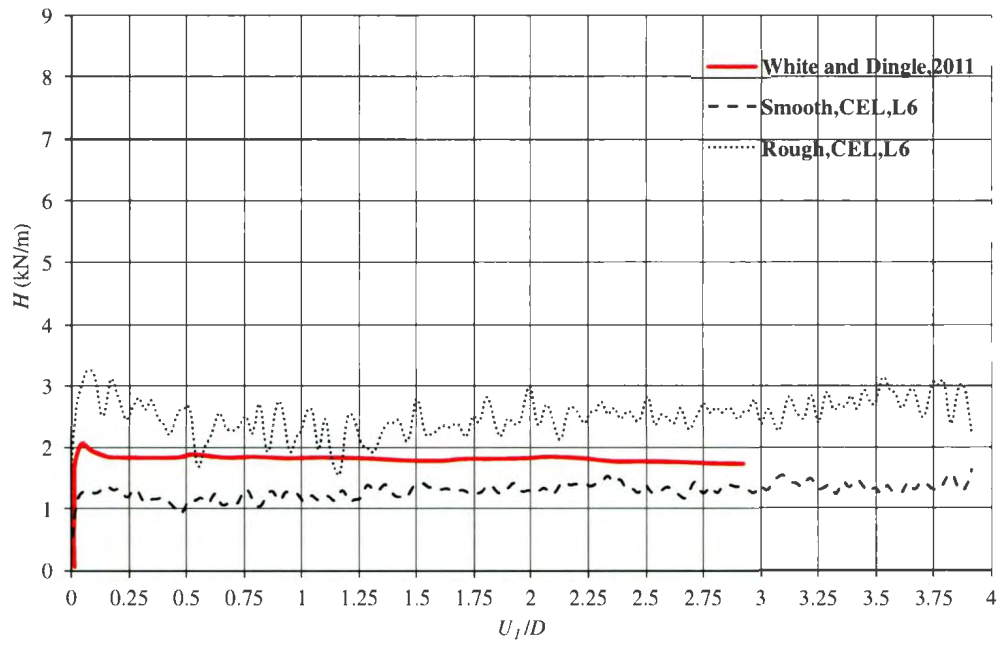


Fig. 5.8(a) Pipe resistance during lateral movement (Case-L6)

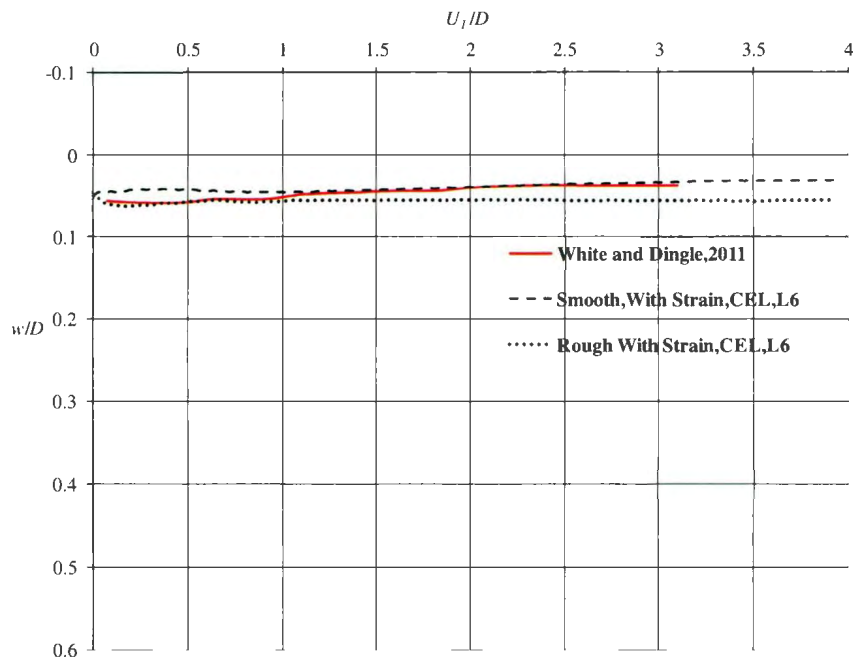


Fig. 5.8(b) Pipe invert trajectory (Case-L6)

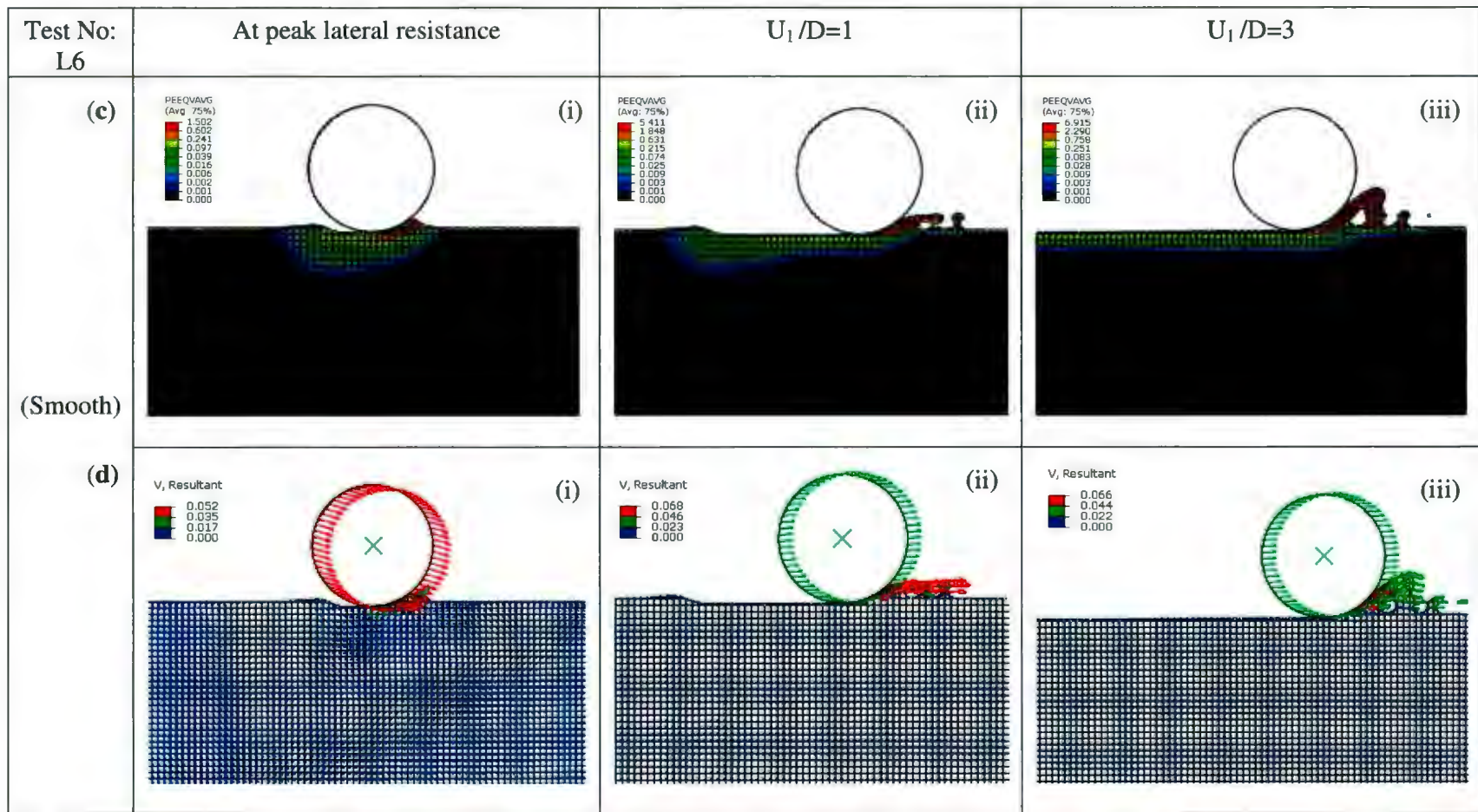


Fig. 5.8 (c) Equivalent plastic strain around pipeline and (d) Velocity field during pipe lateral movement at (i) breakout point (ii) lateral displacement of one pipe diameter (iii) lateral displacement of three pipe diameter.

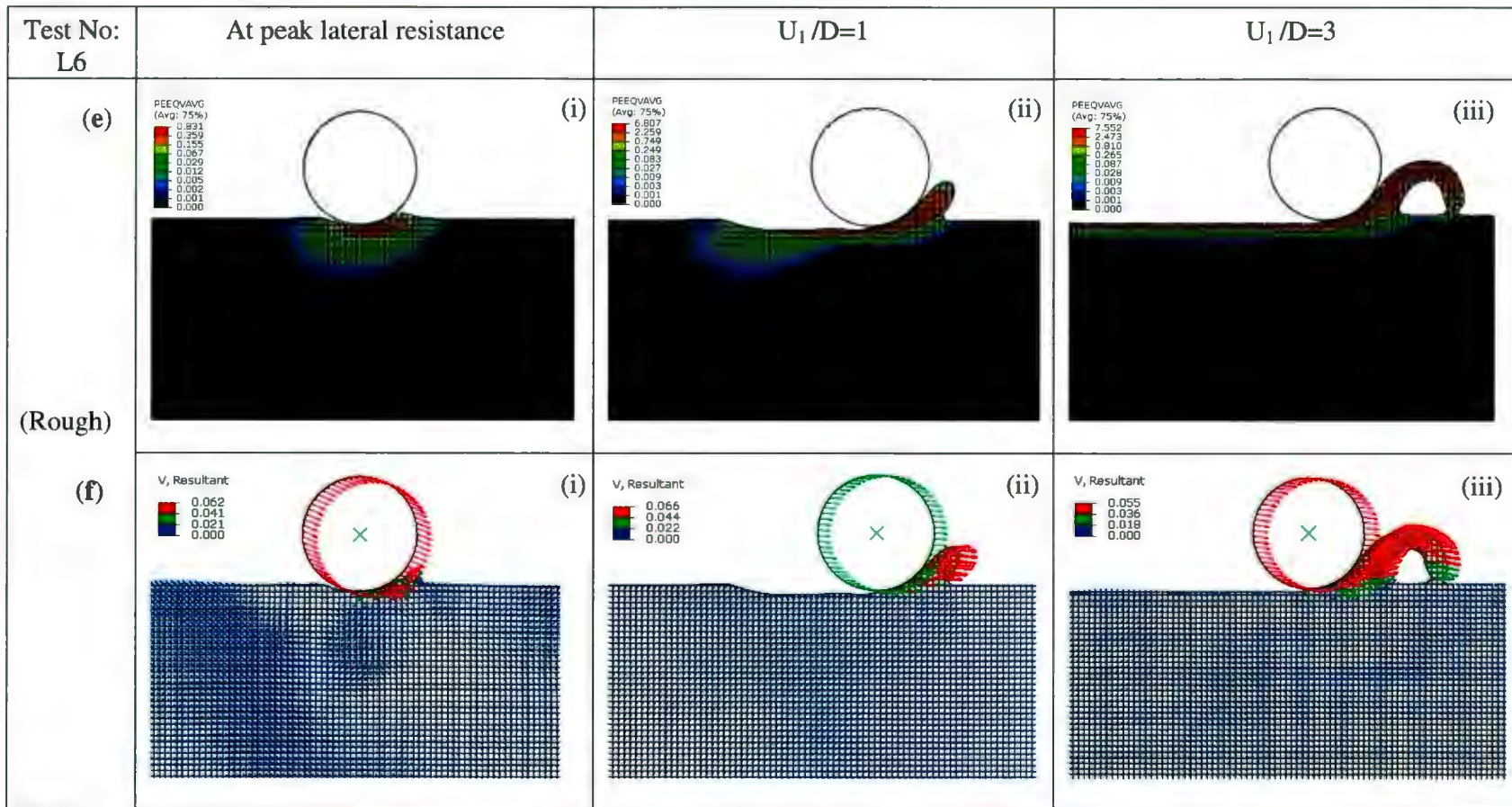


Fig. 5.8 (e) Equivalent plastic strain around pipeline and (f) Velocity field during pipe lateral movement at (i) breakout point (ii) lateral displacement of one pipe diameter (iii) lateral displacement of three pipe diameter.

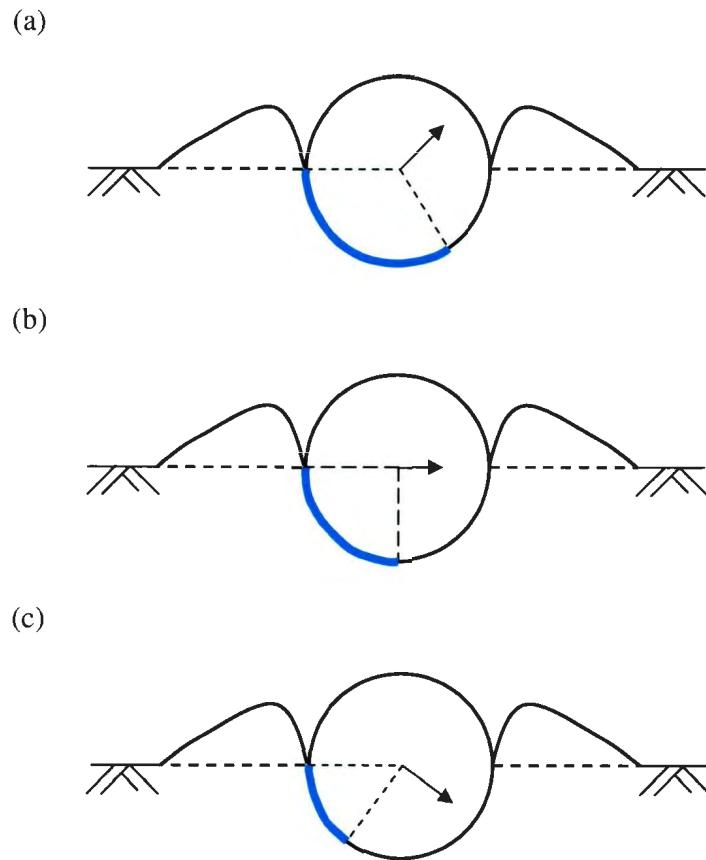


Fig. 5.9 Variation of pipe rear end surface area with pipe travel direction.

value at large displacement. For a given lateral displacement the lateral force is higher for rough pipe/soil interface condition. For a very low applied vertical load (e.g. Test L3, applied vertical load is 1.0 kN/m) the horizontal resistance is almost zero when smooth pipe/soil interface condition is used as shown in Fig. 5.5(a). The peak lateral resistance is termed as “breakout resistance” and the approximately constant lateral resistance at large

displacement is termed as “residual resistance.” The breakout and residual resistance under various test conditions are discussed in the following sections.

The breakout resistance is defined as the highest lateral resistance and generally develops within $0.2D$ lateral movement. The breakout resistance is higher for rough pipe/soil interface conditions. The comparison between numerical and centrifuge test results show that the breakout resistance obtained from centrifuge tests is higher than that of finite element models even with a rough pipe/soil interface for higher initial embedments (L1-L3 and D1). However, for very shallow initial embedment (L4-L6) finite element models with rough pipe/soil interface give higher breakout resistance than centrifuge tests. One of the reasons behind this is the effects of suction at the rear end of the pipe. During vertical penetration, soil around the pipe comes in contact with the pipe. In subsequent lateral movement suction develops in the rear end of the pipe in centrifuge test. The magnitude of lateral force from suction depends on contact area of the pipe with soil. The higher the initial pipe embedment the higher the pipe rear surface contact with soil, and thus higher suction. That means the suction force is less in shallow embedded tests (L4-L6) than deeper embedded tests (D1 and L1-L3).

The suction force also depends on the direction of pipe movement. The direction of pipe movement is related to applied vertical load and initial depth of embedment. This is schematically shown in Fig. 5.9. For example, as shown in Fig. 5.9(a) if the initial depth of penetration is high and the applied vertical load is low then the pipe will move in

inclined upward direction. The contact area behind the pipe is shown by a thick line. Similarly, the contact areas behind the pipe for pure horizontal and inclined downward movement are shown in Figs. 5.9 (b) and 5.9(c), respectively. It is clear from this figure that the contact area behind the pipe for suction is higher in Fig. 5.9(a). Therefore, in centrifuge tests higher breakout resistance was observed in D1 and L1-L3. In the present finite element analyses this suction force could not be modelled using ABAQUS CEL and therefore less breakout resistance is calculated for these four cases.

5.2.2.2 Pipe Invert Trajectory

Figures 5.2(b) to 5.8(b) show the trajectories of the invert of the pipe during lateral movement. As light pipes are considered in the present study, the pipes move up with lateral displacement at constant depth of embedment. The higher the applied vertical load the higher the depth of embedment at residual state. Very light pipe (e.g. L3) moves to the seabed at residual stage. Figure 5.5(b) shows that the finite element prediction of pipe invert trajectory for test L3 is somehow different in shape from other tests. In this simulation, the pipe is penetrated to a depth of $0.25D$ and then displaced laterally under a very light applied vertical load of 1.0 kN/m. Therefore, during lateral movement the smooth pipe easily climbed up the berm that has been formed by the initial vertical penetration and then moved essentially on the original seabed as shown in Figs. 5.5(c) and 5.5(d). However, when a rough interface condition is used some soil has been ploughed and there is a small berm in front of the pipe even at large displacement. The

passive resistance from the berm with soil/pipe interaction contributes in lateral pipe resistance during its lateral travel.

5.2.2.3 Effects of applied vertical load

The lateral loading in centrifuge tests D1 (Dingle et al., 2008) and L2 (White and Dingle, 2011) were done approximately from the same initial embedment. The soil shear strength profile is also the same in these tests. The only difference is the applied vertical load; test D1 was conducted under 3.39 kN/m while test L2 was conducted under 2.8 kN/m applied vertical load. Comparison between Fig. 5.2(a) and Fig. 5.4(a) show higher lateral force in Test D1 both in numerical analyses and centrifuge tests as the applied vertical load is higher. Similar conclusions can be drawn from comparing the simulation of Tests L3 and L4 although there is a slight difference in initial embedment.

5.2.2.4 Very shallowly embedded pipes

The tests L5 and L6 are for very shallowly embedded pipes ($w/D = 0.02$ and 0.05). Numerical simulation of these cases are shown in Figs. 5.7 and 5.8. Test L5 and L6 were conducted under an applied vertical load of 2.1 and 4.4 kN/m, respectively. The comparison between numerical analysis and physical test results show that the horizontal resistance is higher in both L5 and L6 when rough soil/pipeline interface condition is used. Higher breakout resistance is calculated for the Case-L6 than Case-L5 (Figs. 5.7(a) & 5.8(a)). In finite element analyses it is also found that the lateral force slightly increases

with lateral displacement especially in Case L6. It is noted that while the numerical and centrifuge test results show some reasonable comparison, there are several other factors that is very difficult to characterize. One of them is the undrained shear strength of the soil near the mudline. While T-bar tests have been widely used for seabed shear strength measurement, the shear strength obtained from T-bar near the mudline is not accurate. Moreover, the shear strength of soil in the berm in front of the pipe is also very difficult to measure. In this study, the intact shear strength at the mudline, with remoulding and strain rate effects is used for soil shear strength in the berm.

Figures 5.2 (e & f) to 5.8(e & f) show the plastic shear strain and velocity vectors with lateral movement of the pipe. Large shear strain is developed near the bottom of the pipe, which has been successfully modelled using ABAQUS CEL without any numerical issues. However, it is noted that accurate estimation of lateral resistance depends on undrained shear strength of soil in this narrow zone. Estimation of undrained shear strength near the mudline is very difficult.

5.2.2.5 Comparison of velocity field

Dingle et al. (2008) showed the soil velocity field around the pipe during the lateral displacement using PIV technique. Soil velocity field at six different pipe lateral displacements shown in Fig. 5.10 are discussed here. Two of them (A & B) are near the lateral breakout resistance, two (E & F) are near the lateral residual resistance and the remaining two (C & D) are in between the breakout and residual resistances. The velocity

fields observed in centrifuge modeling are compared with the present finite element modeling, (Fig. 5.11). The results show that the direction of movement varies with lateral displacement, and at the residual condition the pipe displaced almost horizontally for the case analyzed here. The soil velocity fields obtained from the present FE analyses with rough soil/pipe interface conditions are very similar to the velocity field observed in the centrifuge.

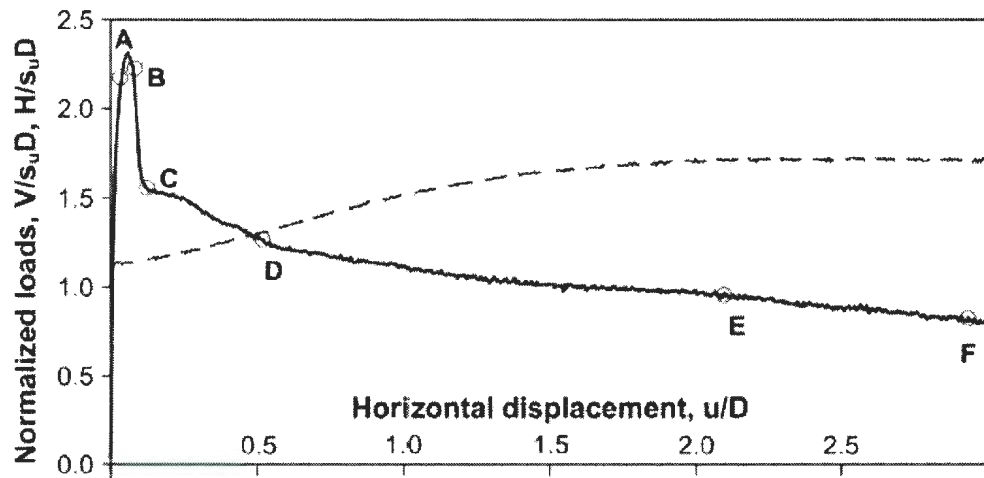


Fig. 5.10 Six pipe locations (A, B, C, D, E & F) on load-displacement plot (Dingle et al., 2008).

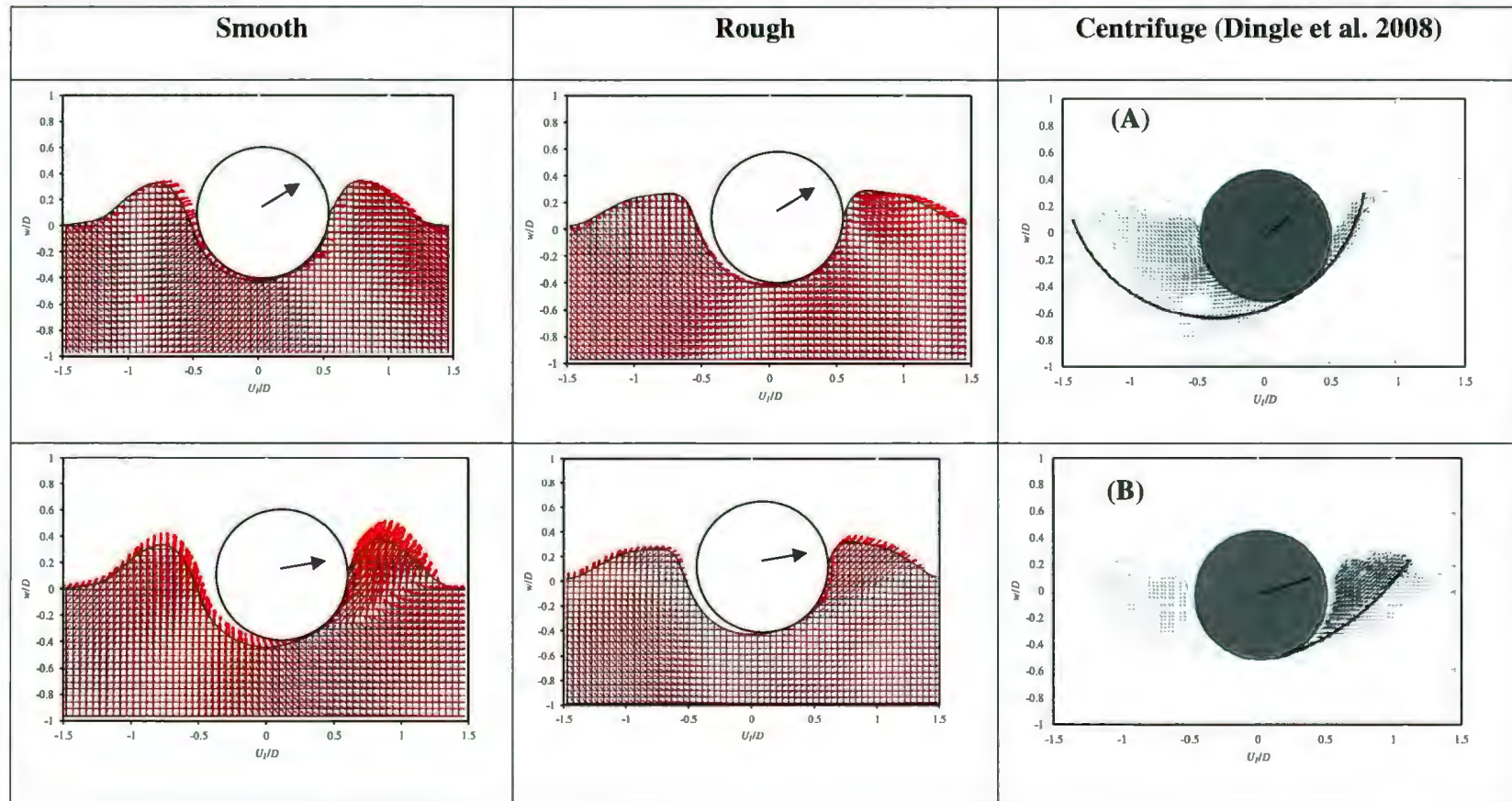


Fig. 5.11 (a) Predicted and observed velocity vectors at pipe lateral displacement of 0.04D (location A) and 0.1D (location B)

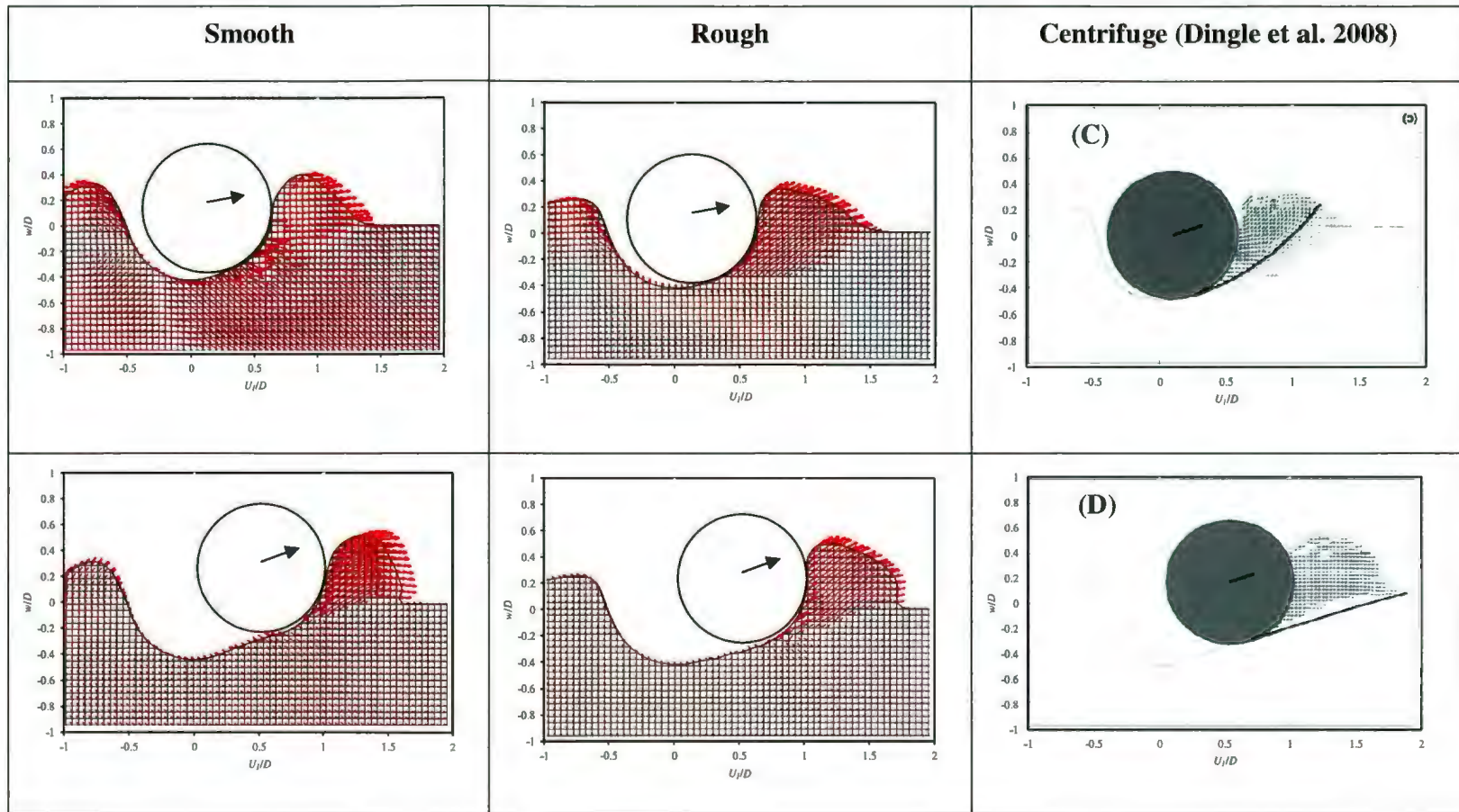


Fig. 5.11 (b) Predicted and observed velocity vectors at pipe lateral displacement of $0.15D$ (location C) and $0.53D$ (location D)

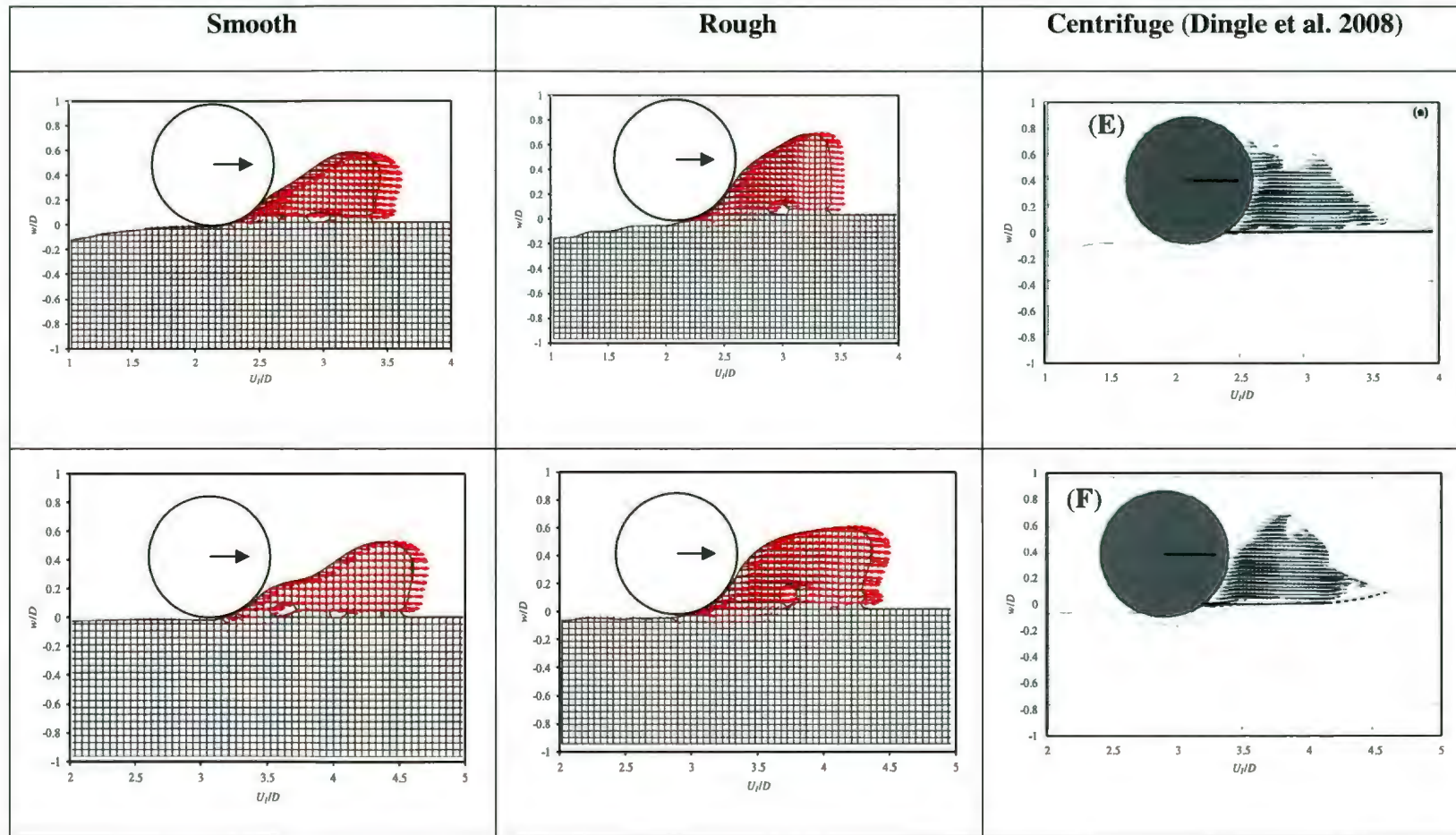


Fig. 5.11 (c) Predicted and observed velocity vectors at pipe lateral displacement of $2.11D$ (location E) and $2.95D$ (location F)

5.3 Alternative interpretation of pipe lateral resistance

Attempts have been taken in the past to develop simplified solutions for estimating force and resistance during lateral movement. To develop such solutions, pipe lateral resistance obtained from numerical analysis or physical model tests were plotted in terms of effective embedment (w') (Chatterjee et al., 2009; Wang et al., 2010; White and Dingle, 2011). The effective embedment is defined as:

$$\frac{w'}{D} = \frac{w}{D} + \frac{1}{S_{t,berm} D} \sqrt{\frac{A_{berm}}{\eta}} \quad (5.1)$$

Details of effective embedment are given in Section 2.5.2.1 of this thesis.

The normalized lateral resistance and pipe invert location obtained from the present finite element model is plotted in Fig. 5.12 and Fig. 5.13, respectively, for smooth and rough interface conditions. Finite element simulations for L5 and L6 are not shown in these figures as the initial depth of embedment is very small and very little change in depth of embedment occurred during lateral displacement. The pipe moves upward with lateral movement. The horizontal resistance also decreases as the pipe moves upward. The arrows show the breakout resistance. A narrow variation in lateral resistance is observed for smooth pipe but a wider variation is observed for rough pipe.

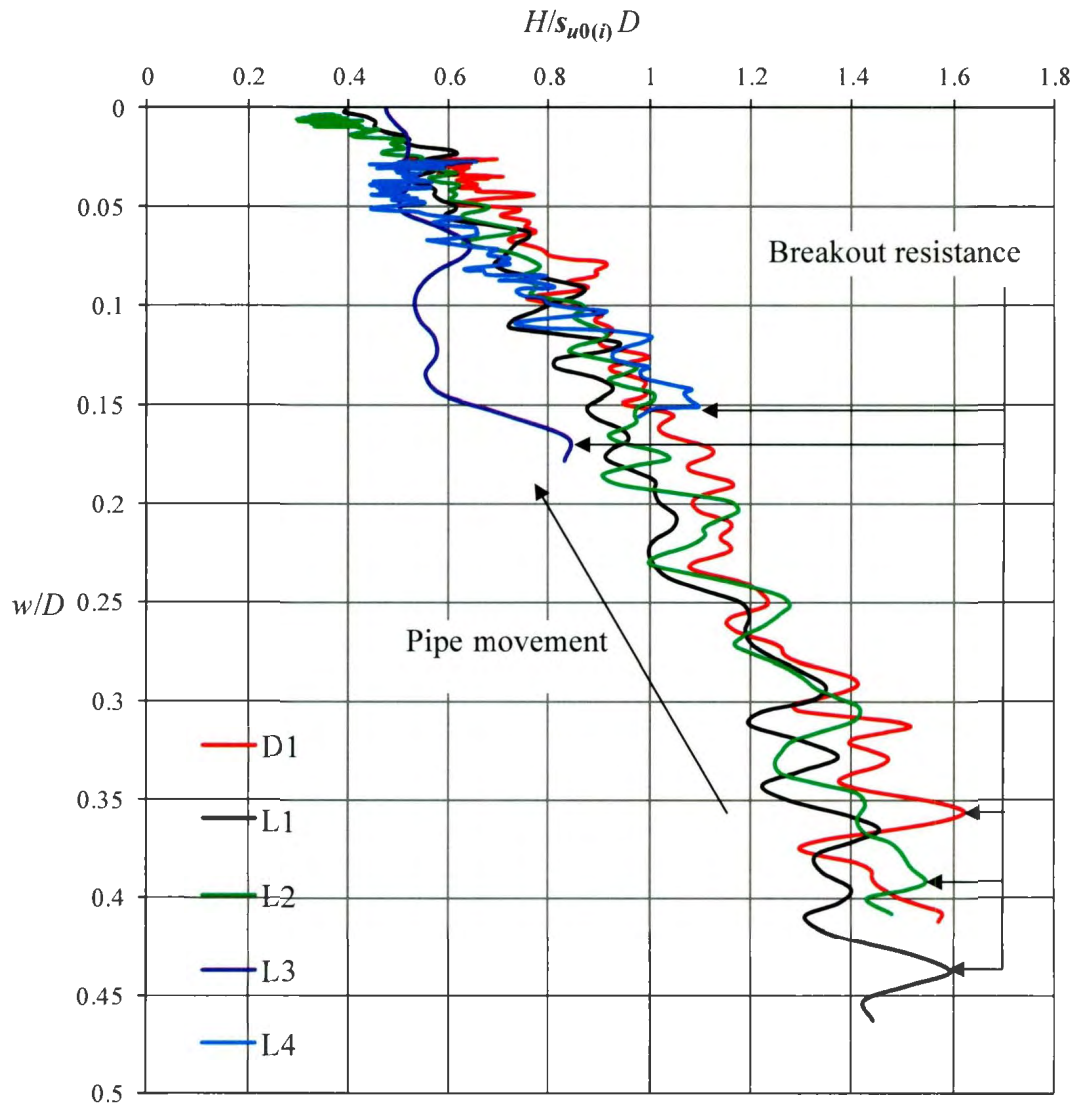


Fig. 5.12 Variation of smooth pipe lateral resistance with embedment from CEL analysis

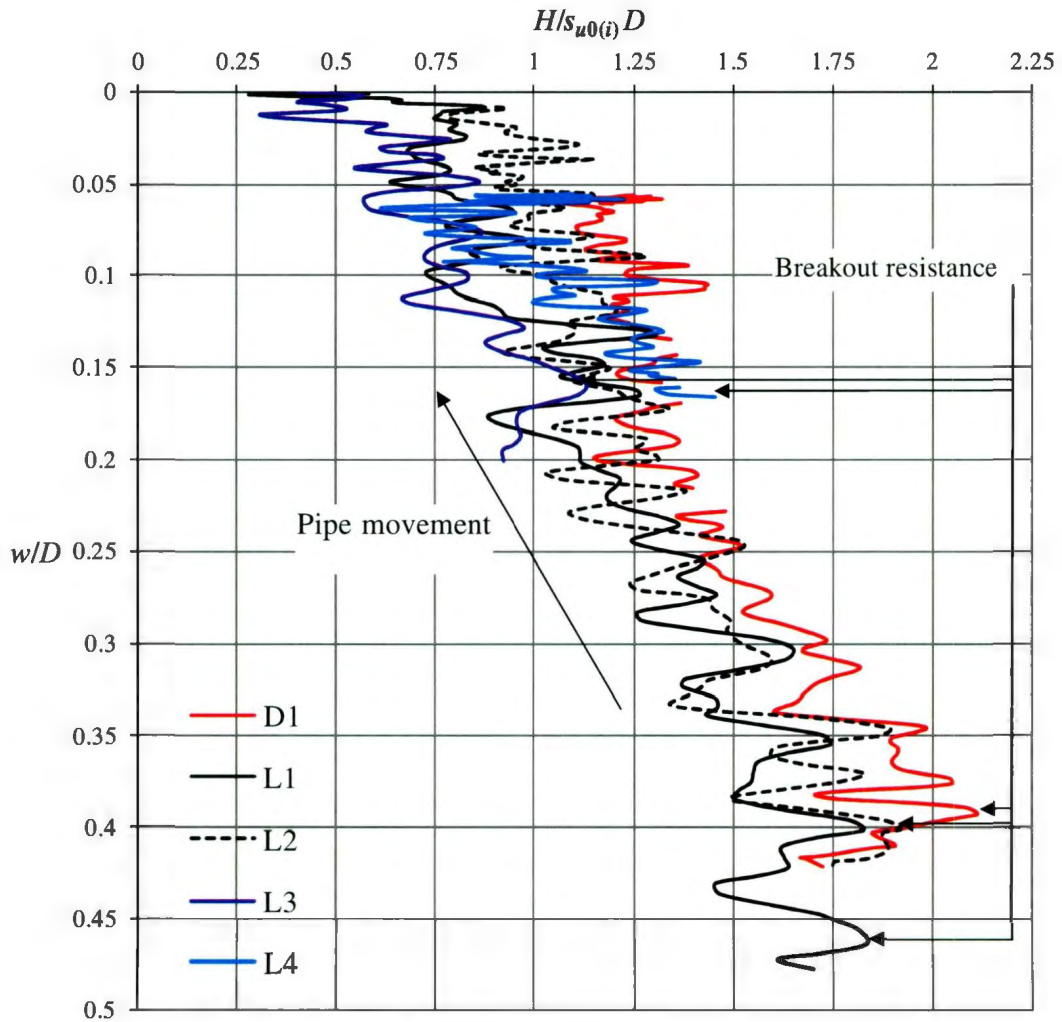


Fig. 5.13 Variation of rough pipe lateral resistance with embedment from CEL analysis

Previous studies show that fluctuation in lateral resistance can be reduced with the help of effective embedment concept (Wang et al., 2010; White and Dingle, 2011). Using Eq. 5.1, the effective embedment is calculated from the location of the invert of the pipe and

soil ploughing during lateral displacement. The value of $S_{t,berm} \times \sqrt{\eta} = 6.7$ is used as suggested by White and Dingle (2011). Figures 5.14 and 5.15 show the variation of lateral resistance with normalized effective embedment. Although the calculated resistance is still scattered, it shows a clear trend of decreasing lateral resistance with decrease in effective embedment. The numerical results obtained in the present study are compared with the following empirical equation.

$$\frac{H}{s_{u0}D} = a \left(\frac{w'}{D} \right)^b \quad (5.2)$$

Where a and b are model parameters. Wang et al. (2010) suggested $a = 2.3$ and $b = 0.9$ while White and Dingle (2011) recommended $a = 2.8$ and $b = 0.75$.

Figure 5.14 shows that the empirical equation by Wang et al. (2010) underestimates the lateral resistance, but White and Dingle (2011) is close to the numerical prediction for smooth pipe. Note that, the present analyses are performed only for light pipe whereas Wang et al. (2010) is based on both light and heavy pipes. On the other hand both empirical models give lower horizontal force if rough pipe/soil interface condition is used as shown in Fig. 5.15.

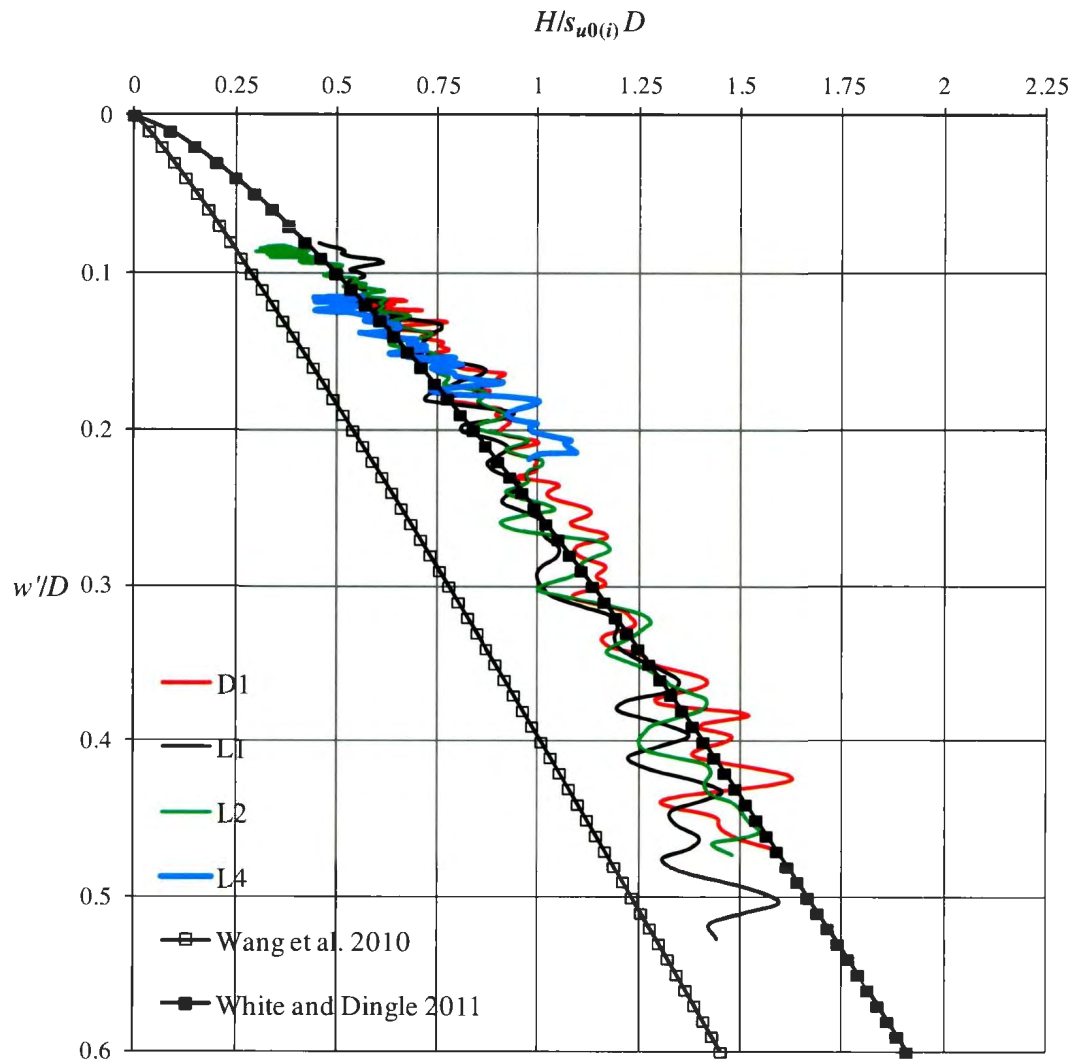


Fig. 5.14 Variation of smooth pipe lateral resistance for CEL analysis with effective embedment (w' = effective embedment)

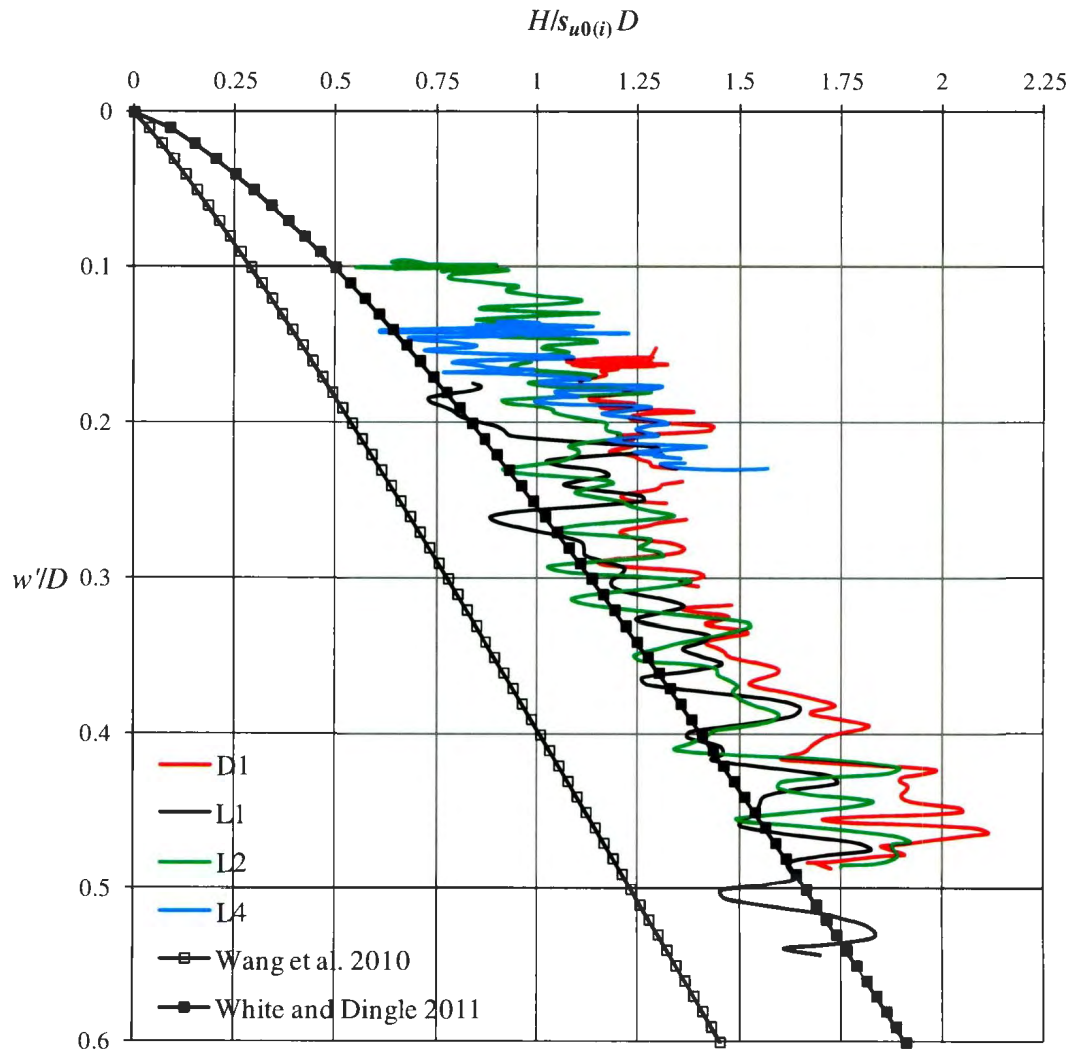


Fig. 5.15 Variation of rough pipe lateral resistance for CEL analysis with effective embedment

5.4 Comparison with Other Analytical Solutions

Pipe lateral resistance has two main parts: (i) pipe breakout resistance and (ii) pipe residual resistance. Based on the experimental database, analytical models have been proposed by Bruton et al. (2006), Cardoso and Silveira (2010) and White and Dingle (2011) to calculate breakout and residual resistance. The lateral breakout resistance obtained from the present finite element models are compared with the analytical model of Bruton et al. (2006) as shown in Eq. 2.7, in Chapter 2 and also with centrifuge test data (Table 5.1). The comparison is shown in Fig. 5.16. The vertical axis shows the normalised breakout resistance and the horizontal axis shows the normalised initial pipe embedment. As discussed before, centrifuge tests showed higher breakout resistance with higher the initial embedment, which is shown in Fig. 5.16. The analytical model by Bruton et al. (2006) underestimates the lateral breakout resistance observed in centrifuge tests except Test D1. Note that, the analytical model by Bruton et al. (2006) is not only a function of $(w/D)_{init}$ but also depends on applied vertical load and undrained shear strength of soil which are different in centrifuge tests and the analyses performed in this study. That is why the points obtained from this analytical model do not show a general trend in Fig. 5.14 as they are plotted only with $(w/D)_{init}$. The present FE analyses give a reasonable comparison with centrifuge test results. For the initial pipe embedment depth of less than $0.2D$, centrifuge test results are in between the finite element model results for smooth and rough pipe.

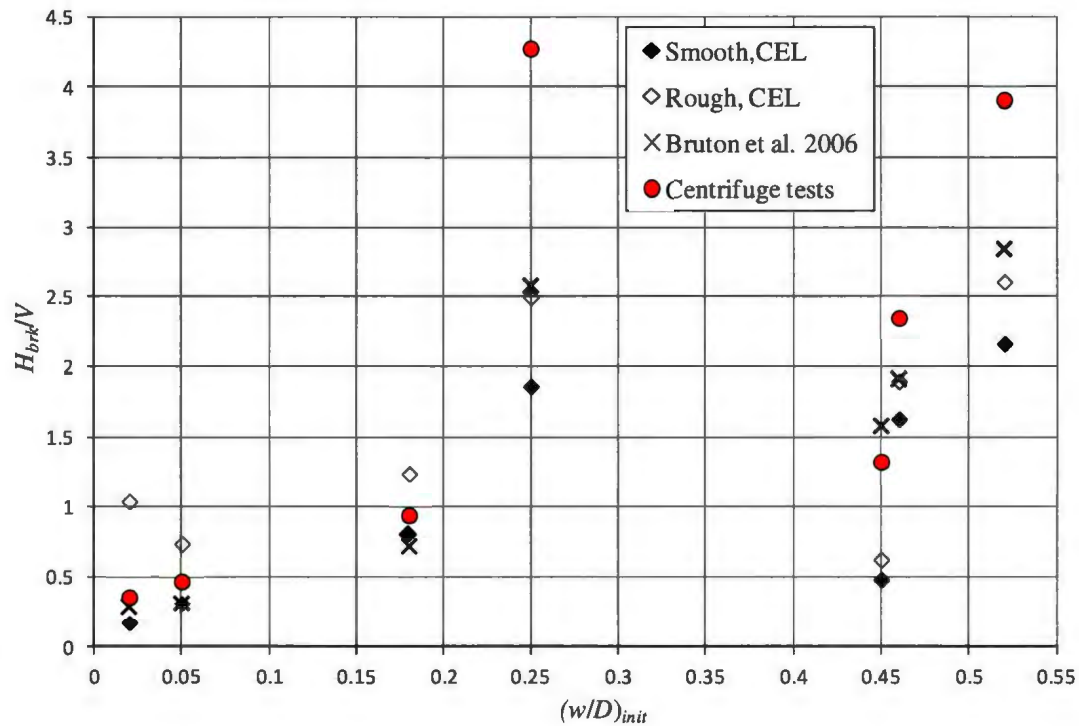


Fig. 5.16 Comparison of lateral breakout resistance

Similarly the residual resistances from the present finite element model are compared with the analytical solutions and centrifuge test results in Fig. 5.17 and 5.18. In finite element modelling, the average value of the lateral resistance for the final $0.5D$ lateral displacement is defined as pipe residual resistance. Figure 5.17 shows the normalised pipe residual resistance (H_{res}/V) with initial pipe embedment and Figure 5.18 is for residual resistance with initial embedment time over square root of over-penetration ratio (R). Both plots show that the analytical solutions of Bruton et al. (2006) (Eq. 2.10, in Chapter 2) and Cardoso and Silveira 2010 (Eq. 2.11, in Chapter 2) give higher residual resistance than the values obtained in the present finite element model and centrifuge tests. Again, in

these two analytical models the residual resistance is also a function applied vertical load and undrained shear strength of the soil which are not constant in different centrifuge tests simulated in this study, and therefore the values calculated with these models are scattered in Figs. 5.15 and 5.16. The solid line in Fig. 5.18 shows the best fit line of centrifuge test results proposed by White and Dingle (2011). The values of residual resistance in centrifuge tests is slightly lower that obtained in the present finite element models with rough pipe/soil interface. The use of appropriate pipe/soil interface condition ($\alpha < 1$) might simulate the centrifuge test results closer. As mentioned before, unfortunately this option is not working in the current version (6.10-EF1) of ABAQUS CEL.

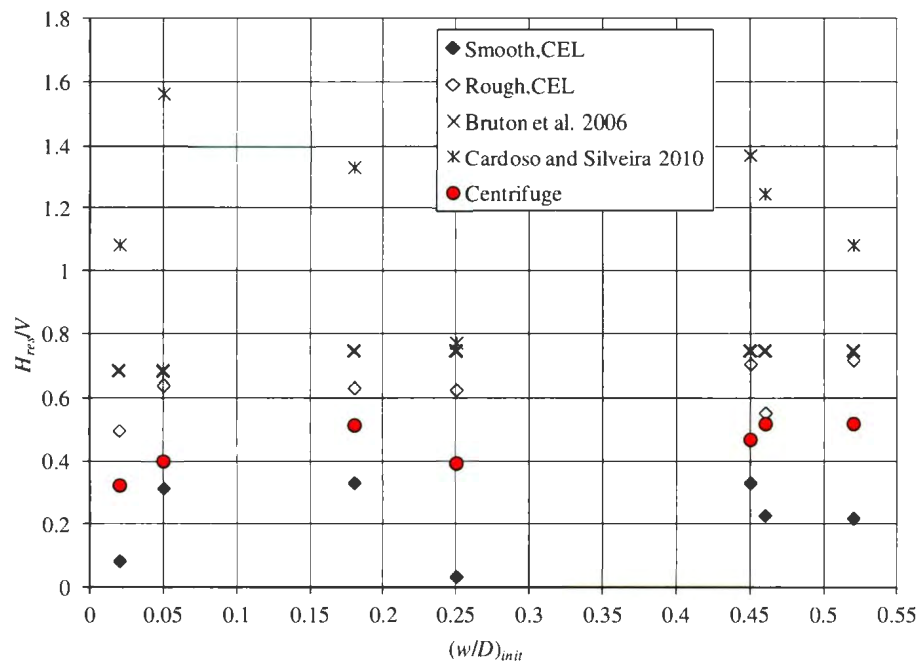


Fig. 5.17 Variation of lateral residual resistance with initial pipe embedment

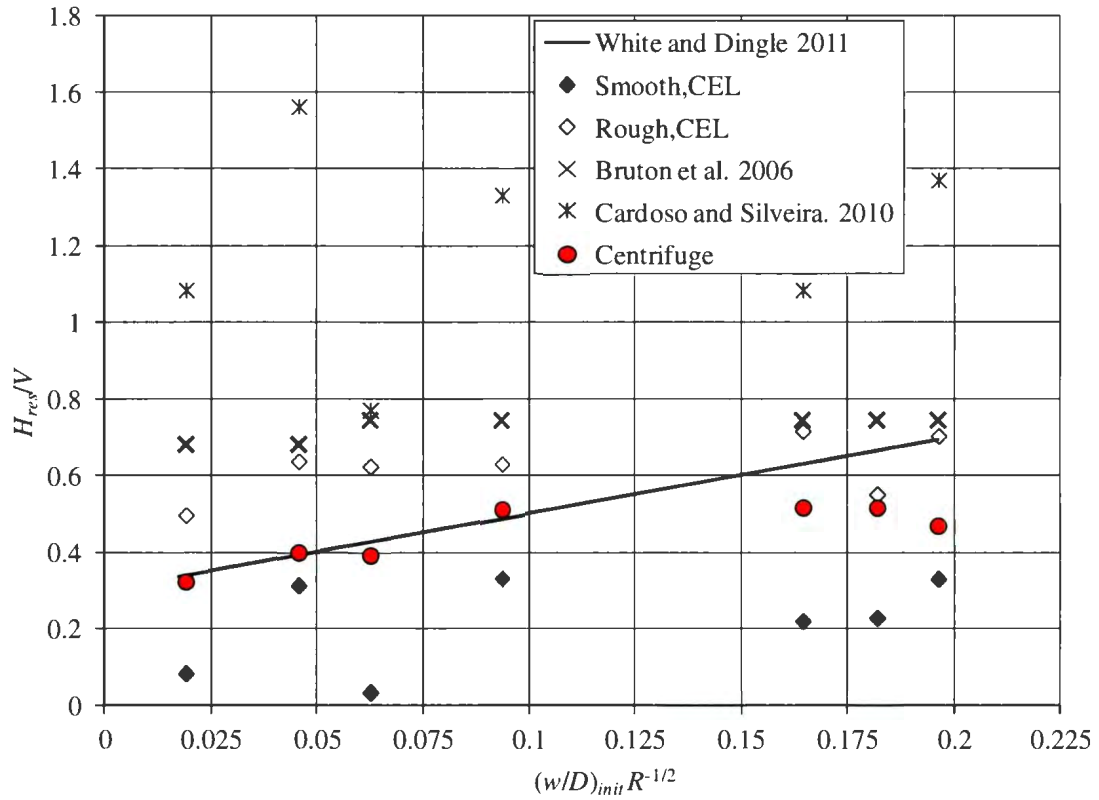


Fig. 5.18 Comparison of lateral residual resistance

5.4 Conclusion

Partially embedded pipelines under lateral displacement have been modelled using ABAQUS CEL finite element software. Strain softening and strain rate effects on undrained shear strength have been modelled. Lateral load versus lateral displacement plots are shown, and from this plot two critical values for design are identified: (i) breakout resistance and (ii) residual resistance. The finite element models developed in

the present study are compared with seven centrifuge test results conducted at the University of Western Australia.

The pipe was first pushed to the desired depth and then moved laterally. The comparison between vertical penetration resistance and centrifuge test results are discussed in Chapters 3 and 4. The lateral force versus lateral displacement in the first four centrifuge tests (cases-L1 to L4), where the initial embedment is at least $0.18D$, match well with numerical models if rough soil/pipe interface conditions are used. However, for very shallowly embedded pipes (cases-L5 and L6), the centrifuge test results are in between the numerical models of smooth and rough pipes. Using the effective embedment concept, the lateral resistance is plotted for both smooth and rough pipes and then compared with available analytical models. Analytical solution of Wang et al. (2010) always underestimates the lateral resistance whereas White and Dingle (2011) is close for smooth pipe. Finally, the lateral breakout and residual resistance are compared with available analytical solutions. Higher residual resistance is found from the available analytical solutions when compared with the present finite element and centrifuge test results.

Chapter 6

Conclusions and Recommendations for Future Research

6.1 Conclusions

During offshore pipeline installation in deep water a pipeline can be embedded a fraction of its diameter into the seabed. However, during operation these partially embedded subsea pipelines can experience very large lateral displacements typically from either thermal expansion or a submarine land slide. Both of them are fundamentally large deformation phenomenon. Few finite element techniques have been developed/used in the past to address these issues — some of them are very simplified while some are the advancement of these models. Almost all the numerical analyses conducted at the early stage used the wished in place (WIP) pipe concept for calculating vertical and lateral pipe resistance using finite element software. Very limited analyses are available for pushed in place (PIP) pipe. The analysis using WIP pipe is a small strain analysis while the PIP pipe is for large strain analysis.

One of the advancements in the finite element modelling technique is the use of Eulerian framework. Large deformation problems can be modelled numerically in this framework. Coupled Eulerian Lagrangian (CEL) approach, recently incorporated in ABAQUS FE software, is used for numerical modelling in this study.

In Chapter 3, the successful use of ABAQUS CEL for modelling vertical penetration of on-bottom offshore pipelines in deep sea conditions is presented. The soil is modelled as ideal clay; that is, the undrained shear strength does not vary with strain rate or strain softening. However, the undrained shear strength of soil is varied with depth. The pipe is penetrated to $0.45D$ where D is the diameter of the pipe. The formation of a berm during penetration and vertical penetration resistance are consistent with the centrifuge test results. Plastic strains around the pipeline and soil flow mechanism during vertical pipe penetration are explained and compared with the observed centrifuge phenomenon. Analyses were conducted successfully without any numerical issues, such as mesh tangling, as typically encountered in small strain analysis using Lagrangian framework.

Several researchers showed that the undrained shear strength of soil depends on shear strain rate. Moreover, strain softening behaviour is common in offshore clays. Modelling of such behaviour of clay cannot be done using the built-in soil constitutive models available in ABAQUS. Therefore, in this study, a strain softening and strain rate dependent model is implemented in ABAQUS CEL using user subroutines. The analyses using this model are presented in Chapter 4. It is shown that the prediction of vertical resistance and berm formation improved significantly if this new soil constitutive model is used. The FE results from the developed model are compared with the existing analytical, theoretical and experimental results. Closer agreement is observed and a parametric study is conducted to show the effects of various soil parameters on predicted

vertical resistance. Parametric study shows that the pipe penetration resistance is influenced by rate parameters rather than softening parameters.

The response of pipelines under a lateral displacement is presented in Chapter 5. Again, the strain softening and strain rate dependent model mentioned before is used for modelling the soil. The pipe is first embedded into the desired depth and then displaced laterally. A total of seven centrifuge tests are simulated numerically. The breakout resistance and residual resistance obtained from FE analysis are compared with centrifuge test results and analytical models. The residual resistance obtained from the present finite element analyses compares well with the centrifuge test result. Excellent comparison of breakout resistance from FE model and centrifuge tests is not found. One of the reasons is that ABAQUS CEL cannot model the suction behind the pipe when it moves laterally.

6.2 Recommendations for Future Research

In the present study the vertical penetration and lateral displacement of deep water offshore pipelines has been successfully modelled. Although a number of important features have been simulated in this study, there are some limitations which might be addressed for further improvement of the model.

- The roughness of the pipe surface should be modelled properly. The maximum shear resistance at the pipe/soil interface cannot be defined in ABAQUS CEL (e.g. Fig. 4.4(b)). Therefore, analyses have been performed only for smooth and rough

conditions. It is expected that these limitations will be solved in the new version of ABAQUS CEL and then it could be used.

- For calculating breakout resistance the suction force behind the pipe should be calculated properly. ABAQUS cannot model such behaviour. A different type of modelling technique could be used in the future.
- During installation, a pipeline might experience dynamic loading, which might be considered to simulate the more realistic conditions. The strain softening effects might be significant and as-laid embedment might increase for dynamic loading as found in some field observations (Westgate et al. 2010b).
- There is a great uncertainty in undrained shear strength of soil in the berm and near the mudline. Accurate measurement/estimation will improve the prediction of vertical and lateral resistance.
- Soil water mixing and its effects on pipe lateral resistance can be addressed using appropriate tools (e.g. computational fluid dynamics tools).

References

- ABAQUS, 6.10EF-1. 2010. Dassault Systèmes, Waltham, MA, United States.
- Abdalla, B., Pike, K., Eltaher, A., and Jukes, P. 2009. A coupled eulerian lagrangian finite element model of ice-soil-pipe interaction. *In* Proceedings of the 19th International Offshore and Polar Engineering Conference, ISOPE 2009, June 21, 2009 - June 26, pp. 474-479.
- AGA, P. 1992. Weight coating design for submarine pipeline on-bottom stability. Final report comparing TAMU test to SINTEF model. PR-178-918, American gas association.
- Aubeny, C.P., Shi, H., and Murff, J.D. 2005. Collapse loads for a cylinder embedded in trench in cohesive soil, *International Journal of Geomechanics*, **5**(4): 320-325.
- Barbosa-Cruz, E.R. and Randolph, M.F. 2005. Bearing capacity and large penetration of acylindrical object at shallow embedment. *In* Proceedings of the 1st International Symposium on Frontiers in Offshore Geotechnics, ISFOG 2005, pp. 615-621.
- Bransby, M.F., Zajac, P., and Amman, S. 2008. Finite element analysis of the vertical penetration of 'on-bottom' pipelines in clay. *In* Proceedings of the 18th International Offshore and Polar Engineering Conference, ISOPE 2008, July 6, 2008 - July 11, pp. 245-249.
- Brennodden, H. 1991. Troll phase-I verification of expansion curve analysis and consolidation effects. STF69 F91011, SINTEF.

Brown, H.k., Burns, P.S., and Christon, A.M. 2002. Coupled eulerian-lagrangian methods for earth penetrating weapon applications. SAND2002-1014, Sandia National Laboratories, California, USA.

Bruton, D.A.S., Boreas, A., White, D.J., Carr, M., and Cheuk, J.C.Y. 2008. Pipe-soil interaction during lateral buckling and pipeline walking-the SAFEBUCK JIP. *In* Proceedings of the Offshore Technology Conference, Houston, Texas, USA. OTC 19589.

Bruton, D.A.S., White, D.J., Cheuk, C.Y., Bolton, M.D., and Carr, M.C. 2006. Pipe-soil interaction behaviour during lateral buckling, including large amplitude cyclic displacement tests by the safebuck JIP. *In* Proceedings of the Offshore Technology Conference, Houston, USA. OTC 17944.

Cardoso, O.C. and Silveira, M.S.R. 2010. Pipe-soil interaction behaviour for pipelines under large displacements on clay soils-A model for lateral residual friction factor. *In* Proceedings of the Offshore Technology Conference, Houston, Texas, USA. OTC 20767.

Cathie, D.N., Jaeck, C., Ballard, J.C., and Wintgens, J.F. 2005. Pipeline geotechnics - state-of-the-art. *In* Proceedings of the 1st International Symposium on Frontiers in Offshore Geotechnics, ISFOG 2005, pp. 95-114.

Chartarjee, S., Randolph, M.F., and White, D.J. 2012a. The effects of penetration rate and strain softening on the vertical penetration resistance of seabed pipelines, *Géotechnique*, **62**(7): 573-582.

Chatterjee, S., White, D.J., and Randolph, M.F. 2012b. Numerical simulation of pipe-soil interaction during lateral movements on clay, *Géotechnique*, **62**(8): 693-705.

Chatterjee, S., White, D.J., and Randolph, M.F. 2011. Lateral movement of pipelines on a soft clay seabed: LARGE deformation finite element analysis. *In* Proceedings of the ASME 2011 30th International Conference on Ocean, Offshore and Arctic Engineering, OMAE2011, June 19, 2011 - June 24, 2011, Vol. 7, pp. 799-807.

Cheuk, C.Y. and White, D.J. 2011. Modelling the dynamic embedment of seabed pipelines, *Géotechnique*, **61**(1): 39-57.

Cheuk, C.Y., White, D.J., and Bolton, M.D. 2007. Large-scale modelling of soil-pipe interaction during large amplitude cyclic movements of partially embedded pipelines, *Canadian Geotechnical Journal*, **44**(8): 977-996.

Dingle, H.R.C., White, D.J., and Gaudin, C. 2008. Mechanisms of pipe embedment and lateral breakout on soft clay, *Canadian Geotechnical Journal*, **45**(5): 636-652.

Dunlap, W.A., Bhojanala, R.P., and Morris, D.V. 1990. Burial of vertically loaded offshore pipelines in weak sediments. *In* Proceedings of the Offshore Technology Conference, Houston, Texas, USA. OTC 6375.

Dutta, S., Hawlader, B., and Phillips, R. 2012. Finite element modeling of vertical penetration of offshore pipelines using coupled eulerian lagrangian approach. *In* Proceedings of the 22nd International Offshore and Polar Engineering Conference, ISOPE 2012, Rhodes, Greece, pp. 343-349.

Einav, I. and Randolph, M.F. 2005. Combining upper bound and strain path methods for evaluating penetration resistance, *International Journal for Numerical Methods in Engineering*, **63**(14): 1991-2016.

Gourvenec, S. and Randolph, M.F. 2003. Effect of strength non-homogeneity on the shape of failure envelopes for combined loading of strip and circular foundations on clay, *Géotechnique*, **53**(6): 575-586.

Green, A.P. 1954. The plastic yielding of metal junctions due to combined shear and pressure, *Journal of Mechanics and Physics of Solids*, **2**: 197-211.

Hu, J.E.H., Leung, C.F., Chow, Y.K., and Palmer, C.A. 2009. Centrifuge model study of SCR motion in touch down zone. *In Proceedings of the ASME 2009 28th International Conference on Ocean, Offshore and Arctic Engineering, OMAE 2009, May 31, 2009 - June 5, Honolulu, Hawaii, USA, Vol. 7, pp. 221-229.*

ISO, O. 2003. Petroleum and natural gas industries specific requirements for offshore structures part-04: Geotechnical and foundation design considerations. 19901-4, International organization for standardization.

Karal, K. 1977. Lateral stability of submarine pipeline. *In Proceedings of the Offshore Technology Conference, Houston, USA, pp. 71-75, OTC 2967.*

Lyons, C.G. 1973. Soil resistance to lateral sliding of marine pipelines. *In Proceedings of the Offshore Technology Conference, Houston, USA. pp. 479-482, OTC 1876.*

Martin, C.M. and Randolph, M.F. 2006. Upper-bound analysis of lateral pile capacity in cohesive soil, *Géotechnique*, **56**(2): 141-145.

Merifield, R., White, D.J., and Randolph, M.F. 2008. The ultimate undrained resistance of partially embedded pipelines, *Géotechnique*, **58**(6): 461-470.

Merifield, R.S., White, D.J., and Randolph, M.F. 2009. Effect of surface heave on response of partially embedded pipelines on clay, *Journal of Geotechnical and Geoenvironmental Engineering*, **135**(6): 819-829.

Morris, D.V., Webb, R.E., and Dunlap, W.A. 1988. Self burial of laterally loaded offshore pipeline in weak sediments. *In Proceedings of the Offshore Technological Conference*, Houston, Texas, USA. OTC 5855.

Morrow, D.R. and Bransby, M.F. 2011. Pipe-soil interaction on clay with a variable shear strength profile. *In Proceedings of the 2nd International Symposium on Frontiers in Offshore Geotechnics*, ISFOG 2010, November 8, 2010 - November 10, pp. 821-826.

Murff, J.D., Wagner, D.A., and Randolph, M.F. 1989. Pipe penetration in cohesive soil, *Géotechnique*, **39**(2): 213-229.

Quiros, W.G. and Little, L.R. 2003. Deepwater soil properties and their impact on the geotechnical program. *In Proceedings of the Offshore Technology Conference*, Houston, USA. OTC 15262.

Randolph, M.F. and White, D.J. 2008. Upper-bound yield envelopes for pipelines at shallow embedment in clay, *Géotechnique*, **58**(4): 297-301.

Randolph, M.F. and Houlsby, G.T. 1984. Limiting pressure on a circular pile loaded laterally in cohesive soil, *Géotechnique*, **34**(4): 613-623.

SINTEF. 1987. Pipe-soil interaction test on sand and soft clay. STF60 F7018.

SINTEF. 1986b. Pipe-soil interaction test, stiff clay. STF60 F86072.

- SINTEF. 1986a. Pipe-soil interaction test, soft clay. STF60 F86023.
- Small, S.W., Tamburello, R.D., and Piaseckyj, P.J. 1972. Submarine pipeline support by marine sediments, *Journal of Petroleum Technology*, **24**: 317-322.
- Tho, K.K., Leung, C.F., Chow, Y.K., and Swanddiwudhipong, S. 2009. Application of eulerian finite element technique for analysis of spudcan and pipeline penetration into the seabed. *In Proceedings of the 12th Jack Up Conference*, City University, London.
- Tho, K.K., Leung, C.F., Chow, Y.K., and Palmer, A.C. 2012. Deep cavity flow mechanism of pipe penetration in clay, *Canadian Geotechnical Journal*, **49**(1): 59-69.
- Verley, R. and Lund, K.M. 1995. Soil resistance model for pipelines placed on clay soils. *In Proceedings of the 14th International Conference on Offshore Mechanics and Arctic Engineering (OMAE)*, Copenhagen, Denmark, June 18, 1995 - June 22, Vol. 5, pp. 225-232.
- Wagner, D.A., Murff, J.D., Brennodden, H., and Sveggen, O. 1989. Pipe-soil interaction model, *Journal of Waterway, Port, Coastal and Ocean Engineering*, **115**(2): 205-220.
- Wang, D., White, D.J., and Randolph, M.F. 2010. Large-deformation finite element analysis of pipe penetration and large-amplitude lateral displacement, *Canadian Geotechnical Journal*, **47**(8): 842-856.
- Westgate, Z.J., Randolph, M.F., White, D.J., and Li, S. 2010a. The influence of sea state on as-laid pipeline embedment: A case study, *Applied Ocean Research*, **32**(3): 321-331.

Westgate, Z.J., White, D.J., Randolph, M.F., and Brunning, P. 2010b. Pipeline laying and embedment in soft fine-grained soils: Field observations and numerical simulations. In Offshore Technology Conference 2010, OTC 2010, May 3, 2010 - May 6, Vol. 1, pp. 326-340

White, D.J. and Dingle, H.R.C. 2011. The mechanism of steady friction between seabed pipelines and clay soils, *Géotechnique*, **61**(12): 1035-1041.

White, D.J. and Cheuk, C.Y. 2008. Modelling the soil resistance on seabed pipelines during large cycles of lateral movement, *Marine Structures*, **21**(1): 59-79.

Zhou, H. and Randolph, M. 2009. Numerical investigations into cycling of full flow penetrometers in soft clay, *Géotechnique*, **59**(10): 801-812.

